UNIVERSITY OF LIVERPOOL

The link between mRNA 3' tagging and Nonsense-Mediated mRNA Decay (NMD) in *Aspergillus nidulans*

Thesis submitted in accordance with the requirements of

The University of Liverpool for the degree of

Doctor in Philosophy by

Amir Mossanen-Parsi

June 2018

ABSTRACT

The focus of this study was to characterise the nonsense-mediated mRNA decay (NMD) complex and its link to mRNA 3' tagging in *Aspergillus nidulans*. The human histone H2a and H3 encoding transcripts were the first mRNAs reported to be oligouridylated. This was shown to involve Upf1, which is recruited by the stem-loop binding protein (SLBP) in response to DNA synthesis being blocked; Upf1 recruitment promotes 3' tagging of the histone transcript which in turn leads to their rapid degradation. Other NMD components have not been implicated in the regulatory response. Initial work looking at the H2A transcript suggested that a similar response occurs in *A. nidulans* when DNA synthesis is blocked. In addition to the tagging factors, CutA and CutB, we tested a number of key NMD and decay factors to obtain a general view of histone mRNA regulation with the aim of gaining crucial information on the mechanism and function of tagging. Additionally, we investigated the role of two putative NMD factors, Smg6 and Upf3, and the specific role of particular domains within Smg6 and Upf1. Our studies confirmed that both Smg6 and Upf3 are required for NMD in *A. nidulans*. Additionally, we have shown that both Dcp2 mediated decapping and Smg6 dependent endonuclease cleavage contribute to NMD in *A. nidulans*, similar to the situation in mammalian systems. Disruption of the NMD component Upf1, Upf2, Upf3 and Smg6 fully supress NMD and partially supress histone regulatory response to hydroxyurea treatment. Simultaneous disruption of certain NMD and decay factors displayed additivity and led to full disruption of histone mRNA regulation. Based on our data, one important possibility is the parallel function of the Lsm1-7 activated decapping pathway and a second pathway involving the NMD complex but not Smg6 mediated mRNA cleavage. Histone mRNA degradation data demonstrated that the disruption of CutA and CutB had a minor impact on histone mRNA regulation, whereas their disruption had a major impact on histone transcripts within polysomes. Western analysis demonstrated that both CutA and CutB were associated with ribosomal fractions. This Suggests that the CutA and CutB enzymes are involved in regulating translationally active histone transcripts and their disruption results in extension of histone mRNA half-life within the polysomes. However, this does not have a major effect on the overall histone mRNA turnover. These results are consistent with a model in which the tagging factors may recruited to transcripts harbouring a terminating ribosome possibly by Upf1. Subsequently, both the NMD components and engagement of the Lsm1-7 complex separately facilitate histone mRNA decapping and translational repression.

Acknowledgements

A sincere thanks to Professor Mark X. Caddick for his continuous support with help, guidance and extreme patience. I would also like to thank Dr Bahram Ebrahimi, Dr Igor Morozov and Dr Christopher Clarke for all their useful advice. Particular thanks go to our group members and the members of Lab G. Finally, I would like to thank my family, especially my mother Sohaila Tootoonchi and father Dr Masoud Mossanen-Parsi for their endless support and my daughter Ava for bringing happiness and joy in the final year of my PhD.

Abbreviations

APS	Ammonium Persulfate
bp	base pair
cDNA	complementary deoxyribonucleic acid
cRT-PCR	circularisation RT-PCR
DNA	Deoxyribonucleic acid
DMSO	Dimethyl sulfoxide
dNTP	Deoxynucleotide phosphate
EDTA	Ethylenediaminetetraacetic acid
g	gram
Kb	Kilobase
LB	Luria broth
mg	Milligram
ml	mililitre
MOPS	3-(N-morpholino) propanesulfonic acid
MQ	MilliQ
mRNA	messanger ribonucleic acid
mRNP	messenger ribonucleoprotein
PCR	polymerase chain reaction
PEG	Polyethylene glycol
RNA	Ribonucleic acid
RPM	Revolutions per minutes
SDS-PAGE	Sodium dodecyl sulfate polyacrylamide gel electrophoresis
TBST	Tris buffered saline with tween® 20
TEMED	Tetramethylethylenediamine
3’-UTR	3 prime untranslated region
5’-UTR	5 prime untranslated region
µl	microlitre

List of Tables

List of Figures

CHAPTER 5

CONTENTS

Chapter 1: Introduction

1.1 Gene expression

Gene expression is the process by which genetic information is transmitted, primarily through the synthesis of proteins, for cell maintenance, growth, proliferation, and differentiation. There are two key steps involved in making a protein; transcription and translation. Transcription of protein coding genes is when the genetic information encoded in DNA is transcribed by RNA polymerase. In eukaryotes this is mediated by RNA polymerase II, producing a primary transcript that undergoes various co- and post-transcriptional modifications to form the mature messenger RNA (mRNA). Translation in eukaryotes occurs after transcription is complete and the mRNA has been exported from the nucleus, the ribosomes completing the flow of information from the DNA by decoding the RNA to protein (Li and Xie, 2011). To live, cells must be able to control both transcriptional and translational patterns in order to adjust the quantity and nature of proteins it manufactures (Miller and Pearce, 2014). Although the primary component of gene regulation occurs at the level of transcriptional initiation, cells also regulate protein levels through the enzymatic breakdown of RNA transcripts and existing protein molecules that it no longer needs or that are detrimental to its health (Miller and Pearce, 2014). In addition, faulty or damaged proteins are recognised and rapidly degraded within cells, thereby eliminating the consequences of mistakes made during protein synthesis (Cooper, 2000).

1.2 mRNA maturation

In eukaryotic cells, newly transcribed mRNA is initially modified by adding specific structures at its ends; the 5' terminal 7-methylguanosine (m^7G) cap and the 3' terminal poly(A) tail (Zhao et al., 2017). Modifying the transcript is required to permit mRNA transfer from the

nucleus to the cytoplasm for subsequent rounds of translation (Zhao et al., 2017). The m^7G-cap structure protects the mRNA from 5'-3' exonucleolytic degradation, it is recognised and bound by the cap-binding protein, eukaryotic translation initiation factor 4E (eIF4E) (Zhao et al., 2017). The mRNA poly(A) tail, which is a vulnerable to 3'-5' exonuclease activity of the deadenylases and the exosome, is protected by poly(A) binding protein (Pab1) (Dunn, 2005).

The eukaryotic genes are discontinuous as they contain protein coding regions (exons) disrupted by noncoding regions (introns) (Lee and Rio, 2015). The introns are spliced out by the spliceosome from the precursor messenger RNA (pre-mRNA) to join protein coding exons into mature mRNA (da Costa, Menezes and Romão, 2017). Vertebrates have relatively long introns and short exons; this relationship is reversed in lower eukaryotes (Li, Xu and Ma, 2017). Eukaryotes have lost and gained introns in response to strong selective pressures over time as part of their dynamic intron evolution (Li, Xu and Ma, 2017). It was suggested that natural selection favours short introns in the highly expressed genes of nematodes and humans to minimise the cost of transcription (Li, Xu and Ma, 2017). However, the density of introns in a gene does not show a strong correlation with the level of gene expression. However, it was found that organisms that reproduce rapidly have a lower intron density than organisms with longer life cycles (Li, Xu and Ma, 2017). For instance, Homo sapiens have an average of 8.1 introns per gene, *Caenorhabditis elegans* with 4.7, *Arabidopsis thaliana* with 4.4 and *Drosophila melanogaster* with 3.4; whereas unicellular species with short life spans were found to have fewer introns (Stajich, Dietrich and Roy, 2007). Studies of intron densities in a variety of single-celled species have revealed great variation. For instance, the yeasts *Schizosaccharomyces pombe* and *Saccharomyces cerevisiae* have low intron densities with 0.9 and 0.05 introns per gene, respectively. However, the

euascomycete fungi *Neurospora crassa* and *Aspergillus nidulans* have much higher intron densities at 2-3 per gene (Stajich, Dietrich and Roy, 2007).

With advances in genome sequencing, it is apparent that organismal complexity is to a great extent dependent on the pre-mRNA splicing (Lee and Rio, 2015). Although the numbers of genes in mouse and human genomes are similar, alternative pre-mRNA splicing (AS) occurs in approximately 63% of mouse genes compared with 95-100% of human genes (Lee and Rio, 2015). Therefore, one characteristic of AS is to expand the form and function of the proteome by creating multiple transcript variants produced from a single gene locus (Lee and Rio, 2015). It has been reported AS can function in several modes such as exon skipping and alternative use of 5′ and 3′ splice sites which regularly occur whereas more rare events such as intron retention and the inclusion of mutually exclusive exons can also take place (da Costa, Menezes and Romão, 2017). AS participates in various biological processes, such as metabolism, differentiation, pluripotency, adhesion, cell proliferation, adaptation and apoptosis; in contrast its aberrant activation can lead to many human diseases such as various types of cancers (da Costa, Menezes and Romão, 2017).

In mammalian, during splicing a multiprotein assembly termed the exon junction complex (EJC) is loaded 20-24 nucleotides upstream of the exon-exon junctions by the splicing machinery (Figure 1.1) (Hir, Saulière and Wang, 2015). The EJC is composed of an inner heterotetrameric core consisting of eIF4A3, MAGOH, Y14 and MLN51 (Tian et al., 2017). The EJC core components are linked to the mRNA via eIF4A3 which is a DEAD-box RNA helicase (Bhuvanagiri et al., 2010). eIF4A3 binding to the Y14–MAGOH dimer inhibits its ATPase activity and stabilises the binding of EJC components to the mRNA (Bhuvanagiri et

al., 2010). EJC core components are accompanied with other regulatory factors which remain associated with mRNA until translation (Tian et al., 2017). The composition of EJCs is highly dynamic, where the EJC core factors act as a binding platform for a number of proteins called the EJC peripheral factors; these promote EJC functionality during mRNA transport to the cytoplasm (Hir, Saulière and Wang, 2015, Bhuvanagiri et al., 2010). In the cytoplasm, the EJC acts as an anchor for various mRNA processing factors during translation (Hir, Saulière and Wang, 2015).

Translation begins with the recognition of the cap structure by the eIF4E protein; eIF4G then serves as a scaffolding protein to recruit other translation initiation factors such as eIF4A, eIF4B and Pab1 to form the eIF4F complex (Hir, Saulière and Wang, 2015, González-Almela et al., 2018).

The interactions between mRNA 5' end through eIF4G and mRNA 3' end through Pab1 results in a closed-loop conformation which has been shown to be important for the translation initiation (von der Haar, Ball and McCarthy, 2000). Upon the formation of the eIF4F complex, the small 40S ribosomal subunit carrying additional initiation factors; eIF1, eIF1A, eIF3, eIF5 and the ternary complex eIF2-Met-$tRNA_i^{Met}$-GTP forms the 43S pre-initiation complex (González-Almela et al., 2018). Subsequently, the 43S pre-initiation complex interacts with the 5' end of the mRNA forming the 48S initiation complex which scans mRNA from 5' to 3' until it detects the start codon in an appropriate sequence context (Langley, 2015). Finally, eIF5B binds the 48S complex which promotes the release of eIFs in a GTP-dependent manner, resulting in a fusion with the large 60S ribosomal subunit to form the elongating 80S ribosome (González-Almela et al., 2018).

Through the pioneer round of translation the translating ribosome subsequently displace EJCs on the transcript (da Costa, Menezes and Romão, 2017). However, when the mRNA molecule is defective, the ribosome will fail to displace these distal EJCs and consequently results in the formation of a decay-inducing complex (da Costa, Menezes and Romão, 2017).

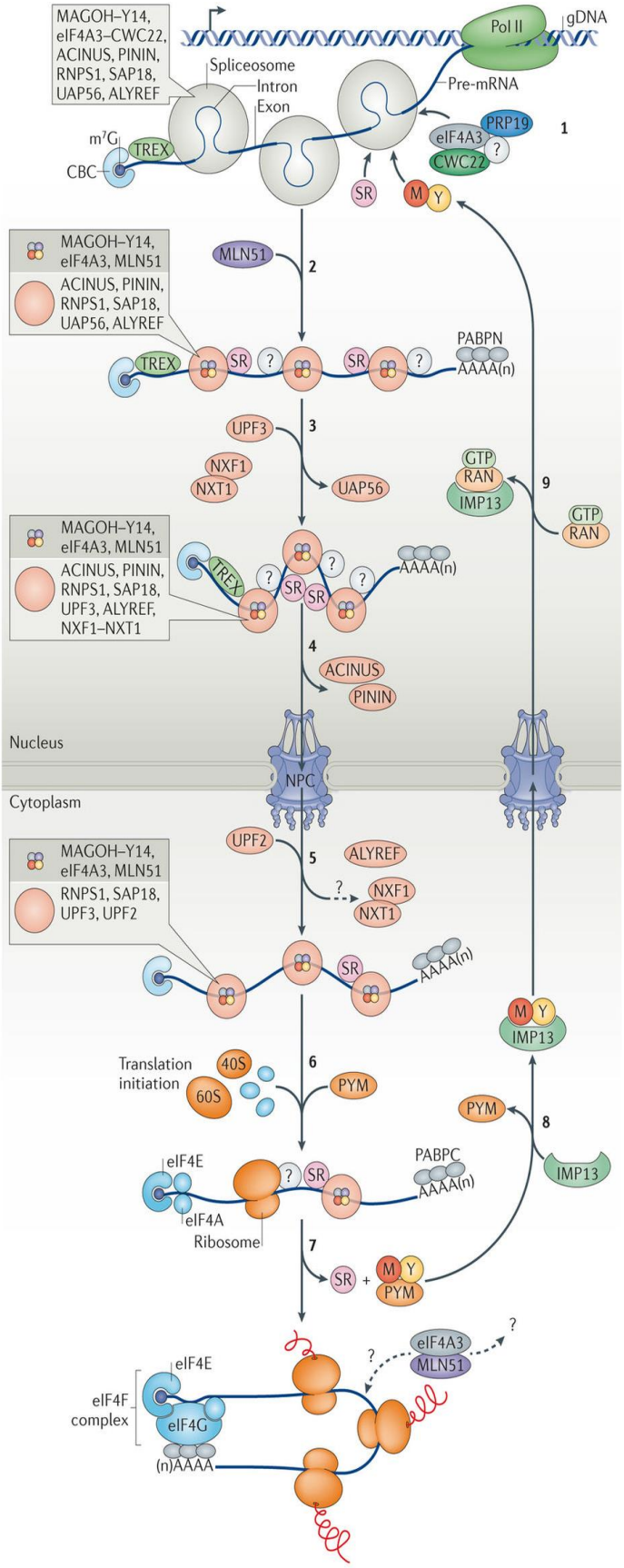

Figure 1.2 The assembly of EJCs on mRNA. In human cells, following splicing, the EJCs are assembled on the spliced mRNA by the spliceosome. EJC peripheral factors restricted to the nucleus leave the EJC before the mRNP enters the cytoplasm through the nuclear pore complex (NPC). Several factors involved in mRNA splicing, transport, translation and processing along with the EJC core proteins; eIF4A3, MAGOH, Y14 and MLN51 remain associated with the mRNP. Once in the cytoplasm, Upf2 joins the EJC whereas the nuclear transport factors; ALYREF, NXF1 and NXT1 dissociate rapidly. In cytoplasm, untranslated mRNAs bound by cap-binding complex (CBC) and nuclear poly(A) binding protein (PABPN) are exchanged with the translation initiation factors eIF4E and PABPC, respectively. Circularisation of the mRNA through the interaction of PABPC with translation factors bound at the cap facilitates successive rounds of translation. Following EJC disassembly and SR protein release, eIF4A3 and MLN51, as well as SR proteins, can potentially rebind to translated mRNAs or shuttle back to the nucleus. PYM has been identified to mediate efficient EJC components disassembly and recycling. Figure taken from Hir, Saulière and Wang, (2015).

1.3 General mechanism of mRNA decay

The balance between mRNA synthesis and decay adjusts transcript abundance to the needs of the cell for specific proteins (Braun and Young, 2014). Previous studies have revealed that the two processes are closely related (Braun and Young, 2014). Transcript decay is a major component of overall mRNA metabolism and plays a key role in determining intracellular levels of mRNA molecules under certain stress conditions or when the transcript is defective (Deutscher, 2006). Significant advances have been made in our knowledge of the mRNA regulatory mechanism over the past 20 years (Kiledjian, 2015). In all organisms tested from all kingdoms of life, mRNA degradation is a prevalent activity. Overall, the emerging picture is that despite the immense complexity of specific mRNA degradation pathways, there are substantial similarities in mechanisms of mRNA degradation between bacteria, archaea, and eukaryotes, underlining its major, and long-standing, importance (Houseley and Tollervey, 2009).

Although the general pathways of mRNA decay remain constant, many of the key endo/exonucleases and trans-acting factors have been identified and found to be highly conserved across eukaryotes (Table 1) (Houseley and Tollervey, 2009). Several deadenylases have been uncovered; PARN, Pan2/Pan3 and the CCR4/Caf1/Not complex, all functioning to remove the 3' end poly(A) tail (Houseley and Tollervey, 2009). Subsequently, the deadenylated mRNA can be efficiently degraded by the exosome complex. This complex consists of a core of nine subunits arranged in a ring-like structure, with 3'-5' exonuclease activity; associated with several ribonucleases such as PM/Scl-100 (Rrp6 in *Saccharomyce cerevisiae*) or Rrp44 (Dis3 in *S. cerevisiae*) proteins (Houseley and Tollervey, 2009). In addition to the decay of the mRNA from the 3' end the 5' cap structure can be removed by

the cytoplasmic decapping complex which is composed of the catalytic subunit Dcp2 and its coactivator, Dcp1 (Houseley and Tollervey, 2009). Additionally, several enhancers of decapping in humans, such as PatL1 (Pat1 in *S. cerevisiae*), DDX6 (Dhh1 in *S. cerevisiae*), Edc3, Scd6 and the Sm-like (Lsm) protein complex (Lsm1-7) are thought to modulate its decapping activity *in vivo* (Antic et al., 2015). Once the cap is removed, the 5' end is degraded by the exonuclease Xrn1 (Houseley and Tollervey, 2009). In some circumstances, mRNA degradation is initiated by endonucleolytic cleavage. Internal cleavage produces free 5' and 3' ends, which in turn can be degraded by Xrn1 and/or the exosome, respectively (Houseley and Tollervey, 2009).

The absence of any one mRNA degradation factor does not commonly result in a complete inhibition to mRNA degradation in either eukaryotes or prokaryotes (Houseley and Tollervey, 2009). This signifies that multiple proteins are able to identify the same target transcripts and compensate for the deleted protein, which enhances the robustness of mRNA degradation (Houseley and Tollervey, 2009).

Table 1 mRNA decay factors. List of major proteins involved in general mechanisms of NMD and mRNA decay in eukaryotes.

	Protein	Function	Reference
3' tagging			
	CutA	A nucleotidyltransferase that catalyses the addition of nucleotides (C/U) to the 3' end of mRNA in *A. nidulans.* Putatively forming a complex with CutB.	(Morozov et al., 2012)
	CutB	A nucleotidyltransferase that catalyses the addition of nucleotides (C/U) to the 3' end of mRNA in *A. nidulans.* Putatively forming a complex with CutA.	(Morozov et al., 2012)
NMD			
	Upf1	A 5'-3' DNA and RNA helicase with nucleic acid-dependent ATPase activity essential for NMD, competing with Pab1 for interaction with eRF3.	(Azzalin and Lingner, 2006)
	Upf2	Involved in both mRNA nuclear export and mRNA surveillance.	(Melero et al., 2014)
	Upf3	A part of a post-splicing multi-protein complex involved in both mRNA nuclear export and mRNA surveillance.	(Melero et al., 2014)
	Smg6	Is thought to provide a link to the mRNA degradation machinery as it has endonuclease activity required to initiate NMD.	(Nicholson et al., 2014)
Decay			
3'-5' decay	Ccr4	3'-5' exonuclease, a catalytic subunit of deadenylase complex.	(Laribee et al., 2015)
	Caf1	3'-5' exonuclease, a catalytic subunit of deadenylase complex.	
	Rrp44	The catalytically active component of exosome complex involved in both an RNase II–like hydrolytic 3'-exonuclease activity and a PIN-domain endonuclease activity.	(Schneider et al., 2014)
	Ski3	An exosome enhancer.	(Fromont et al., 2014)
5'-3' decay	Dcp1	A subunit of decapping complex, the enzymatic activity of Dcp2 is critically dependent on the Dcp1.	(Fillman and Lykke-Andersen, 2005)
	Dcp2	The catalytic subunit of the Dcp1:Dcp2 complex.	(Fillman and Lykke-Andersen, 2005)
	Dhh1	A DEAD-box RNA helicase, an activator of mRNA decapping. It interacts with both decapping and deadenylase complexes. It binds to mRNA and also associates with Edc3 and Pat1.	(Sesma and Haar, 2014)
	Pat1	It appears to function as a scaffold protein to form a multisubunit assembly to activate mRNA decapping. It binds to Dhh1, Lsm1-7 complex, Dcp1, Dcp2 and Xrn1.	(Fourati et al., 2014)
	Scd6	It associates with eIF4G subunit of eIF4F translation initiation complex.	(Fromont et al., 2014)
	Edc3	Sm-like, decapping enhancer.	(Fourati et al., 2014)
	Lsm1-7	A cytoplasmic heteroheptameric complex of Sm-like proteins, required for mRNA decapping.	(Zhou et al., 2013)
	Lsm2-8	A nuclear heteroheptameric complex of Sm-like proteins, required for mRNA splicing.	(Zhou et al., 2013)
	Xrn1	5'-3' exonuclease degrades mRNA containing a free 5' monophosphate end.	(Harigaya and Parker, 2012)

1.4 Regulation of aberrant transcripts

Gene expression is a controlled and monitored throughout the multi-step process of gene expression; from DNA to RNA to protein. In some cases, DNA damage can be repaired but aberrant mRNA and protein may not, thus a number of different mechanisms have evolved to detect and eliminate these aberrant gene products. In the case of mRNA synthesis, various defects can arise including somatic rearrangements at the DNA level and germ-line mutations, the latter accounting for hundreds of inherited genetic disorders, especially cancers (Chakrabarti et al., 2011). Additionally, errors can arise much more frequently during transcription and pre-mRNA splicing than in DNA replication (Allan Drummond and Wilke, 2009). In all organisms, DNA is duplicated with remarkable fidelity to ensure the faithful transfer of genetic information from one generation to the next through the combined action of accurate DNA polymerases and post-replication DNA mismatch repair, which result in a DNA mutation rate estimated to be lower than 1×10^{-9} per base pair (bp) (McCulloch and Kunkel, 2008). For example, it was found that the yeast transcriptome contains on average 4.0 errors per million base pairs. It was demonstrated that transcription errors are more than a 100 times more frequent. However, these errors are not equally distributed across the transcriptome. Transcripts synthesised by RNA polymerase II (RNAPII) contain the least number of errors (3.9×10^{-6} per bp), followed by ribosomal RNA molecules synthesised by RNAPI (4.3×10^{-6} per bp), mitochondrial RNA (9.3×10^{-6} per bp) and transcripts synthesised by RNAPIII (1.7×10^{-5} per bp); suggesting that each RNA polymerase has a unique error rate (Gout et al., 2017).

Protein synthesis is the next step in gene expression; it is also the stage which harbours the greatest potential for errors (Mohler and Ibba, 2017). Translation in prokaryotic and

eukaryotic cells has an error rate in the range of 1 x 10^{-3} to 1 x 10^{-4} per bp, under normal physiological conditions, leading to the incorrect incorporation of amino acids into proteins (Araújo et al., 2018). Although, it was recently reported for bacterial cells, that mistranslation arises approximately once every 200 codons (Meyerovich, Mamou and Ben-Yehuda, 2010). However, various mechanisms, such as molecular chaperones, proteasomes and autophagy, can remove defective proteins so that the cell usually does not suffer significant damage. However, defects in the translational machinery can lead to dysfunction or disease due to an increased level of errors (Araújo et al., 2018).

Translation plays a significant role in the regulation of gene expression and is implicated in the control of cell growth, proliferation, and differentiation. In eukaryotes, during the first round of translation, transcripts containing premature termination codons (PTC) can be recognised and rapidly degraded via a surveillance pathway known as nonsense-mediated mRNA decay (NMD) which involves a series of protein-protein interactions (Chakrabarti et al., 2011). NMD is an evolutionarily conserved process and, for the most part, components of the NMD complex in mammalian cells have been identified by their homology to those in yeast or by their physical interaction to previously identified members of the NMD complex, emphasising the significance of this pathway in evolutionary terms (Gardner, 2010).

Initially, it was discovered that the level of β-globin mRNA in patients with β^0-thalassemia was repressed by NMD, subsequent studies in many species, have revealed that expression of between 4% and 25% of protein-coding genes are altered when NMD is reduced or eliminated (Muir, Gasch and Anderson, 2017). A consistent issue with such studies is the difficulty in determining whether the altered expression of any single gene in an NMD-

deficient cell is either due to a direct effect of NMD or whether the altered expressions of NMD substrates have an indirect consequence on the mRNA of other genes.

To establish whether a transcript is a direct substrate of NMD, a number of different strategies have been utilised (Muir, Gasch and Anderson, 2017) such as:

- isolating transcripts that copurify with the NMD factors
- measuring mRNA half-life after NMD inhibition, followed by monitoring immediate versus delayed effects on expression
- measuring changes in mRNA abundance following reactivation of NMD

Together, such studies have shown that around 20-50% of transcripts that have increased expression in NMD-deficient cells are direct NMD substrates (Muir, Gasch and Anderson, 2017). Remarkably, the abundance of a number of transcripts, which appear to be substrates of NMD remains unchanged in NMD-deficient cells (Muir, Gasch and Anderson, 2017).

A key function of NMD is to prevent accumulation of non-functional or potentially harmful truncated proteins in the cell (Fiorini, Boudvillain and Le Hir, 2012). Consequently, NMD can reduce the phenotypic impact of a mutation. However, in cases where NMD silences an aberrant transcript that nevertheless has the potential to produce a functional product, NMD can exacerbate the effect. PTC-containing transcripts may evade NMD in two ways; by the incomplete action of NMD in the degradation of PTC-containing transcript or by a specific mechanism that allows the transcript to evade NMD to ensure protein synthesis (Smith, Blencowe and Graveley, 2008). For example, DMD (Duchenne muscular dystrophy) is a disorder which arises due to 5’ PTCs in the dystrophin gene prompting an NMD response

which drastically reduces the synthesis of the truncated protein. 3’ PTCs on the other hand are linked to a milder form of the disorder called BMD (Becker muscular dystrophy) since they can escape NMD and resulting in the synthesis of C-terminally truncated dystrophin protein (Bhuvanagiri et al., 2010).

It was concluded that the augmentation or inhibition of NMD efficiency could offer potential therapeutic strategies and applications in medicine (Bhuvanagiri et al., 2010). In theory, NMD could be stimulated or inhibited for therapeutic results depending on its effect on target proteins. Although, only inhibition of NMD has been developed clinically against diseases which could be favourably affected by the increased synthesis of the mutated proteins. A much deeper understating of the NMD pathway and its manipulation are required in order to develop strategies that can modulate NMD as a therapeutic strategy for PTC-related inherited disorders (Han et al., 2017).

NMD can significantly reduce the abundance of PTC-containing transcripts, but does not eliminate them completely (Smith, Blencowe and Graveley, 2008). Furthermore, PTC-containing isoforms are not degraded immediately, their degradation occurs only after a pioneer round of translation, which may occur near the nuclear pore during or soon after export of the mRNA from the nucleus (Smith, Blencowe and Graveley, 2008). Therefore, PTC-containing transcripts are present in the cell, especially inside the nucleus, due to the temporal lag between splicing and degradation rather than incomplete surveillance (Smith, Blencowe and Graveley, 2008).

The key NMD proteins are the three up frame-shift (Upf) suppressor proteins with Upf1 acting as the central regulator of the NMD pathway, which is highly conserved across all eukaryotes. Upf1 is a phosphoprotein whose activity in multicellular organisms is regulated by cycles of phosphorylation and dephosphorylation. The four ''suppressor with morphological effect on genitalia'' (Smg) proteins; Smg1, Smg5, Smg7 and Smg6 have been shown to mediate the phosphorylation/dephosphorylation cycles of Upf1 which allows the formation of an Upf1-Upf2-Upf3 surveillance complex that is believed to trigger the mRNA degradation machinery (Peccarelli and Kebaara, 2014). However, the detailed role of these Smg proteins and how they mediate Upf1 phosphorylation/dephosphorylation cycles is yet to be determined.

A defining step in recruiting Upf1 and promoting NMD is the failure of two eukaryotic release factors, eRF1 and eRF3 to release ribosomes that terminate at a PTC (Singh, Rebbapragada and Lykke-Andersen, 2008). Typically, a number of ribosomes are engaged with the transcript in order to allow repeated rounds of translation. At the end of each round of translation, eRF3 is recruited by eRF1 to the translating ribosome as it associates with the termination codon. Generally, eRF3 interacts with poly(A) binding protein (Pab1), an interaction which promotes both deadenylation and the dissociation and recycling of ribosomes (Morozov et al., 2012). In the case of NMD the interaction between eRF3 and Pab1 does not occur and Upf1 is recruited to the terminating ribosome through an interaction with eRF3. This can take place, for example, where there is a premature termination codon (PTC) positioned such that the poly(A) tail and associated Pab1 cannot easily associate with eRF3, and is exacerbated if there is an exon junction complex 3' to the PTC.

Based on work in *S. cerevisiae* and mammals, deadenylation of transcripts to approximately fifteen adenine residues results in Pab1 dissociation (Parker, 2012). As the Pab1-eRF3 interaction is central to ribosome recycling, it has been proposed that in the absence of Pab1, deadenylation will result in eRF3 recruiting of Upf1 to the stalled ribosome, which triggers an NMD-like response, leading to repression of translational initiation, mRNA decapping and degradation, all of which mirror the role of the NMD factors in regulating gene expression (Figure 1.2) (Morozov et al., 2012). However, no confirmation of this model or detailed understanding of NMD factors specificity for terminating ribosomes at termination codons is yet available. Additionally, the mechanisms and factors responsible for the recognition and dissociation of stalled ribosomes remain to be fully elucidated.

The importance of the NMD components is highlighted by the fact that they not only impact on the expression of PTC-containing transcripts, but also play an important role in modulating the expression levels of a large number of genes (Ottens and Gehring, 2016). Moreover, under specific stress conditions, NMD components are important players in regulating the abundance of functional mRNAs. An example of this is the regulation of histone transcripts by Upf1 in response to repression of DNA synthesis in human cells (Mullen and Marzluff, 2008).

In addition to NMD, two other mRNA surveillance pathways have also been discovered: non-stop decay (NSD) and No-Go decay (NGD). Like NMD, these both monitor mRNAs for translational errors to prevent the production of aberrant proteins. mRNAs that lack an in-frame termination codon or exhibit stop codon read-through, leads to the ribosome translating the poly(A) tail and stalling at the 3’ end (Jamar, Kritsiligkou and Grant, 2017,

Krebs, Goldstein and Kilpatrick, 2017). Premature transcriptional termination and polyadenylation is the main source of NSD substrates (Krebs, Goldstein and Kilpatrick, 2017).

NSD substrates are targeted by a set of factors called the Super killer (Ski) proteins (Krebs, Goldstein and Kilpatrick, 2017). The ribosome is released from the mRNA by the action of Ski7 (Krebs, Goldstein and Kilpatrick, 2017). Ski7 has a GTPase domain similar to eRF3 and probably binds to the ribosome in the A site to stimulate release (Krebs, Goldstein and Kilpatrick, 2017). Ski7 promotes the subsequent recruitment of Ski complex proteins and the exosome, leading to 3'-5' decay of the NSD substrates (Krebs, Goldstein and Kilpatrick, 2017). The Ski complex is an evolutionarily conserved complex which consists of three proteins; this complex is functionally and physically associated with the exosome (Krebs, Goldstein and Kilpatrick, 2017). The three proteins that embody the Ski complex are the DExH RNA helicase, Ski2, a tricopeptide repeat protein, Ski3, and WD repeat protein, Ski8 (Jamar, Kritsiligkou and Grant, 2017). Moreover, in the absence of Ski7 the decay of NSD substrates can proceed by decapping and 5'-3' decay (Krebs, Goldstein and Kilpatrick, 2017). NSD substrate vulnerability to decapping could be due to the pioneer ribosome displacing PABPs as it penetrates the poly(A) tail (Krebs, Goldstein and Kilpatrick, 2017). Rrp44 also known as Dis3 is the catalytic subunit of the exosome which promotes both endonucleolytic and exonucleolytic digestion of NSD substrates (Shoemaker and Green, 2012).

mRNAs can contain a range of potential stall-inducing characteristics such as rare codons, pseudoknots, GC-rich sequences, damaged RNA bases or strong secondary structures which can cause translating ribosomes to stall known NGD (Shoemaker and Green, 2012). NGD is

the least understood of the decay pathways (Krebs, Goldstein and Kilpatrick, 2017). NGD substrates are targeted by the recruitment of two proteins, Dom34 and Hbs1, which are homologous to eRF1 and eRF3, respectively (Saito, Hosoda and Hoshino, 2013). Therefore, Hbs1 is closely related to Ski7 and it is thought that it can function in both NSD and NGD (Jamar, Kritsiligkou and Grant, 2017). The Dom34–Hbs1 complex binds to the ribosome A site and promotes the dissociation of the stalled ribosomes (Jamar, Kritsiligkou and Grant, 2017). NGD substrate decay is initiated by an endonuclease cleavage, it was suggested that Dom34 may be the active endonuclease involved in initiating decay, as one of its domains is nuclease like (Krebs, Goldstein and Kilpatrick, 2017). Subsequently, the 5' and 3' fragments are digested by the exosome and Xrn1, respectively (Krebs, Goldstein and Kilpatrick, 2017).

Endonucleolytic cleavage has been implicated in all three NSD, NGD and NMD surveillance pathways. However, the factors responsible for the cleavage of NSD and NGD substrates are incompletely defined with the exception of Smg6 which has a defined role in the cleavage of NMD substrates (Shoemaker and Green, 2012). The endonucleolytic cleavage is a potent mechanism for triggering mRNA decay which circumvents the need for the normal initial steps in mRNA decay, decapping and deadenylation, which are typically rate limiting and tightly regulated (Shoemaker and Green, 2012). mRNA cleavage is likely to be an irreversible process (Shoemaker and Green, 2012). More studies are needed to uncover the role of the endonuclease cleavage involved in NSD, NGD and NMD pathways.

1.5 mRNA 3' end tagging

The first reports of the addition of a short run of non-templated nucleotides to the 3' end of cytoplasmic RNA molecules (termed 3' tagging) were for small noncoding RNAs and their

degradation products in both animal and plant systems, where it was shown to be associated with degradation, maturation and the modulation of function (Shen, 2004). In prokaryotes, mRNA degradation is initiated by the addition of oligo (A) to the mRNA 3' end and subsequent binding of Hfq protein, a homologue of the eukaryotic Sm-like proteins (Valentin-Hansen, Eriksen and Udesen, 2004). The human H2a and H3.3 histone encoding transcripts were the first mRNAs reported to be oligouridylated (Mullen and Marzluff, 2008). This was shown to involve Upf1, which is recruited by the stem-loop binding protein (SLBP) in response to DNA synthesis being blocked. Upf1 recruitment promotes 3' tagging of the histone transcript which in turn leads to their rapid degradation (Mullen and Marzluff, 2008). Human histone transcripts are unusual in that they are not polyadenylated but the SLBP functionally replaces poly(A) binding protein (Mullen and Marzluff, 2008).

Most mRNA uridylation events reported to date involve the addition of just one or two uridine monophosphate residues. It was shown that mRNA monouridylation is sufficient to promote decapping in a cell-free system; this stimulatory effect increased with longer oligo(U) tails, reaching a plateau between five and ten nucleotides (Song and Kiledjian, 2007, Norbury, 2013). It remains to be determined whether increasing oligo(U) tail length similarly increases decapping efficiency *in vivo* (Norbury, 2013).

Cytoplasmic deadenylation generally triggers the removal of the 5' cap and exonucleolytic degradation of the residual body of the mRNA. Shortening of the poly(A) tail prevents PABP binding and favours recruitment of the Lsm-Pat1 complex, which preferentially binds short terminal oligo(A) and oligo(U) regions and stimulates decapping (Norbury, 2013). Following decapping, Xrn1 degrades the accessible 5' end of the mRNA whilst the 3' end is degraded by the exosome (Norbury, 2013).

mRNA decapping is generally preceded by deadenylation, however this concept has been challenged by observation into the fission yeast *S. pombe*, where the poly(A) tail length of decapped *act1* mRNA was similar to that of capped transcript (Rissland and Norbury, 2009). Similar to decapping in *S. pombe*, uridylation does not require prior deadenylation; loss of tagging in *S. pombe* resulted in mRNA stabilisation, which suggested the involvement of tagging in mRNA degradation (Norbury, 2013). Similar observations were made in *A. nidulans* where it was shown that prior deadenylation is also not required for either decapping or tagging in the presence of a PTC (Figure 1.2) (Morozov et al., 2012).

These findings are consistent with observations in *A. nidulans*, including Upf1 regulated mRNA 3' tagging of polyadenylated transcripts, which is mediated by CutA and CutB enzymes (Figure 1.2) (Morozov et al., 2012). It was demonstrated that disruption of either CutA or CutB led to a dramatic reduction in mRNA 3' tagging and a significantly increased proportion of PTC-containing transcripts associated with ribosomes in *A. nidulans* (Morozov et al., 2012). No mRNA tagging was observed when both CutA and CutB were disrupted (Morozov et al., 2012). Additionally, in a Δ*upf1* mutant strain, 3' tagging of short poly(A) tails was reduced but not completely lost (Morozov et al., 2012). Regarding these observations, what remains unclear are the links between mRNA 3' tagging and the factors mediating mRNA degradation in both the regulation of functional transcripts and the elimination of deadenylated or aberrant transcripts.

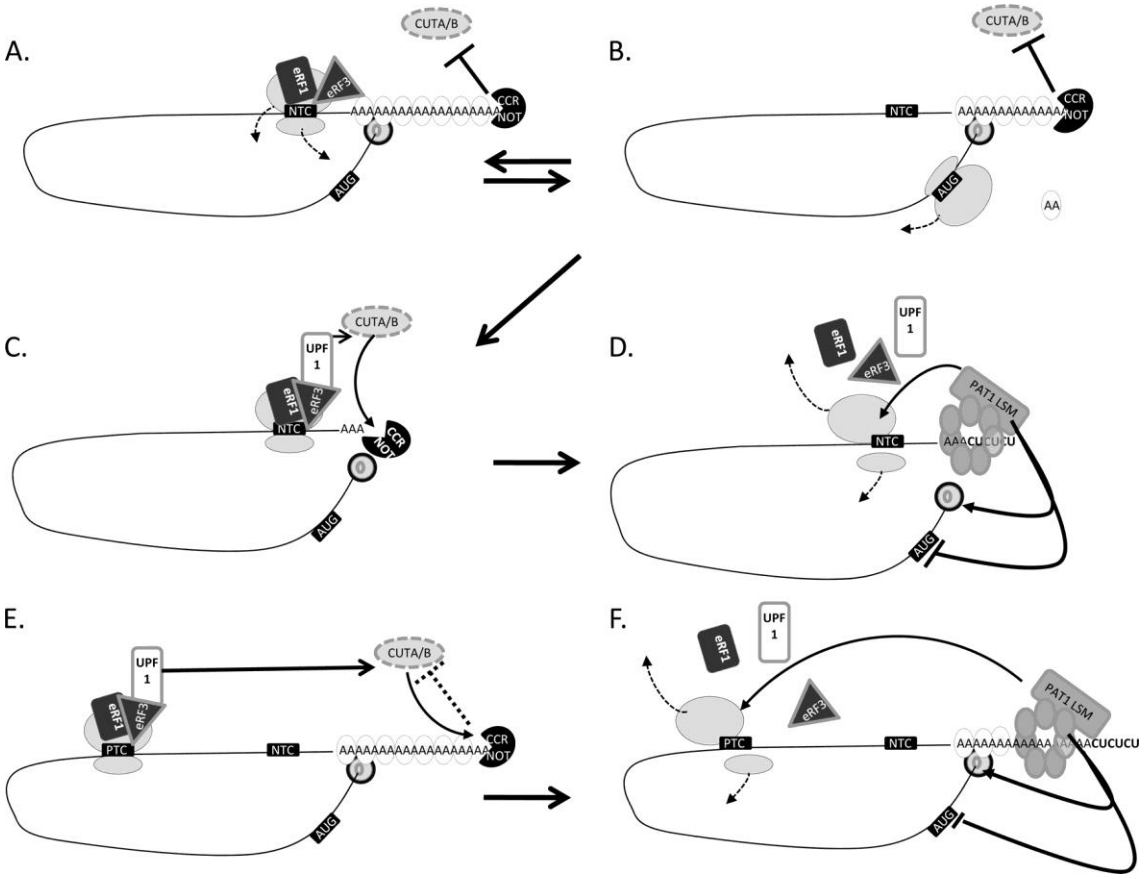

Figure 1.5 Translational termination of deadenylated transcripts promotes an NMD-like response. During translation the cap binding complex at the mRNA 5'–end associates with Pab1 associated with the 3' poly(A) tail through an interaction mediated by eIF4G. This interaction is important for efficient translational initiation and ribosome recycling. Recruitment of eRF3 by eRF1 to terminating ribosome at NTC leads to interaction with Pab1 which is required for efficient ribosome dissociation and initiate new round of translation (A and B). Poly(A) tail degradation to approximately 15 adenine residues by Ccr4-Caf1-Not complex in *A. nidulans* is proposed to cause Pab1 dissociation resulting in eRF3 recruiting Upf1, triggering an NMD like response. In addition, Pab1 binding to long poly(A) tails prevents mRNA 3' oligouridylation (Lim et al., 2014) by CutA and CutB in *A. nidulans* where tagging generally occurs in transcripts with short poly(A) tails (Morozov et al., 2012) (C and D). During NMD terminating ribosome at PTC recruits Upf1 through its interaction with eRF3, this triggers mRNA 3' tagging which is known to help recruit the Lsm-Pat1 complex which is poly(A) independent (E and F). Although 3' tagging is not required for NMD-induced transcript degradation, its loss leads to decapping becoming dependent on deadenylation. Figure taken from Morozov et al. (2012).

1.6 *A. nidulans* as an experimental system

The ascomycete, *A. nidulans* is a filamentous fungus which was originally used and established as a model genetic system by Pontecorvo et al. (1953). In the late 1960s, John Clutterbuck, isolated a strain of *A. nidulans* that had a mutation he called *velvet*. The velvet allele, *veA1*, which is recessive, results in colonies with even conidiation, which resulted in it being adopted as the standard wild-type strain. Colonies will not overgrow each other, so distinct isolates can be grown in close proximity facilitating the use of simple growth tests for phenotypic analysis. The organism can grow as either a haploid or a diploid, so mutations can be easily isolated in the haploid phase but characterised by cis-complementation tests. It is homothallic, so theoretically any strain can be crossed to any other. Finally, *A. nidulans* has proven to be a remarkably useful model for higher eukaryotes, with many of its genes having close homologues in animal and plant systems (Hu, Qin and Liu, 2018).

S. cerevisiae has been used extensively as the model of choice for studies in eukaryotic mRNA degradation and translation. However, it lacks cytoplasmic mRNA oligouridylation, mRNA splicing is rare and mRNA decay in this organism principally occurs through the deadenylation-dependent decapping pathways. In all these respects, *A. nidulans* represents a good alternative. Additionally, due to ease of its manipulation and the wealth of literature available including recent observations of mRNA 3' tagging supports its use. In particular it has the potential for providing a fuller understanding of the link between the NMD factors and 3' tagging in mRNA degradation of both normal and aberrant transcripts.

1.7 Project aims

Recent unpublished work in *A. nidulans* indicates that addition of a short run of pyrimidine nucleotides to the 3' end of histone transcript, mediated by CutA and CutB, is associated the response to disruption of DNA synthesis. This response is in part regulated by the NMD factors and associated with reduced transcript levels. This is consistent with a model in which the addition of a 3' tag increases the affinity of mRNA molecules for recruitment of the Lsm1-7 complex, which, in conjugation with other proteins including Pat1, Dhh1, Scd6, Ecd3, Dcp1, Dcp2, Ski3 and Rrp44, stimulates efficient mRNA decay, ribosome recycling and translational repression (Morozov et al., 2012). The aim of this thesis was to test this model by investigating the role of these different factors in regulating normal and abnormal transcripts in order to determine how their roles are linked to the 3' end tagging.

Chapter 2: Materials and Methods

2.1 Buffers and solutions for general molecular biology

Appendix 1a

2.2 *A. nidulans* strains, oligonucleotides and maintenance

2.2.1 Oligonucleotides

All synthetic oligonucleotides used in this project were purchased from Sigma Aldrich UK. These are listed in Table 2.1.1.

Table 2.1.1 Primer sequences used in mutant validation

Oligonucleotide	Primer sequence (5' – 3')
Upf1 F1	ACCGGGAAGTCGTAACGA
Upf1 F2	CGAGTTGCTTTCCGGTTGCT
Upf1 F3	CGAGCTTGACGACGCTGAAA
Upf1 R3	GTGGCTGCAGGCAGATCAGA
Upf1 R4	TCGGATCATCGTTGCCGTAA
Upf1 C134S F	GAATGCTATAACTCTGGCACCAAGAATGTC
Upf1 C134S R	CTTGGTGCCAGAGTTATAGCATTCTAG
Upf1 K451Q F	CCCGGTACTGGAGAGACAGTCACTTCAGC
Upf1 K451Q R	AAGTGACTGTCTCTCCAGTACCGGGAGGA
Upf1 RR811AA F	CTTGAGTGATCCTGCCGCTCTAAATGTTGCGCTT
Upf1 RR811AA R	CGCAACATTTAGAGCGGCAGGATCACTCAAGAAAC
Upf1 Fusion F1	CCATGCCATCTTCCAAGGACA

Upf1 Fusion F2	GCCCTCTAACGTTGCCGTTG
Upf1 Fusion R1	CCGGGAGGACCTTGAATCAG
Upf1 Fusion R2	TTTCTCGCGACCCTGGAAAG
Upf1 intF1	ACGGAGGCCAGGTTTTAGTT
Upf1intR1	ACACTCGGGTTCAGCAGACT
10400 CM1For	TGTGCCGTGGCTGAAACGGC
10400 CM1 Rev	GCCGTTTCAGCCACGGCACA
10400 CM3 For	GTTACCAACGCCCGTACTAC
10400 CM3 Rev	TAGTACGGGCGTTGGTAACT
AN10400_F1	AGGAGGGTGCGAAAGAAGTT
AN10400_F2	AAATCCTGGACGCCCGATCT
AN10400_R3	CGGGACGAGTCAGGAGGTGT
AN10400_R4	ACCAGCGTACCACCCAGATA
AN10400_IntF	GAATGGAGACGAGTCGAAGG
AN10400_IntR	GAAGTCCGCAACTGATGGAT
ANID 00505 F (8F)	ACATAGTCGCCGAGGAACAC
ANID 00505 R (8R)	CCTGAGTTAGGCCTGGAGGT
Int.Fwd_DCP1	CGATCAACAGAATCGAAGCA
Int.Rev_DCP1	AAGACCCAAAGCCCGTAAAT
Dcp2_Int_R	AGGATCGTGATTGGTGAAGC
Dcp2_Int_F	AGTGGAACTGTCGGCTCATC
LSM5 intF	AGTCTCGCATTGGAATCGTC
LSM5 intR	AGGAGGATTTTTGGCAGCTT

Dhh1 intF	TGATGCAAATCCAGATCCAA
Dhh1 intR	GTTTTGCCTGTGCCATTCTT
RRP44_Int_R1	GCCAAAGAGGAAAGTGTGA
RRP44_Int_R2	GGCGTCATTTCCCACAGT
LSM1 intF	ACGAGATGGGAGAAAGCTGA
LSM1 intR	GCCGAGCTCTTGTAGCTTGT
CutB seq For	AATGCCGCCAACTCTACATC
CutB_seq_Rev	CGAGCATGTGCAATTGTTTC
cutA_Int_F0	CACAATACGAAATCTGGGTAATACG
cutA_int_R2	ACAAGGTTCTGTTGGGCAAG
Pat1 intF	CATCCCTTTATTGCGTTGCT
Pat1 int R	GCGTATGGGTAAGCACCAAGT
xrn1 Int F2	GTCTCGATGCCGATCTGATT
xrn1 Int R2	TGGAGGTTTGGCAGATTAGG
Int_scd6 forward	ATTTCCGTTGCCTTCCTTCT
Int_scd6 reverse	CTTGAGGTGGTTGTTGCAGA
Int_nkuA forward	CGCCCAACGACCCTGACG
Int_nkuA reverse	TCCCCGCCGAATTTGTATGC
Int.Fwd_Af.pyrG	ACATCCTCACCGATTTCAGC
Int.Rev_Af.pyrG	TCCCAGCCTTCTTTCTGGTA
pyrG 3' F	CGCATCAGTGCCTCCTCTCAGAC
cid2_R4	AGGTTAGGGAGGCAGAGAGG
eRF3 end R4	GCCTCCTCTTACCTCGACCT

Table 2.2.2 *A. nidulans* strains used in this study

Genotype	Stock Number	Source
Wild-Type (WT): *veA+*	1048	This laboratory
AfpyrG pyroA$_4$ ΔnkuA (*pyrG89*)	505	This laboratory
uaZ$_{14}$ pantoB$_{100}$	230	This laboratory
Δupf1 pyroA$_4$ ΔnkuA (*pyrG89*)	670	This laboratory
Δupf1 uaZ$_{14}$ pantoB$_{100}$	1229	This work
nmdA1 pantoB$_{100}$	196	This laboratory
Δupf3 pyroA$_4$ ΔnkuA	849	This laboratory
Δupf3 uaZ$_{14}$ pyroA$_4$ ΔnkuA	988	This work
Δsmg6 pyroA$_4$ ΔnkuA	770	This laboratory
ΔcutA ΔcutB ΔnkuA	1024	This laboratory
Δlsm1 pyroA$_4$ ΔnkuA	880	This laboratory
Δlsm5 pyroA$_4$	946	This laboratory
Δlsm8 hxA$_5$ pantoB$_{100}$	906	This laboratory
Δpat1 uaZ$_{14}$ pantoB$_{100}$	948	This laboratory
Δrrp44 pyroA$_4$ ΔnkuA	1033	This laboratory
Δdhh1 pyroA$_4$ ΔnkuA	779	This laboratory
Δxrn1 pantoB$_{100}$ pyroA$_4$ ΔnkuA	973	This laboratory
Δski3	974	This laboratory
Δdcp1 pantoB$_{100}$ pyroA$_4$ ΔnkuA	972	This laboratory
Δdcp2 hxA$_5$ pantoB$_{100}$ pyroA$_4$ yA$_2$	740	This laboratory
Δdcp2 uaZ$_{14}$ pantoB$_{100}$	947	This laboratory

Δ*scd6 uaZ*$_{14}$ *pantoB*$_{100}$ *pyroA*$_4$	969	This laboratory
Δ*edc3 uaZ*$_{14}$ *pyroA*$_4$ Δ*nkuA*	835	This laboratory
Δ*ccr4 pyroA*$_4$ *pabaB*$_{22}$ *riboB*$_2$	655	This laboratory
Δ*caf1 pyroA*$_4$	955	This laboratory
Δ*upf1* Δ*lsm1 pantoB*$_{100}$	966	This laboratory
Δ*upf1* Δ*lsm5*	1196	This work
Δ*upf1* Δ*pat1 uaZ*$_{14}$ *pantoB*$_{100}$	965	This laboratory
Δ*upf1* Δ*dhh1 pyroA*$_4$	1124	This work
nmdA1 Δ*lsm1 pantoB*$_{100}$	967	This laboratory
Δ*cutA* Δ*cutB* Δ*lsm1 pyroA*$_4$	831	This laboratory
Δ*lsm5* Δ*lsm8*	1142	This work
Δ*dcp2* Δ*smg6 uaZ*$_{14}$ *pantoB*$_{100}$ *pyroA*$_4$	786	This laboratory
Δ*dcp2* Δ*rrp44 uaZ*$_{14}$ *pyroA*$_4$	1031	This work
upf1^{C134S} *pantoB*$_{100}$	1333	This work
upf1^{K451Q} *pyroA*$_4$	1334	This work
upf1^{RR811AA} *pyroA*$_4$	1354	This work
upf1^{C134S} *uaZ*$_{14}$ *pyroA*$_4$	1330	This work
upf1^{K451Q} *uaZ*$_{14}$ *pyroA*$_4$	1331	This work
upf1^{RR811AA} *uaZ*$_{14}$	1332	This work
smg6$^{D13A\ D251A}$	1362	This work
smg6$^{D13A\ D251A}$ *uaZ*$_{14}$	1363	This work
Δ*dcp2 smg6*$^{D13A\ D251A}$	1359	This work
Δ*dcp2 smg6*$^{D13A\ D251A}$ *uaZ*$_{14}$	1360	This work

cutA Δ*ct*	728	This laboratory
CutB:S-tag: *AfpyrG pyroA*$_4$ Δ*nkuA* (*pyrG89*)	1153	This work
CutA:S-tag:*AfpyrGpabaB*$_{22}$ *riboB*$_2$ Δ*nkuA* (*pyrG89*)	1217	This laboratory
CutA:GFP: *AfpyrG pyroA*$_4$	1241	This laboratory
CutB:S-tag CutA:GFP	1298	This work
Δ*lsm1 CutB:S-tag*: *AfpyrG pantoB*$_{100}$ (*pyrG89*)	1200	This work
eRF3:S-tag: *AfpyrG* Δ*nkuA* (*pyrG89*)	1156	This work
Δ*lsm1 eRF3:S-tag*: *AfpyrG pantoB*$_{100}$ (*pyrG89*)	1197	This work
Δ*cutA*Δ*cutB eRF3:S-tag: AfpyrG pantoB*$_{100}$ (*pyrG89*)	1224	This work

2.3 *A. nidulans* solutions and media

Appendix 1b

2.4 Maintenance and growth of *A. nidulans* strains

A. nidulans stock cultures were kept as conidia using premade glycerol stocks from the Protect Microorganism Preservation System (Technical Service Consultant Ltd) at - 80 ˚C. For the preparation of conidial suspensions to inoculate liquid cultures, strains were grown on minimal media (MM) (Appendix 1b) containing 3% agar (w/v) with appropriate supplements for 3-4 days at 37 ˚C. Conidial were scrapped from the plates and resuspended in 10 ml 0.01% Tween, and grown in 200 ml MM in 1 litre flask. Liquid cultures were incubated at 30 ˚C in an orbital incubator at 180 rpm for 16 hours. Mycelia were harvested by filtration through Miracloth (Calbiochem Corp.), washed with cold water, dried by blotting with paper towel and frozen in liquid nitrogen.

2.5 *A. nidulans* genetic techniques

2.5.1 Crosses

For sexual crosses the procedure is as described by Todd et al. (2007). The parental strains, with complimentary auxotrophic and preferably colour markers, were inoculated alternately on a fully supplemented agar plate. After 3 days of incubation at 37 ˚C, the junction of growth between the two parental strains was transferred to unsupplemented MM agar plate with $NaNO_3$ as nitrogen source. The mycelia were inoculated under the surface of a thick layer of agar (~50 ml/ dish). The plates were incubated for 14 days or more at 37 ˚C. Mature cleistothecia were picked and rolled on a 1% MM plate to clean it from cell debris. The cleistothecia were then individually squashed in a vial containing 2 ml of sterile water and vortex vigorously. A loop full of ascospore suspension was then inoculated onto complete medium (CM) (Appendix 1b) and incubated at 37 ˚C for 2 days. Ascospore suspensions that appeared to have the re-assortment of markers were plated out in dilution series onto fully supplemented MM. After three days, 23 progenies were randomly picked and inoculated onto a master plate, which also containing both parental strains and a wild-type control. The master plates were incubated at 37 ˚C for three days before replica plating onto test media.

2.5.2 Plate tests

Progeny were grown on differently supplemented media (Minimal media with 1% (w/v) agar) to check the growth requirements and morphology. Plates were scored after two days of incubation at 37 ˚C.

2.6 Generating *A. nidulans* mutants

The protocol for transformation in this study was based on the method developed by Dr Joan Tilburn (Tilburn et al., 1983), and modification made by Dr Berl R.Oakley (Szewczyk et al., 2007). All the glassware was acid washed to remove any traces of detergent which could rupture the protoplasts (Magdalena Mos 2010).

2.6.1 Generation of *A. nidulans* protoplasts

10^8 of fresh conidia were inoculated into 25 ml fully supplemented CM and grown overnight at 30 °C with agitation at 180 rpm. After 14 hours growth, the culture was harvested using a sterile funnel lined with miracloth (Calbiochem). The cells were transferred to a new falcon tube containing 8 ml of CM, 8 ml of 2 x protoplasting solution (1.1 M KCl, 0.1 M citric acid pH 5.8, and 2 g of VinoTaste Pro lysing enzyme (Novozymes). The cells were incubated with gentle shaking at 30 °C for 2 hours. Then the protoplasts were filtered through a sterile sintered glass funnel containing glass wool and washed with an equal volume of protoplast wash solution (1 M sorbitol, 10 mM Tris-HCl, pH 7.5). The mixture was centrifuge at 3,100 g (Megafuge 1.0R, Heraeus) for 12 minutes at 4 °C. The supernatant was discarded and the pellet re-suspended with 1 ml protoplast wash solution and transferred to a 1.5 ml tube. The mixture was centrifuge at 6,500 g for 2 minutes and the washing step was repeated for another 2 times. The pellet was re-suspended in 500 µl transformation solution (1 M sorbitol, 10 mM $CaCl_2$, 10 mM Tris-HCl, pH 7.5). Protoplasts were counted and diluted to 1 x 10^8 for transformation.

2.6.2 Transformation of *A. nidulans* strain

Up to 50 µl DNA (~60 ng per µl) was added to 150 µl protoplasts and the mixture was transferred to a plastic universal containing 50 µl PEG solution (60% Polyethylene glycol 6000 10 mM $CaCl_2$, 20 mM Tris-HCl, pH 7.5) and incubated on ice for 20 minutes. 1 ml PEG solution was added and the mixture was incubated at room temperature for 5 minutes. Then, 5 ml transformation solution was added and the mixture was incubated on ice. Then, 15 ml of regeneration media (MM with 1 M sucrose, 1% glucose) were added into the mixture and layered on top of regeneration media plates. Plates were incubated at 30 °C overnight and transferred to 37 °C for additional two days until transformants had appeared.

2.7 *Escherichia coli* strains, growth, maintenance and manipulation

The *E. coli* strain used in this project was DH5-alphaTM (*DH5α*) (Thermo).

2.7.1 *Escherichia coli* growth and maintenance

E. coli was grown on Luria-Bertani (LB) agar, or in LB liquid media in orbital incubator (200 rpm), at 37 ˚C for all standard protocols. Long term storage of *E.coli* strains was achieved using a Protect Microorganism Preservation System (Technical Service Consultant Ltd) and stored at - 80 ˚C.

2.7.2 Antibiotics and plasmids

PCR products were cloned into pGEMT-EasyTM (Promega) which has an ampicillin resistance gene. For selection and maintainence of plasmids within the *E. coli*, 50 µg/ml ampicillin (amp) was added to the solid or broth media.

2.7.3 Plasmid DNA isolation

Small scale plasmid preps were performed using the GeneJET Plasmid Miniprep Kit (Thermo Scientific) according to the manufacturer's instructions.

2.7.4 Restriction digests

Restriction digests of plasmids were performed with standard restriction enzymes (NEB) according to the manufacturer's instructions. Plasmid DNA was normally digested for at least 120 minutes at 37 ˚C.

2.7.5 Ligation of DNA fragments

All DNA fragments were ligated using the T4 DNA Ligase (Promega) according to the manufacturer's instructions.

2.7.6 DNA purification

DNA fragments from agarose gels were extracted using QIAquick Gel Extraction Kit (Qiagen) according to the manufacturer's instructions.

2.8 Molecular techniques for the manipulation of DNA

2.8.1 Genomic DNA extraction

Genomic DNA extraction was carried out from strains grown in SC with 1% (w/v) agar. Hyphae and conidia were transferred to a sterile 2.0 ml microcentrifuge tube containing glass beads (180 µm) and 1 ml of extraction buffer (100 mM Tris pH 8.0, 1.4 M NaCl, 10 mM EDTA, 2% CTAB). The mixture was homogenised using a PowerLyzer® 24 Bench Top Bead-Based Homogeniser (MO-Bio) at 3,000 rpm for 90 seconds. The suspension was incubated at

65 ˚C for 10 minutes before centrifugation for 2 minutes. 700 µl of supernatant was transferred to a new 2 ml tube containing 4 µl RNase (100mg/ml) and the tube was incubated at 37 ˚C for 30 minutes. An equal volume of phenol: chloroform: Isoamyl alcohol (v/v, 25:1) was added. The mixture was vortexed and centrifugated at maximum speed for 2 minutes. 600 µl of the aqueous phase were transferred to a new 2 ml tube and the chloroform extraction was repeated. An equal volume of isopropanol was added to the aqueous phase and the mixture was incubated on ice for 5 minutes. Then, the mixture was spun at maximum speed for 5 minutes and the pallet was washed twice with 70% ethanol. Pellets were air dried on bench for 5 minutes before dissolving it with 150 µl nuclease-free water. The genomic DNA was used directly for PCR or stored at - 20 ˚C.

2.8.2 Nucleic acid quantification

The quantity of DNA and RNA was measured with NanoDrop-1000 (Thermo Scientific) using a 1 µl sample per measurement.

2.8.3 Agarose gel electrophoresis of DNA and RNA

Agarose gel electrophoresis of DNA was performed in Fisher brand horizontal electrophoresis gel tanks (Fisher Scientific) using agarose (Bioline) at a concentration between 1% to 2% (w/v) in 1X TAE (0.4 M Tris-acetate, 1 mM EDTA) buffer. Gels were run at 100 V until the bromophenol dye reached ¾ of the gel length. DNA was stained by the addition of 2 µl Midori Green (NIPPON Genetics EUROPE) per 100 ml agarose gel for visualization under the UV light using the U-Genius (Syngene Imager). Hyperladder 1 or Hyperladder 1kb (Bioline) were used as a molecular weight marker.

2.8.4 Polymerase Chain Reaction (PCR) from genomic and plasmid DNA

2.8.4.1 Standard PCR

PCR analysis was carried out using:

2X BioMixTM Red (Bioline)	5 µl
Genomic DNA (0.1 µg)	1 µl
Forward primer (10 µM)	0.1 µl
Reverse primer (10 µM)	0.1 µl
Nuclease-free water	3.8 µl

All the forward and reverse primers used in this experiment are listed in Table 2.1.1 The standard PCR program was as follows:

Pre-denaturation	95 °C, 3 minutes
30 cycles Denaturation	95 °C, 30 seconds
Primers annealing	60 °C, 30 seconds
Extension	72 °C, 1 minute
Final Extension	72 °C, 5 minutes

2.8.4.2 Fusion PCR

PCR amplification of DNA fragments to be fused together was performed using the Phusion High-Fidelity DNA Polymerases (Thermo Scientific). The two PCR fragments to be fused were synthesised with an overlapping region of approximately 25 bp by inclusion of this sequence at the 5’ ends of the relevant primers. The fragments were amplified individually using two different PCR reactions. Where appropriate the oligonucleotides were designed to harbour specific mutations. Annealing temperature and extension times varied with primers and

product sizes. PCR products of the correct size were gel extracted and then combined as the DNA substrates for the second Fusion PCR reaction. The reaction mixture for fusion PCR as below:

2 flanking DNA fragments (~100ng)	1 µl
DNA-TAG fragment (200ng)	1 µl
Primer F1 (20 mM)	1.25 µl
Primer R3 (20 mM)	1.25 µl
dNTPs (10 mM)	1 µl
Phusion High-Fidelity DNA Polymerases	1 µl
Nuclease-free water	43.5 µl

The fusion PCR was performed using the program as follow:

Pre-denaturation	98 °C, 30 seconds
35 cycles Denaturation	98 °C, 10 seconds
Primers annealing	62 °C, 30 seconds
Extension	72 °C, 3 minutes
Final Extension	72 °C, 5 minutes

2.8.4.3 cRT-PCR and RNA-Seq

20 µg of total RNA was treated with 25 U of DNase I (Thermo Fisher) and 40 U of RNasin (invitrogen) in 50 µl reaction for 30 minutes at 37 °C. The RNA was then purified with equal volume of phenol/chloroform and precipitated with ethanol. For decapped transcripts (to analyse the decapped mRNAs only), 5 µg of DNA-free RNA was treated by rAPid Alkaline Phosphatase (Roche, cat. No 04-898-133-001) for 30 minutes at 37 °C followed by

phenol/chlorophorm purification and precipitated with ethanol. The remaining DNase I treated RNA (dephosphorylated) was incubated with 2.5 U of TAP (Epicentre Biotechnologies) and 20 U of RNasin in 20 µl, containing 1-fold TAP buffer (supplied) for 45 minutes at 37 °C. RNA was purified as above and resuspended in 16 µl of DEPC-H_2O. Circularisation of the remaining decapped RNA was performed in 200 µl, containing 10 U of T4 RNA ligase 1 (Thermo Fisher, EL0021) and 20 U of RNasin for 16 hours at 16 °C. The samples were then extracted and purified with ethanol as above and were suspended in 12 µl of DEPC-H_2O.

Then 5 µl of the RNA was used to perform reverse transcription (cDNA) using SuperscriptII (Invitrogen). The cDNA synthesis was performed as followed: RNA was combined with 1.5 µl of the mixture 1 (2 volumes of random hexamer primers (10 µM): 1 volume of dNTPs (25 mM each): 3 volumes H_2O) and was incubated for 5 minutes at 65 °C followed by incubation on ice for 5 minutes. Then 3 µl of mixture 2 (2 volumes of the 5X First strand buffer: 1 volume of the 100 mM DTT) was added to the RNA:primer:dNTP solution and incubated for 2 minutes at room temperature followed by addition of 0.5 µl Reverse Transcriptase and incubated for 90 minutes at 42 °C. 1 µl of the cDNA was diluted 10-fold in 25 µl PCR reaction using Q5 Hot Start High-Fidelity 2X Master Mix (New England Biolabs) and primers tailed with universal sequences to amplify up the joined 5’ and 3’ UTRs. A total of 25 cycles were performed followed by the analysis on 2% agarose gel. The resulted products with the correct size were purified from the gel and sequenced by Pacific Biosciences, University of Liverpool.

2.9 Molecular techniques for the manipulation of RNA

To minimise degradation of RNA by ribonucleases, all the consumables were autoclaved twice. Disposable gloves were worn at all times during the preparation of materials and solutions used, as well as during the extraction and handling of RNA. To prepare the solutions, diethyl pyrocarbonate (DEPC) was added to distilled water and autoclaved.

2.9.1 RNA preparation from *A. nidulans* - Uric acid treatment

Strains were grown in 200 ml minimal medium with nitrate as nitrogen source and incubated overnight at 30 ˚C with agitation at 180 rpm. After 16 hours growth 0.1mg/ml uric acid was added to the cells for 2 hours prior to harvesting. This step was carried out to induce the expression of *uaZ* gene. Mycelia were harvested and washed with cold water twice and pressing it between the paper towels before transfer immediately to liquid nitrogen. Then, approximately 0.5 g frozen mycelia were placed in pre-filled VWR® Reinforced bead mill tubes containing 600 µl of lysis buffer (100 mM Tris-Cl pH 8.0, 600 mM sodium chloride, 10 mM EDTA, 5% sodium dodecyl sulphate, SDS) and 600 µl of phenol. The cells were homogenised using a PowerLyzer® 24 Bench Top Bead-Based Homogeniser (MO-Bio) at 4,000 rpm for 90 seconds. Supernatants were phenol:chloroform (1:1) extracted followed by 5 M lithium acetate precipitation. Pellets were then washed with 70% ethanol before dissolving in DEPC-water. RNA concentrations of each sample were determined spectrophotometrically.

2.9.2 RNA preparation from *A. nidulans* - Hydroxyurea treatment

Cells were grown to the logarithmic phase in synthetic complete (SC) medium and incubated overnight at 30 ˚C with agitation at 180 rpm. After 16 hours growth hydroxyurea (1.5 mg

ml^{-1}) was added to the cultures to inhibit DNA synthesis, 20 minutes prior to the first sample being taken. Mycelia were harvested pressing it between the paper towels before transfer immediately to liquid nitrogen. Then, approximately 0.5 g frozen mycelia were placed in pre-filled VWR® Reinforced bead mill tubes containing 600 µl of lysis buffer (100 mM Tris-Cl pH 8.0, 600 mM sodium chloride, 10 mM EDTA, 5% sodium dodecyl sulphate, SDS) and 600 µl of phenol. The cells were homogenised using a PowerLyzer® 24 Bench Top Bead-Based Homogeniser (MO-Bio) at 4,000 rpm for 90 seconds. Supernatants were phenol:chloroform (1:1) extracted followed by 5 M lithium acetate precipitation. Pellets were then washed with 70% ethanol before dissolving in DEPC-water. RNA concentrations of each sample were determined spectrophotometrically.

2.9.3 Northern blotting

2.5 grams of agarose (Bioline) was melted in 206 ml DEPC water. When cooled, 25 ml of 10X MOPS (20mM MOPS, 5 mM sodium acetate, 1mM EDTA) and 14 ml formaldehyde were added to the agarose solution. This was mixed and poured into the gel mould. RNA samples were prepared by adding 10 µl 2X sample buffer (50 µl formamide, 18 µl 37% formaldehyde (~2.2 M), 10 µl 10X MOPS buffer and 3 µl 10X Dye Solution (50% glycerol, 0.3% bromophenol blue). Samples were then denatured at 65 ˚C for 15 minutes and immediately transferred to ice before loading. The gel was submerged in 1X MOPS and the samples were run for 1 hour at 110 V. After electrophoresis, the RNA was transferred from the gel to the Zeta Probe GT (BioRad) blotting membrane in 10X SSC (1.5 M NaCl, 0.15 M Na-Citrate, pH 7.0) overnight. Then, the membrane was rinsed in 2X SSC twice for 10 minutes and air dried. RNA was fixed to the blot by vacuum drying for 45 minutes at 80 ˚C. The membrane was then hybridised at 65 ˚C to DNA probes radiolabelled with ^{32}P – dCTP. Imaging was

conducted using a Molecular Dynamics STORMTM scanner and quantification was done using ImageQuant TL Software (GE Healthcare Life Sciences).

2.9.4 Polysomal analysis

The method was adopted from Morozov et al. (2012) with some modifications. Mycelia from overnight cultures were harvested immediately after 10 minutes treatment with cycloheximide (0.1 mg ml^{-1}) to trap elongating ribosomes (t_0); and where appropriate with Hydroxyurea (1.5 mg ml^{-1}) 10 minutes prior to cycloheximide treatment (t_{20}). Harvested mycelia were washed with 20 mM Tris-HCl, pH 8.0, 140 mM KCl, 1.5 mM $MgCl_2$ and 0.1 mg ml^{-1} cycloheximide; frozen in liquid nitrogen; and stored at − 80 °C. Approximately 0.5 g mycelia was ground in liquid nitrogen with a mortar and pestle, and the powder was resuspended in 1 ml ice-cold RNA lysis buffer (20 mM Tris-HCl, pH 8.0, 140 mM KCl, 1.5 mM $MgCl_2$, 0.1 mg ml^{-1} cycloheximide, 1% Triton X-100, 1 mg ml^{-1} heparin, 0.5 mM DTT and 1 µl RNasin). Cell debris was removed by centrifugation at 4,000 × *g* for 5 minutes at 4 °C. The supernatant was clarified by further centrifugation at 10,000 × *g* for 5 minutes at 4 °C. Aliquot (800 µg) of RNA was layered on 10 ml of 10 to 50% (w/v) sucrose gradient and centrifuged at 37,000 rpm at 4 °C for 170 minutes. The gradient was fractionated with the BioLogic LP system at a flow speed of 0.8 ml min^{-1} (Bio-Rad). The gradient was collected at 0.8 ml/min/tube. 1 ml phenol and 10 µl 10% SDS were added. RNA was precipitated by adding 2 volumes of 100% ethanol, 70 µl 3 M sodium acetate (pH 5.0). The RNA was again precipitated by addition of 10 µl 3 M sodium acetate (pH 5.0) and 2.5 volumes of 100% ethanol. The resulting samples were subjected to Northern analysis.

2.10 Molecular techniques for analysing proteins

2.10.1 Protein isolation

Approximately 0.5 g mycelia was ground in liquid nitrogen with a mortar and pestle, the powder was resuspended in 800 µl lysis buffer (25 mM Tris-HCl, pH 8.0, 150 mM NaCl, 1% Trition-X, 1:100 protease inhibitor cocktail (Sigma, P8215). Depending on the experiment, RNAse or RNase inhibitor were added to the samples; vortexed and shaken on ice for 10 minutes. Cell debris was removed by centrifugation at 4,000 × *g* for 5 minutes at 4 ˚C. 600 µl of supernatant was transferred to a new Eppendorf tube. The supernatant was clarified by further centrifugation at 10,000 × *g* for 5 minutes at 4 ˚C. 500 µl of the supernatant was transferred to a new Eppendorf tube. Cell lysate was used directly for protein quantification and visualisation by Western blot analysis.

2.10.2 Antibodies

Immunogen affinity purified primary goat polyclonal anti-S tag anti-body (Cat. No. ab19321) was obtained from Abcam. GFP (Green Fluorescent Protein) Monoclonal Antibody, Mouse (C163) from Thermo Fisher Scientific (Cat. No. 33-2600). Affinity purified secondary anti-body raised in donkey against goat IgG and conjugated to horseradish peroxidase (HRP): sc-2056 was obtained from Santa Cruz Biotechnology, INC.

2.10.3 Protein analysis of ribosomal fractions

800 µg of RNA was layered on 10 ml of 10 to 50% (w/v) sucrose gradient and centrifuged at 37,000 rpm at 4 °C for 170 minutes. The gradient was fractionated with the BioLogic LP system at a flow speed of 0.8 ml min^{-1} (Bio-Rad). The gradient was collected at 0.8 ml/min/tube. Sodium lauroyl sarcosinate (NLS) and trichloroacetic acid (TCA) were added to

final concentrations of 1% and 20% (v/v), respectively, and the solution was precipitated on ice for 15 minutes. Centrifugation was carried out at maximum speed for 15 minutes at 4 °C and the supernatant was discarded. 1 ml chilled aceton (100%) was added and left at -20 °C overnight. Centrifugation was carried out as described above. Pellets were incubated with 3 µl of 200 mM NaOH on ice for 5 minutes. The pellets were suspended in 30 µl of solubilisation buffer (50 mM Tris-HCl, pH 8.0, 2% (w/v) SDS) with the help of a sonicator bath. Centrifugation was carried out at 13000 rpm for 2 minutes to pellet any remaining insoluble material and the supernatant frozen at -80°C. 12.5 µl of 3x loading buffer (187.5 mM Tris-HCl, pH 6.8, 2% (v/v) SDS, 30% (v/v) glycerol, 300 mM DTT, 0.06% (v/v) bromophenol blue) was added to the samples then heated for 5 minutes in a 98°C heat block. Fractions were separated by SDS-PAGE and analysed by Western blot with indicated antibodies.

2.10.4 Western blot analysis

25 µl of the sample was added to 12.5 µL of 3x SDS Loading buffer (2:1). The sample was boiled for 5 minutes at 98 ˚C on a heat block to fully denature the proteins. The boiled sample was spun at maximum speed on a table top centrifuge (micro-centrifuge 1k15, Sigma) for 1 minute to collect all of the condensation to the sample. The samples were separated in 10% acrylamide hand-cast gels (Appendix 1c) in Mini-PROTEAN® Tetra electrophoresis system (Bio-Rad Laboratories) and transferred onto nitrocellulose blotting membrane (Amersham Protran premium 0.45 µm NC, GE Life Sciences, cat. No. 10600003) in Mini Trans-Blot® Cell (Bio-Rad Laboratories). Membrane was blocked with 5% non-fat dry milk in Tris-buffered saline containing 1:1000 Tween-20 (TBST) for 1 hour at room temperature, incubated with primary antibody (1:5000 dilution) in the same solution

overnight. Membrane was washed 3 times with TBST for 30 minutes in total, then incubated with horseradish peroxidase (HRP) coupled secondary antibody (1:5000 dilution) for 1 hour at room temperature, washed 3 times with TBST for 30 minutes in total. Membrane was developed with ECL substrate (Bio-Rad Laboratories), and visualised by ImageQuant LAS 4000 series (GE healthcare life sciences).

2.10.5 Pull-down assay

Approximately 0.5 g mycelia was ground in liquid nitrogen with a mortar and pestle, the resulting powder was transferred to a 2.2 ml tube containing 700 µl lysis buffer (25 mM Tris-HCl (1M), pH 8.0, 150 mM NaCl (2M), 0.1% (v/v) Tergitol® (NP-40), 1 mM DTT (100mM), 10 µl protease inhibitor); vortexed and agitated on ice for 10 minutes. Cell debris was removed by centrifugation at 4,000 × *g* for 5 minutes at 4 ˚C; then 600 µl of supernatant was transferred to a new 1.5 ml Eppendorf tube. The supernatant was clarified by further centrifugation at 10,000 × *g* for 5 minutes at 4 ˚C; 500 µl of the supernatant was then transferred to a new Eppendorf tube. 500 µL of cell lysate containing 5 µl protease inhibitor was pre-cleared by adding 50 µl of protein A/G agarose beads (Pierce™, cat. No. 20421), incubated at room temperature for 1 hour. 3 µl of immunoprecipitation antibody was added to 40 µL of agarose beads in 500 µl lysis buffer, incubated overnight (O/N) at 4°C. Pre-cleared cell lysate was transferred to agarose beads bound with the antibody, incubated O/N at 4°C. The supernatant incubated O/N (agarose beads: AB: cell lysate) was removed by a brief centrifugation. Washed with 500 µL wash buffer (50 mM Tris-HCl (1M), pH 6.8, 150 mM NaCl (2M), 2 mM EDTA (0.5M), 1 % (v/v) Tergitol® (NP-40), 0.5 % (w/v) sodium deoxycholate, 0.1 % (w/v) 10% SDS) and the protein complex was eluted from the beads.

2.11 Computational analysis

2.11.1 Sequence analysis

PCR Primers and hybridisation probes were designed using Primer3 online tools (http://biotools.umassmed.edu/bioapps/primer3_www.cgi). Geneious software was used for sequence analysis. T-Coffee program was used for multiple alignments of protein sequences using the default parameters (output format: ClustalW, matrix: none, order: aligned). Jalview software was used to look at and edit multiple sequence alignments.

2.11.2 Databases

The Aspergillus genome database (http://www.aspgd.org/)

National Centre for Biotechnology Information (NCBI) database (http://www.ncbi.nlm.nih.gov/)

Conserved domain database (http://www.ncbi.nlm.nih.gov/Structure/cdd/wrpsb.cgi)

2.11.3 Online tools

Basic Local Alignment Search Tool (BLAST) (http://www.ncbi.nlm.nih.gov/)

Protein sequence analysis tools (http://www.expasy.org/)

Chapter 3: The role of NMD factors in *uaZ*$_{14}$ mRNA regulation

Introduction

In mammals, the cap structure of the pre-mRNAs is recognised by cap-binding complex (CBC) (Figure 1.1), which is composed of CBP80 and CBP20 proteins (Choe et al., 2012). It was demonstrated that CBP80/20-bound transcripts undergo a pioneer round of translation, before CBP80/20 is replaced by eIF4E in the cap of most transcripts in the cytoplasm for a steady state translation (Ishigaki et al., 2001). Both CBP80/20 and eIF4E have the ability to recruit the small subunit of the ribosome (40S) to initiate translation in the cytoplasm (Choe et al., 2012). It is believed that NMD occurs only on CBP80/20-bound transcripts which harbour EJCs deposited as a result of splicing (Kim et al., 2009). In human cells, it was found that a large proportion of histone transcripts remain bound to CBP80/20, rather than eIF4E, unlike poly(A)-containing transcripts (Choe et al., 2012). The human histone transcripts contain a stem-loop binding protein (SLBP) that binds to a stem-loop structure at the 3' end instead of poly(A) tail (Choe et al., 2012). A significant portion of CBP80 was detected in polysomal fractions (Kim et al., 2009) and was also highly enriched in the nucleus (Garre et al., 2012). Similar to CBP80 in mammalian cells, yeast cap-binding protein, Cbc1, was also detected in all the polysomal fractions, but was concentrated in the sub-polysomal fractions (Garre et al., 2012) while eIF4E was mainly detected in higher polysomal fractions (Garre et al., 2012). Therefore, it was suggested that Cbc1-bound mRNAs are less efficiently translated than eIF4E-bound transcripts (Garre et al., 2012).

In the filamentous fungus *N. crassa*, it has been shown that the degradation of mRNA through the NMD pathway has at least two branches, one only requires the NMD factors and the other requires EJC and CBC factors in addition to NMD factors (Zhang and Sachs,

2015). However, in *S. cerevisiae*, a number of the EJC and NMD components present in animal systems are absent, and in fission yeast *S. pombe*, while EJC components are present, a role for them in determining mRNA stability via NMD-related pathways was not demonstrated (Zhang and Sachs, 2015). Currently there is no comprehensive understanding of the evolutionary significance of EJC, NMD and CBC factors and their contribution to NMD mechanisms in fungal systems (Zhang and Sachs, 2015).

The genome of *N. crassa* contains homologs of the NMD components Upf1, Upf2, and Upf3, the core EJC components eIF4A3, MAGO, and Y14, and CBC components CBP20 and CBP80 (Zhang and Sachs, 2015). Similarly, the *A. nidulans* homologs for a number of NMD and decay factors have been identified and their role in the regulation of PTC-containing transcripts have also been demonstrated for two of these, NmdA (Upf2) and Upf1 (Morozov et al., 2006; Morozov et al., 2012). In *A. nidulans*, it has been shown that a number of NMD and decay factors fully or partially supress the NMD surveillance complex, however it is still unclear how these factors associate with each other. Moreover, it has been shown that there is a link between mRNA 3' tagging and the NMD factors in *A. nidulans* (Morozov et al., 2012), but again the significance of this modification by the tagging factors CutA and CutB enzymes is unclear.

3.1 The role of Upf3 in *uaZ*$_{14}$ mRNA regulation

Previously it has been demonstrated that disruption of Upf1, Upf2/NmdA and Smg6 lead to full suppression of NMD in *A. nidulans* (Morozov et al., 2012; Morozov and Caddick personal communication). Additionally, these three proteins appear to play a major role in the regulation of histone mRNA in response to HU treatment. Based on work in other organisms

an additional NMD component Upf3 has also been found to be important for NMD-mediated decay. Within the *A. nidulans* genome sequence a Upf3 orthologue, AN0505, has been identified (Figure 3.1.a). *A. nidulans* Upf3 genomic sequence is 55% identical to *Homo sapiens* (AAG60690.1) and 56% identical to *S. cerevisiae* (NP_011586.1) orthologues. Similarly, *A. nidulans* Upf3 amino acid sequence is 28% identical to *H. sapiens* and 25% identical to *S. cerevisiae*.

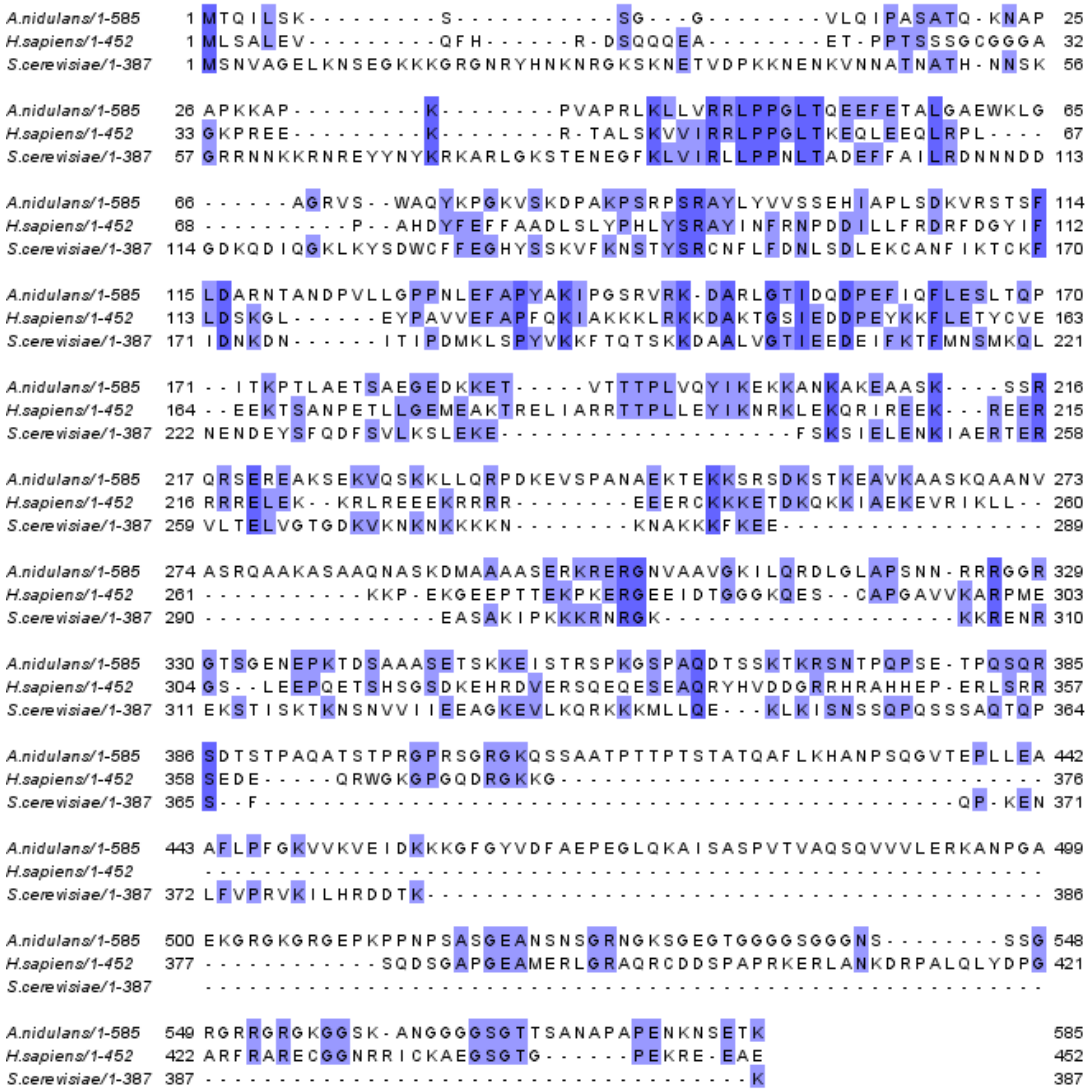

Figure 3.1.a Multiple sequence alignment of Upf3 of *A. nidulans*, *H. sapiens* and *S. cerevisiae*. The amino acid and nucleotide sequence alignments were performed using T-Coffee program. Identical amino acids shaded are highlighted in blue using Jalview software.

The *upf3* loci was deleted using the deletion cassette provided by the fungal genetics stock centre (Caddick, unpublished). Transcript analysis was undertaken to determine if Upf3 was required for NMD in *A. nidulans*, using the structural gene for urate oxidase (*uaZ*). In order to assess the effect of disrupting *upf3*, the Δ*upf3* strain was crossed to introduce the uaZ_{14} allele containing an ochre mutation, terminating the 301-residue *uaZ* protein prematurely after residue 131 in exon 2 (Figure 3.1.b) (Morozov et al., 2006). Strain validation was conducted by growth tests for the uaZ_{14} allele (ability to utilise uric acid as sole nitrogen source) and the Upf3 deletions was confirmed by PCR. The respective strains were then investigated to compare the levels of uaZ^{+} and uaZ_{14} mRNA in both $upf3^{+}$ and Δ*upf3* backgrounds. The uaZ_{14} allele is subject to NMD in the wild-type background due to the presence of the PTC (Morozov et al., 2006). All strains were grown overnight in MM in the presence of nitrate as the sole nitrogen source. Uric acid was added two hours prior to harvesting to induce the transcription of *uaZ* (Morozov et al., 2012). Total RNA was extracted from each strain and quantitative Northern blot analysis was used to monitor transcript levels (Figure 3.2.f).

ggactcgggatttggtgtatggcgtttggcgctgactgggttagactgataagataaagc
tgggaggctgcggccggccatcgcttgcggccatcggaggtggccgatggtctttcatca
ggccatgcgccgcagatttcctgtcccggttctttaaagacggtgatctgcccgtgaagc
tatcgtccgcagctagactgcttagatcttcttcatccgtatcgtctcgtccgttcactaa
gcccatcaccatgtcgaccgttgcagctgcccgctatggtaaggacaatgttcgagtcta
caaggtccacaaggacccgaagactggagttcagaccgtcactgaaatgaccgtctgcgt
cctcctggaaggtgaaatcgatacttcgtaagcgcagcctcccacctctcttagtcctat
agtataaagcgtagaaggacgctaatatagatcacagctacaccaaagccgacaacagcg
tcatcgtcgcaacagactccatcaagaataccatctttattctggccaagcagaaccccg
tcacgcctcccgagctctttggctccattcttggtacccatttcatcaacaagtacaagc
acatccacgtcgcgcataccaacatcatcacgcaccgctggacccgccttaacatcgacg
gcaaaccacactcacactcctttgtccgcgacagcgaggaaacccgcaacgtgcaagtcg
acgtgaccgagggcgtcggcattgatatcaagtcctcaatcaacaagctcaccgtgctca
agagcacgggttcgcaattctggggcttcgtccgcgacgagtacacaacactccccgaag
tatgggaccgcatccttagtaccgatgttgaagcgacgtgggcatggaaaaggttctctg
ggctggatgaggtccgtgggaatgtgcccaagttcgatgagacttgggaggcggcgcgga
acattacgctcaagacatttgccgaggaggagagtgctagtgtccaggcgactatgtaca
agatgggcgagcagattctagcgtaccagccgcttcttgagactgtcgagtactcgttgc
cgaataaacattactttgagattggtgagtcgttaccacatatcctccatttgcttctgc
ggctgactgcttgtttagatctgagctggcacaagggccttaagaacacgggcaaggatg
ctgaggtgtttgttccccagacaaaccctaacggactgatcaagtgcactgtcggccgga
agtccaaggctaagctatagacgtctatagactaggtttttttttttctctattcattg
cacaaggagttgggcgactgtacatagcgggatctggaatatcatttacttctgccacga
aaagccccatagtcatgtaagctgtcaaacgcattgtagggctccaaggaatcatacaag
atctgcgtatgttgacggaagacggcaattggaaaacaattgaacatttaactcccaccc
atgcgctagaaatatcatacaaaagtgata

Figure 3.1.b *uaZ* genomic sequence. *uaZ* (AN9470) has three exons (red) interrupted by two introns (black). In uaZ_{14} an ochre mutation (CAA → TAA) in exon 2, highlighted in blue, terminates *uaZ* protein. Start codon (ATG) and stop codon (TAG) are highlighted in green.

Analysis of the PTC-containing transcript, uaZ_{14}, in the wild-type background, revealed a dramatic reduction in levels compared to the wild-type *uaZ* allele. The equivalent experiment in the Δ*upf1* and Δ*upf3* mutant backgrounds show that the level of PTC-containing transcripts is significantly higher than in the wild-type background. This is consistent with increased stability of NMD substrates in these mutant backgrounds. These data demonstrate the lack of an NMD response in the absence of Upf1 and Upf3 proteins. Furthermore, Upf3 data is consistent with a model in which Upf3, as part of EJC, plays a central role to distinguish aberrant PTC-containing transcripts as in mammalian cells (Imamachi, 2012). Moreover, the deletion of *upf3* in *A. nidulans* resulted in a relatively normal morphology, whereas deletion of *upf1* lead to poor growth (Figure 3.3). This is

consistent with Upf1 having important cellular functions in *A. nidulans* other than its role in NMD, which is consistent with observations in other systems (Isken and Maquat, 2008).

3.2 Mutational analysis of Upf1

Upf1 is a nucleocytoplasmic shuttling protein that associates with the EJC and has been characterised as an essential component of the NMD machinery (Shi et al., 2015). Upf1 is an ATP-dependent RNA helicase which is known to be regulated by phosphorylation, and it contains multiple phosphorylation sites, which are mostly evolutionarily conserved (Durand, Franks and Lykke-Andersen, 2016). Previous studies in mammalian systems have revealed that Upf1 interacts with several NMD factors, such as Upf2, CBP80, Smg1, Smg5-Smg7, Smg6, and eRF1-eRF3 (Imamachi, 2012). Upf1 is a substrate for the protein kinase Smg1 only when assembled with mRNA during NMD (Durand, Franks and Lykke-Andersen, 2016). Upf1 phosphorylation by Smg1 protein kinase results in increased affinity for the Smg5-7 complex and Smg6 (Durand, Franks and Lykke-Andersen, 2016). Simultaneous binding of the Smg5-7 complex and Smg6 to phosphorylated Upf1 are required for NMD (Okada-Katsuhata et al., 2011). It has been shown that the phosphorylation of Upf1 at threonine 28 (T28) is important to induce the binding of Smg6 via its 14-3-3-like domain during NMD (Okada-Katsuhata et al., 2011). Additionally, phosphorylation of Upf1 at Serine 1096 (S1096) by Smg1 kinase is important for Smg5-7 binding to dissociate ribosome and release factors from Upf1 (Figure 3.2.c) (Rissland and Norbury, 2009, Hu, Li and Li, 2013). Despite the fact that Smg5, Smg6 and Smg7 share the same 14-3-3-like domains, there are differing phospho-S/T (serine or threonine) binding properties between the Smg5-7 complex and Smg6 (Okada-Katsuhata et al., 2011). *In vivo* analysis showed that Upf1 can be phosphorylated at S1078 and S1116; however these are not required for NMD (Okada-

Katsuhata et al., 2011). It was suggested that these phosphorylation sites are involved with other SQ-motif directed kinases such as ATR, ATM and DNA-PKcs, which dictate Upf1 to perform its various cellular functions such as histone mRNA decay or the maintenance of genome stability (Okada-Katsuhata et al., 2011). Smg1 is missing from the genome of fungi therefore an alternative kinase or kinases are assumed to act on Upf1 (Lloyd and Davies, 2013). The assembly of Upf1 with these downstream factors is required for the formation of the translational termination complex (Durand, Franks and Lykke-Andersen, 2016). Upf1 sequence identities amongst human, plant, fruit fly, nematode, and yeast are between 40-62%, which is comparable to ribosomal proteins at 59-67% (Imamachi, 2012). Moreover, the sequence identity amongst zebrafish, mouse, and human is over 90% (Imamachi, 2012). Such a high level of conservation is indicative of the key role which Upf1 plays in biological systems.

Previous studies of both yeast and human Upf1 has shown that changing the residue K498 to A (K498A) led to a strong defect in Upf1 ATP hydrolysis and ATP binding (Cheng et al., 2006). The mutation K498A resulted in accumulation of Upf1 with higher levels of phosphorylation than wild-type Upf1 (Durand, Franks and Lykke-Andersen, 2016). Moreover, mutation of arginine at position 865 to alanine (R865A), within the conserved motif VI, has also been found to abolish ATP hydrolysis and ATP binding of human Upf1 (Cheng et al., 2006). In yeast, it has been proposed that the substitution of cysteine 125 with serine (equivalent to C186 of human Upf1) within the CH-domain to be involved in Zn3 binding which could result in loss of NMD (Cooper, 2000).

Based on sequence comparisons using mammalian, yeast and *A. nidulans* Upf1 proteins (Figure 3.2.a), point mutations C134S, K451Q (equivalent to K489Q) and RR811AA (equivalent to R865A) were engineered into the putative cysteine- histidine-rich region (CH-domain) and helicase domain (HD) of *A. nidulans* Upf1 (Figure 3.2.b).

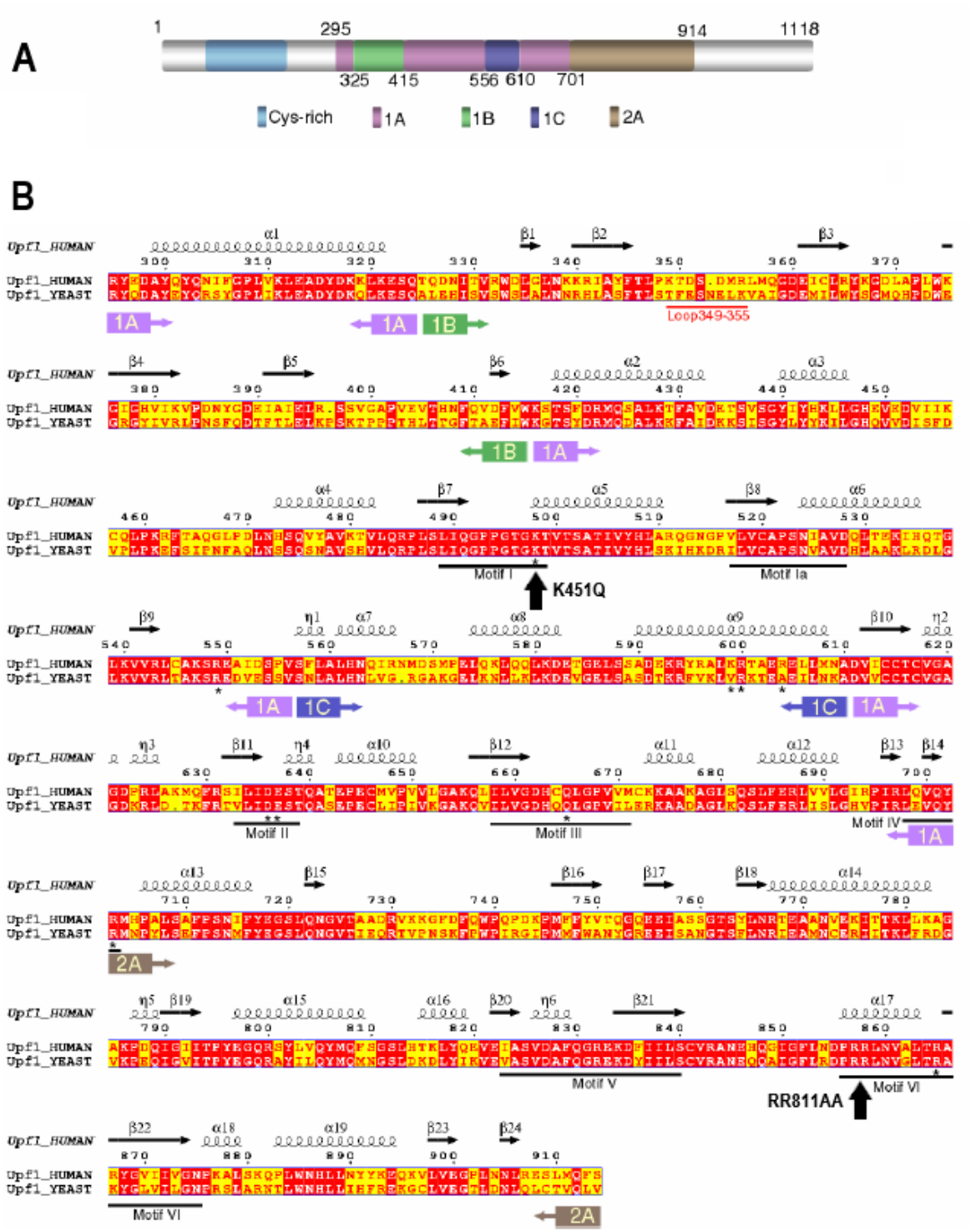

Figure 3.2.a Domain structure of human Upf1 and sequence alignment of the helicase core domain. (A) Schematic diagram showing the Helicase domain of human Upf1 composed of two domains (domains 1 and 2). Both domains contain a 'RecA-like' α/β domain designated as 1A and 2A. In addition to subdomain 1A, domain 1 also contains two insertions, each of which forms a distinct subdomain, denoted as domains 1B and 1C, respectively. (B) Amino acid sequence alignment of HD of human and yeast Upf1 showing conserved helicase motifs (I, Ia, II, III, IV, V, VI). Mutated residues are marked with " * ". Secondary structural elements of Upf1 HD are indicated. The coloring scheme for domains as in (A). Figure taken from Cheng et al., (2006).

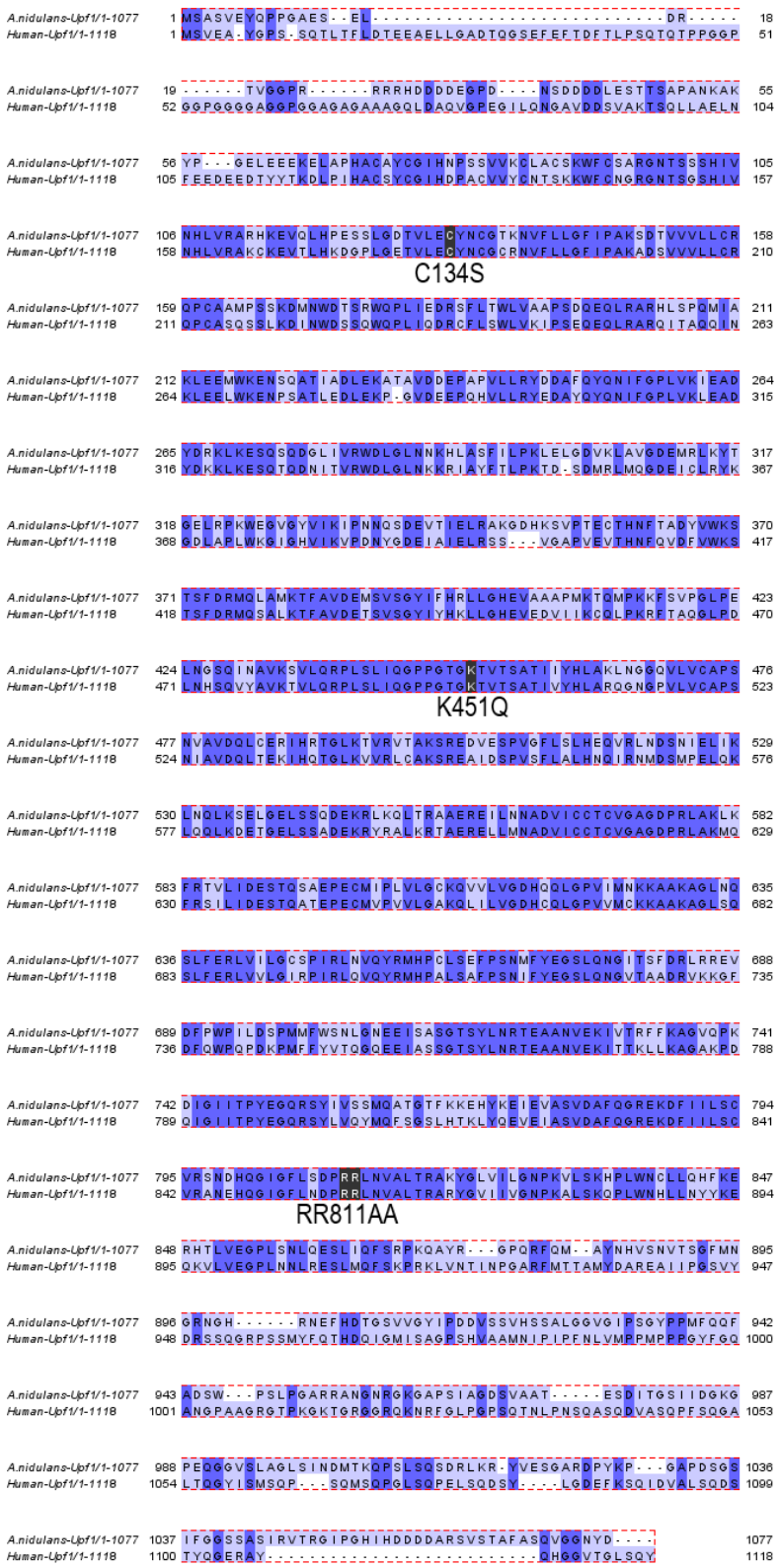

Figure 3.2.b Sequence alignment of human (Q92900-2) and *A. nidulans* (AN0646) Upf1. The amino acid sequence alignment was performed using T-Coffee. Based on sequence comparisons using human and yeast Upf1 proteins (Figure 3.2.a), the equivalent point mutations C134S, K451Q and RR811AA were defined in *A. nidulans* Upf1. The point mutations are marked. *A. nidulans* Upf1 amino acid sequence is 59% identical to human Upf1.

In *S. cerevisiae*, the CH-domain and HD have been shown to be involved in protein-protein interactions with Upf2, eRF3 and CBP80 (Figure 3.2.c) (Imamachi, 2012). Based on *in vitro* studies in human cells, Upf1 interacts with CBP80 via its HD to interact with mRNA cap structure (Benhabiles, Jia and Lejeune, 2016). According to previous studies in mammalian cells it has been shown that there is a direct interaction between CBP80 and Upf1 (Hosoda et al., 2005). This interaction promotes the recruitment of Smg1 associated with Smg5-7 and Smg6 (Benhabiles, Jia and Lejeune, 2016). Generally, Upf1 is known to interact with eRF1, eRF3, and Smg1 to form a complex termed SURF, which subsequently binds to the EJC complex and mRNA decay factors (Kim et al., 2017). Upf2 recruits Upf1 to the EJC, via its CH-domain which stimulates Upf1 helicase activity (Benhabiles, Jia and Lejeune, 2016). Previously in mammalian cells it has been shown that CBP80 is required to promote the recruitment of Upf1 to EJC associated Upf2 (Hosoda et al., 2005). However, their exact role in this process is still unclear. Therefore, assuming a high level of conservation the C134S, K451Q and RR811AA mutations will allow the question of whether these specific interactions are required for NMD in *A. nidulans* to be answered.

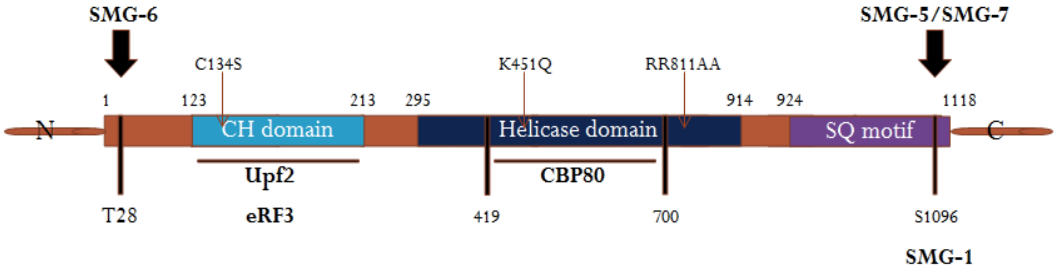

Figure 3.2.c The structure of Upf1. The schematic diagram showing the domains of human Upf1 involved in binding NMD factors are indicated (Imamachi, 2012). The position of mutations, C134S, K451Q and RR811AA in *A. nidulans* are indicated on human Upf1.

Mutant versions of the *upf1* coding region, incorporating the three point mutations, were produced by fusion PCR. To achieve this, complementary forward and reverse primers for the Upf1 gene harbouring the desired nucleotide changes were synthesised. For each mutant allele two gene fragments were produced by PCR, each including an overlapping region of approximately 25 bp which harboured the desired mutation. Fusion was then accomplished using a second round of PCR using the primary PCR products as the DNA template (Appendix 2). Due to the size of Upf1, which is approximately 5.5 kbp, mutant constructs were assembled in two parts with a 500-700 bp overlapping regions (Figure 3.2.d) to facilitate integration by a recombination during transformation (Figure 3.2.e). The mutant alleles were knocked into the Δ*upf1:Af-pyrG*$^{+}$ *(pyrG89)* strain by selecting for resistance to 5-fluoroorotic acid (5-FOA).

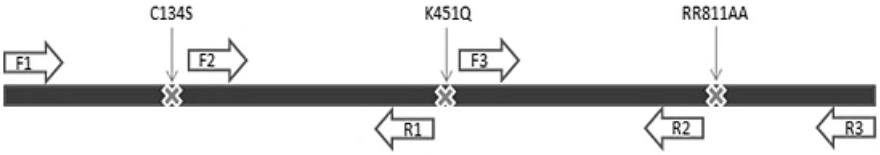

Figure 3.2.d The schematic diagram of fusion PCR. The diagram showing the position of the primers on the Upf1 gene. A combination of primers were used in a multi-step approach to assemble the mutant constructs in two parts with 500-700 bp overlapping regions.

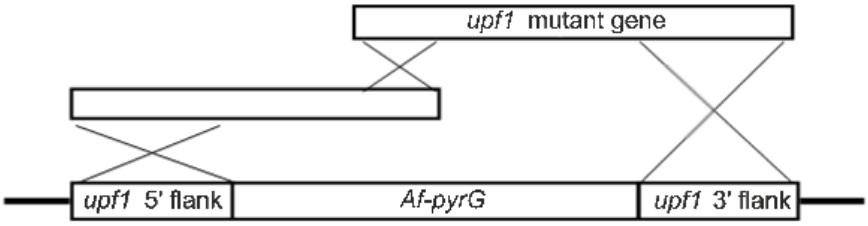

Figure 3.2.e The schematic diagram of homologous recombination. The diagram showing the homologous integration of *Upf1* gene to disrupt *Af-pyrG* gene. Strains that have a functional *Af-pyrG* gene can grow in the absence of uracil but cannot grow in the presence of 5-FOA, because the *pyrG* product, orotidine 5'-phosphate carboxylase, converts 5-FOA into 5-fluorouracil which is toxic. Therefore, transformants in which *Af-pyrG*$^{+}$ has been replaced by the integration of *upf1* derived sequences were selected on the basis of 5-FOA resistance.

Putative transformants were screened by PCR to confirm integration of *upf1* mutant alleles and the point mutations were confirmed by sequencing. Interestingly, they looked phenotypically wild-type (Figure 3.3). The resulting *upf1* mutant strains *upf1* ^{C134S}, *upf1* ^{K451Q} and *upf1* ^{RR811AA} were used to determine if the *upf1* mutant alleles disrupt NMD. The respective *upf1* alleles were crossed into the uaZ_{14} background and the strains subjected to Northern analysis to determine the effect of these mutants on uaZ_{14} transcript level. Based on this analysis it is apparent that both Upf1-K451Q and Upf1-RR811AA disrupt NMD, whereas Upf1-C134S had no effect on uaZ_{14} mRNA stability (Figure 3.2.f). This is consistent with previous results of yeast and human Upf1 where both K451Q (Motif I) and RR811AA (Motif VI) were strongly defective for ATP hydrolysis and ATP binding (Cheng et al., 2006).

Upf1-C134S (C125S In yeast) has been proposed to disrupt NMD (Cooper, 2000). However, this mutation has not been tested in humans or yeast (Langley, 2015). These mutants will be discussed in more detail in chapter 6.

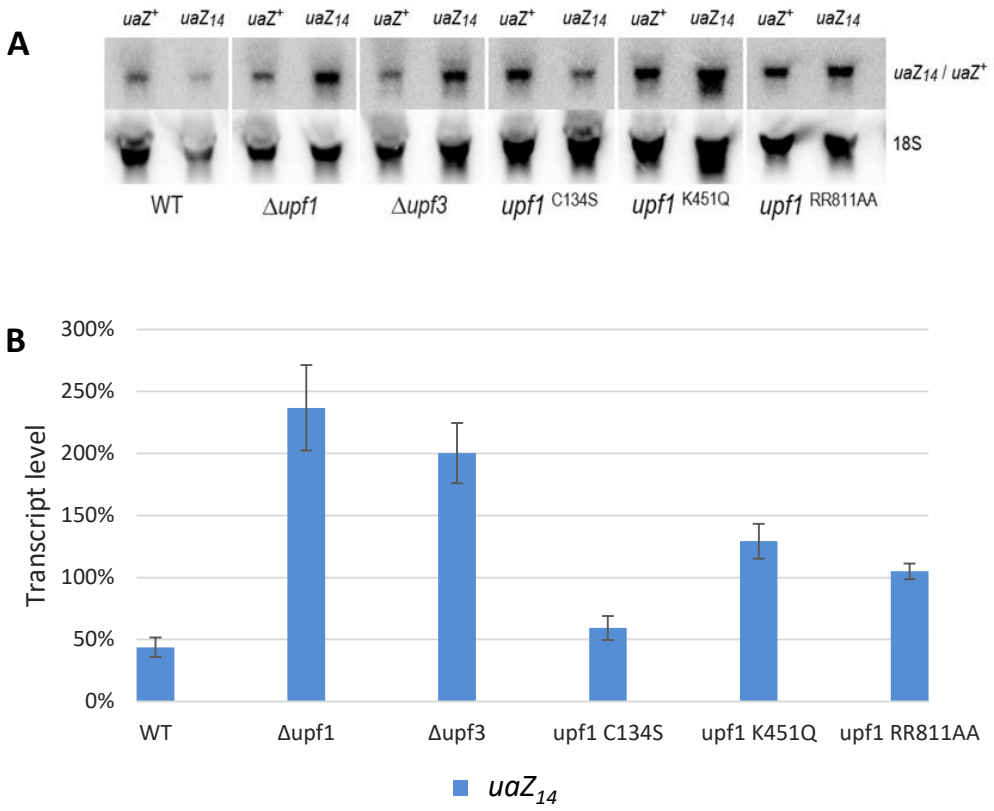

C

		Δ*upf1*	Δ*upf3*	*upf1* C134S	*upf1* K451Q	*upf1* RR901AA
uaZ 14	p-value	0.0160	0.0018	0.1400	0.0030	0.0019
		Sig.	Sig.		Sig.	Sig.

Figure 3.2.f Characterisation of Upf3 and Upf1 mutants with respect to *uaZ$_{14}$* transcript levels. (A) Northern blot analysis of total RNA samples was conducted to monitor the level of *uaZ*$^{+}$ and *uaZ$_{14}$* transcripts in different genetic backgrounds: wild-type (WT), Δ*upf3*, Δ*upf1*, *upf1* C1134S, *upf1* K451Q and *upf1* RR811AA. The phosphorimager data from triplicate experiments were compiled for further analysis. (B) The level of *uaZ$_{14}$* transcript is presented as a percentage of *uaZ*$^{+}$ in the equivalent strain. Bar graph shows calibrated quantitative values normalised to 18S rRNA as a control. n = 3 +/- SD. (C) A t-test was done to determine whether there was a significant difference between the regulatory response in mutants and in the wild-type strain. A p-value of ≤0.05 is considered statistically significant (Sig.).

3.3 The role of endonucleolytic domain of Smg6 in *uaZ$_{14}$* mRNA regulation

Phosphorylated Upf1 associates with the phospho-binding proteins Smg5, Smg6, Smg7 and general mRNA decay factors, resulting in further rearrangements of this complex which leads to mRNA degradation (Hug, Longman and Cáceres, 2016). Smg5 and Smg7 form a complex that promotes mRNA deadenylation and decapping. In contrast, Smg6 is an endonuclease thought to cleave NMD substrates in the vicinity of the PTC, leading to the initiation of NMD-mediated RNA decay (Hug, Longman and Cáceres, 2016, Celik, Kervestin and Jacobson, 2015).

Based on preliminary analysis (Morozov and Caddick, unpublished data) it is apparent that the putative endonuclease Smg6, is required for NMD in *A. nidulans*. To determine if this specifically involves the endonuclease activity we engineered a double mutant, *smg6* $^{D13A\ D251A}$ (Appendix 3) which, based on protein modelling is likely to disrupt the PIN domain (Rigden and Caddick, unpublished data). The *smg6* mutant allele was inserted into the Δ*smg6:Af-pyrG, pyrG89, pyroA4,* Δ*nkuA* strain as a linear DNA construct, replacing *Af-pyrG* and resulting in resistance to 5-FOA. Putative transformants were screened by PCR to confirm reintegration of the *smg6* allele. The point mutations were confirmed by sequencing. The resulting mutant strain, *smg6* $^{D13A\ D251A}$, was morphologically similar to wild-type and Δ*smg6* strains (Figure 3.3).

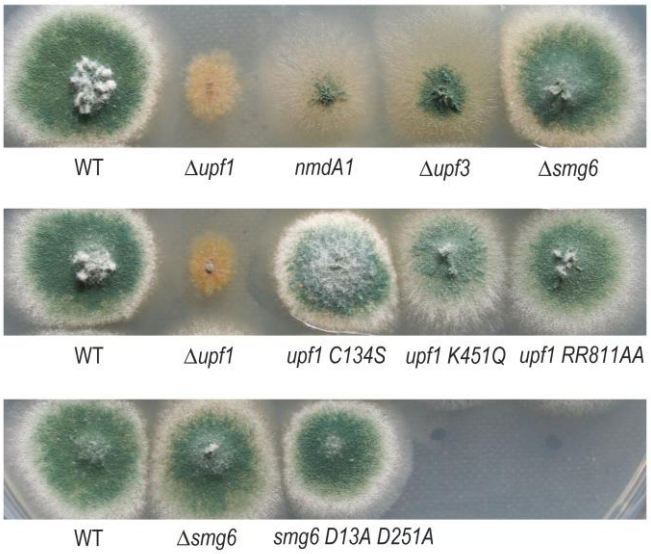

Figure 3.3 Growth phenotype of strains harboring mutations in NMD component genes. Photographs of the colonies of *A. nidulans* wild-type (WT) and mutant strains. All strains were grown on solid MM with required supplements, for 3 days at 37 ˚C. The deletion of *upf1*, *upf2* (*nmdA1*) or *upf3* resulted in poor growth and condition, whereas strains with the *upf1* point mutations (*upf1* C1134S, *upf1* K451Q , *upf1* RR811AA), Δ*smg6* or the *smg6*⁻ allele with the double substitution (*smg6* D13A D251A) disrupting the PIN domain, all showed relatively normal morphology.

Based on quantitative Northern analysis of uaZ_{14} mRNA levels, the catalytic activity of Smg6 is not required for NMD of the uaZ_{14} transcript (Figure 3.4). This suggests that the PIN domain of Smg6 is either not required or that loss of the putative RNA endonuclease activity is masked by RNA degradation mechanism which act in parallel. Moreover, the disruption of NMD associated with the Δ*smg6* allele, suggests that it has a critical role as part of the NMD complex.

3.4 The coordination of decapping and endonuclease cleavage in uaZ_{14} mRNA regulation

Based on other systems, mRNA decapping is a key transition point in mRNA degradation, facilitating rapid 5'-3' degradation which is the major degradation mechanism in a wide range of organisms, extending from *S. cerevisiae* to mammalian systems (Kramer, 2017). In yeast, mRNA decapping is carried out by a single enzyme composed of Dcp1 and the

catalytic subunit, Dcp2, but also requires the functions of specific regulators commonly known as decapping activators (He and Jacobson, 2015). *in vivo* studies of *S. cerevisiae* indicated that the decapping complex interacted directly with only three decapping activators, Edc3, Pat1, and Upf1, and that all three interactions are mediated by Dcp2 (He and Jacobson, 2015). Importantly, in *S. cerevisiae* decapping, mediated by Dcp2, is required for NMD (Hu et al., 2010). However, in animal systems endonuclease cleavage by Smg6 can either replace decapping, as in *D. melanogaster*, or be a component of NMD mediated transcript degradation, as in human cells (Huntzinger et al., 2008).

Previously it has been shown that disruption of either *dcp1* or *dcp2* is not sufficient for the disruption of NMD targeting PTC-containing transcripts in *A. nidulans* (Bharudin, 2017). Our data shows that the PIN domain is not required in *A. nidulans*, but this is consistent with observations in human cells (Nicholson et al., 2014). To elucidate the role of decapping and Smg6 mediated endonucleolytic cleavage in NMD of the uaZ_{14} transcript, the *smg6* $^{D13A\ D251A}$ was crossed to obtain mutant strains: *smg6* $^{D13A\ D251A}$*,* Δ*dcp2 smg6* $^{D13A\ D251A}$, uaZ_{14} *smg6* $^{D13A\ D251A}$ and uaZ_{14} Δ*dcp2 smg6* $^{D13A\ D251A}$. These strains were subject to quantitative Northern analysis assay NMD (Figure 3.4).

Based on Northern analysis, neither *smg6* $^{D13A\ D251A}$ or Δ*dcp2* allele lead to loss of NMD, with the levels of uaZ_{14} mRNA being significantly lower than uaZ^{+} in both backgrounds. Strikingly, disruption of both decapping, via deletion of Dcp2, and the putative Smg6 endonuclease domain, by introducing two amino acid substitutions, led to suppression of NMD. This is consistent with NMD acting to stimulate both decapping and mRNA cleavage and in this respect is equivalent to the situation observed in mammalian systems (Huntzinger et al.,

2008). Furthermore, it supports the putative role of *A. nidulans* Smg6 as an active endonuclease. Importantly, deletion of *smg6* is sufficient to disrupt NMD (Morozov and Caddick, unpublished data), which implies that it forms an essential component within the NMD machinery which is distinct from the specific endonuclease function.

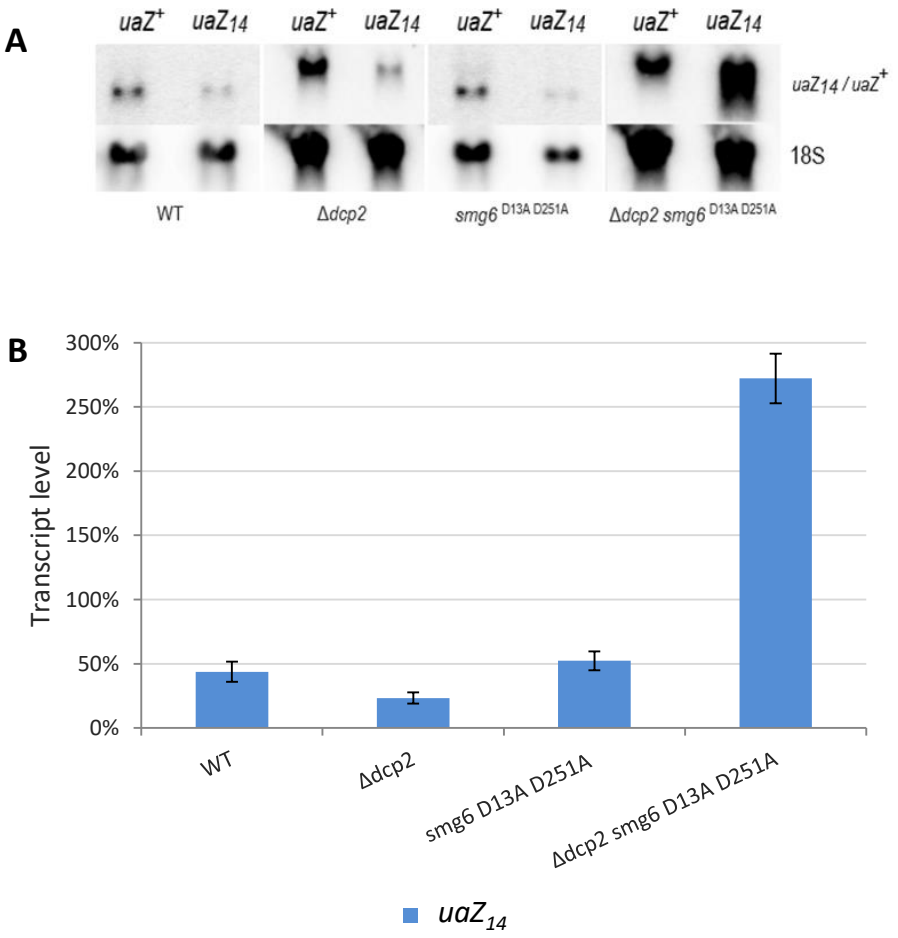

Figure 3.4 Characterisation the role of decapping and Smg6 mediated endonucleolytic cleavage in NMD. (A) Northern blot analysis of total RNA samples was conducted to monitor the level of *uaZ*$^+$ and *uaZ*$_{14}$ transcripts in different genetic backgrounds. The phosphorimager data from triplicate experiments were compiled for further analysis. (B) Bar graph shows calibrated quantitative values normalised to 18S rRNA as a control (B) The average level of *uaZ*$_{14}$ expression, relative to *uaZ*$^+$ is indicated as a percentage, for each strain. n = 3 +/- SD.

3.5 Summary

Previously it has been demonstrated that disruption of Upf1, Upf2 and Smg6 lead to full suppression of NMD in *A. nidulans* (Morozov et al., 2012; Morozov and Caddick personal communication). Further analysis was undertaken to confirm the previous results and also to test an additional NMD factor Upf3 which has been shown to be important for NMD-mediated decay. Our results clearly demonstrated that Upf1 and Upf3 are required for NMD, although the detailed role of the Upf proteins remained to be elucidated in *A. nidulans*. Disruption of Upf1, known as the central component of NMD, lead to reduced tagging for wild-type *gdhA* mRNA and the NMD substrate, uaZ_{14} mRNA (Morozov et al, 2012). Therefore, the mutational analysis of Upf1 was undertaken to further characterise its role in NMD and its possible link to the tagging factors CutA and CutB will be discussed later (Chapter 5). Upf1 mutational analysis data revealed that the Upf1 HD is essential for NMD whereas Upf1 CH-domain had no effect on uaZ_{14} mRNA stability. It is possible that the C134S mutation has not disrupted the activity of the CH-domain. However, this mutation has not been tested so far (Cooper, 2000). Thus further investigation into whether this mutation has an effect on Upf1 interaction with Upf2 is necessary.

In mammalian systems, it has been indicated that simultaneous binding of the Smg5-7 complex and Smg6 to phosphorylated Upf1 are required for NMD (Okada-Katsuhata et al., 2011). Based on previous analysis it is apparent that Smg6 is required for NMD in *A. nidulans*. However, its exact role was unclear. Mutational analysis was used to disrupt the putative PIN domain. Based on this it was found that the PIN domain of Smg6 was not required for NMD. In human cells, it was previously shown that both decapping and Smg6 mediated endonucleolytic cleavage contribute to NMD mediated transcript degradation

(Nicholson et al., 2014). Therefore, further analysis was undertaken to elucidate the role of decapping and Smg6 mediated endonucleolytic cleavage in the regulation of *uaZ*$_{14}$ transcript. We observed that although the PIN domain is not required for NMD in *A. nidulans*, this is not the case for a strain which is defective in mRNA decapping. This is consistent with observations in human cells where NMD involves both decapping and endonuclease cleavage, acting in parallel to degrade the target transcript (Nicholson et al., 2014). Our results provide compelling evidence that the assembly of an active component within the NMD machinery requires Smg6 formation to stimulate both decapping and cleavage of transcripts that terminate at the PTC. Since it has been shown that Smg6 cannot bind mRNA itself, it is highly plausible that Smg6 is being recruited by phosphorylated Upf1 to the EJC through Upf2 and Upf3 which, as in human cells, gives further specificity to the Smg6 recruitment process (Nicholson et al., 2014).

Chapter 4: The role of NMD components in histone mRNA regulation and tagging

Introduction

Chromosomes are composed of negatively charged DNA tightly wrapped around small, positively charged histone proteins to form a complex termed the nucleosome (T. Annunziato, 2008). Nucleosomes consist of two of each H2A, H2B, H3, and H4 histone molecules (T. Annunziato, 2008). In human cells, histone mRNA levels are tightly coupled to DNA replication. Inhibition of DNA replication, which can be induced using hydroxyurea (HU), results in histone mRNA 3' end oligouridylation which leads to rapid degradation, allowing the cell to rapidly adjust the rate of histone protein synthesis (Mullen and Marzluff, 2008). The NMD factor, Upf1, is known to play a key role in this response to the cell cycle, regulating 3' tagging and degradation of histone mRNA (Mullen and Marzluff, 2008).

In *A. nidulans* 3' tagging has been linked to deadenylation dependent mRNA degradation and NMD. Two terminal transferases, CutA and CutB are responsible for this tagging, disruption of both resulting in no 3' tagging being observed (Morozov et al., 2012). In the case of deadenylation dependent mRNA degradation disruption of CutA and CutB leads to an increased transcript stability (Morozov et al., 2012) and in the case of NMD decapping, which in the wild-type background is poly(A) independent, is predominantly associated with deadenylated transcripts (Morozov et al., 2010). Unlike human histone mRNA, in *A. nidulans* the histone transcripts are polyadenylated. However, initial work looking at the H2A transcript suggested that a similar response occurs in *A. nidulans* when DNA synthesis is blocked, with the tagging and accelerated degradation of the transcript (Morozov and Caddick, unpublished data).

In order to confirm these initial observations and characterise both the regulatory system and RNA degradation mechanisms involved, we undertook to monitor histone transcript regulation including analysing the effect of disrupting several key NMD and mRNA decay factors on histone mRNA levels, the regulatory response to the inhibition of DNA synthesis and 3' tagging in *A. nidulans*.

4.1 Deletion of NMD and decay factors

The NMD regulatory complex is known to include a number of factors in addition to Upf1 and Upf2, which prior to this work were the only two characterised in *A. nidulans* (Morozov et al., 2006; Morozov et al., 2013). In order to characterise the role of NMD factors and the terminal transferases CutA and CutB, in the regulation of histone transcript, we assessed strains deleted for genes encoding Upf1, Upf2, CutA, CutB and two additional NMD factors, Upf3 and Smg6.

To investigate the response of histone transcript levels to HU treatment in *A. nidulans*, quantitative Northern blot analysis was used to assay transcript abundance. For Northern analysis, hydroxyurea (1.5 mg ml^{-1}) was added to the cultures to inhibit DNA synthesis for a duration of 20 minutes, samples were harvested immediately prior to HU treatment (t_0) and after 20 minutes in the presence of HU (t_{20}). Total RNA was extracted from the frozen mycelia, resolved by agarose gel electrophoresis, transferred to a nylon membrane and hybridised with ^{32}P radiolabelled probes for the transcripts encoding H2A (AN3468), H3 (AN0733) and 18S rRNA as a loading control.

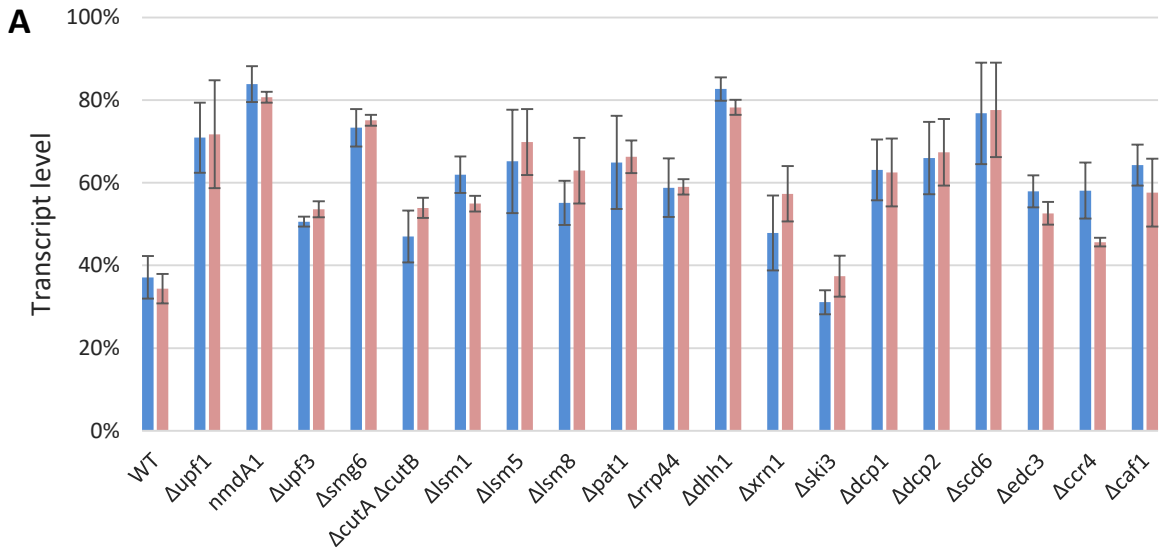

B

		Δupf1	nmdA1	Δupf3	Δsmg6	ΔcutA ΔcutB	Δlsm1	Δlsm5	Δlsm8	Δpat1	Δrrp44	Δdhh1	Δxrn1	Δski3	Δdcp1	Δdcp2	Δscd6	Δedc3	Δccr4	Δcaf1
H2A	p-value	0.0137	0.0011	0.0323	0.0031	0.1453	0.0110	0.0535	0.0364	0.0444	0.0342	0.0008	0.1807	0.1835	0.0222	0.0234	0.0205	0.0161	0.0349	0.0097
		Sig.	Sig.	Sig.	Sig.		Sig.		Sig.	Sig.	Sig.	Sig.			Sig.	Sig.	Sig.	Sig.	Sig.	Sig.
H3	p-value	0.0255	0.0001	0.0045	0.0002	0.0053	0.0036	0.0077	0.0153	0.0020	0.0018	0.0002	0.0195	0.3238	0.0175	0.0100	0.0113	0.0079	0.0196	0.0304
		Sig.	Sig.	Sig.	Sig.	Sig.	Sig.	Sig.	Sig.	Sig.	Sig.	Sig.	Sig.		Sig.	Sig.	Sig.	Sig.	Sig.	Sig.

Figure 4.1.a The effect of NMD and decay factors on histone H2A and H3 mRNA regulation in response to HU treatment. All strains were treated with HU over a 20 minutes time course (t_0-t_{20}), to block DNA synthesis. Aliquots (10 µg) of total RNA were resolved on an agarose gel, transferred to a nylon membrane and hybridised with a ^{32}P radiolabelled probe for H2A and H3 transcripts. Bar graph shows calibrated quantitative values normalised to 18S rRNA as a control, giving the relative expression levels as a percentage of the untreated samples (t_0) for both H2A (Blue) and H3 (red) transcripts after a 20 minutes treatment with HU (t_{20}) for the wild-type and mutant strains. n = 3 +/- SD. (B) A t-test was performed to determine whether there was a significant difference between the HU response in mutants and in the wild-type strain. A p-value of ≤0.05 is considered statistically significant (Sig.).

Assuming that the regulatory response of histone mRNA to HU treatment is mediated primarily at the level of mRNA stability, comparing H2A and H3 expression levels in the wild-type and mutant strains suggests that, disruption of both CutA and CutB, and surprisingly Upf3, led to only limited stabilisation of histone mRNA levels. However, disruption of Upf1, Upf2 and strikingly, Smg6 resulted in a dramatic effect; where their deletion led to a significantly diminished regulatory response for both H2A and H3, compared to the wild-

type (Figure 4.1.a). These data are consistent with a model in which HU treatment induces Upf1 recruitment to the histone transcripts as has been described in human cells (Mullen and Marzluff, 2008). However, these data reveal a novel role for Smg6 and Upf2, both of which appeared to play a major role in the regulation of histone transcripts in *A. nidulans*. This is different to the situation in human cells, where replication-dependent histone mRNA degradation is independent of Upf2 (Kaygun and Marzluff, 2005).

It has been shown that translational termination is linked to mRNA degradation through the action of multiple trans-acting factors, including, Pat1, Dhh1 and Scd6, which are known to have roles in both processes. Scd6, a decapping activator, is an mRNA binding protein that interacts with Dhh1, Dcp2, and Pat1 (Roy and Jacobson, 2013). Pat1 and Scd6 repress translation during 48S initiation complex formation and subsequently affect decapping (Roy and Jacobson, 2013). It has been shown that direct binding of Scd6 to eIF4G blocked 43S complex formation (Roy and Jacobson, 2013). Northern data indicates that the disruption of these proteins, particularly Dhh1 and Scd6, has a significant effect on histone mRNA stability; deletion of *scd6* (AN1055) and *dhh1* (AN10417) supressed the regulatory response to HU treatment, for both H2A and H3, to a third of that of the wild-type (Figure 4.1.a). Δ*dhh1* displays poor growth phenotype, whereas Δ*scd6* showed relatively normal morphology (Figure 4.1.b).

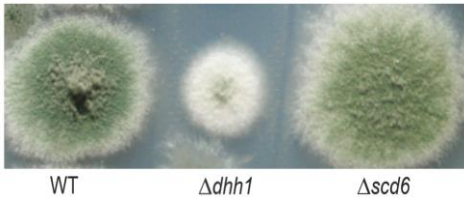

Figure 4.1.b Phenotypic effect of mutations disrupting *dhh1* and *scd6*. Photographs of the colonies of *A. nidulans* wild-type (WT) compared to the Δ*dhh1* and Δ*scd6* strains. All strains were grown on solid MM with required supplement for 3 days at 37 ˚C.

Disruption of *lsm1* (AN6199) and *lsm5* (AN5679) reduced the HU regulatory response, consistent with partial loss of the histone mRNA degradation response (Figure 4.1.a). These data are consistent with a model in which HU treatment induces cytoplasmic Lsm1-7 complex recruitment to the histone transcripts, which then triggers mRNA degradation, as demonstrated in human cells (Mullen and Marzluff, 2008). Moreover, Lsm8 (AN1119) is a subunit of another Lsm heptameric complex termed Lsm2-8, which has Lsm8 in place of Lsm1 (Zhou et al., 2014). However, in *S. cerevisiae* the Lsm1-7 complex is cytoplasmic, whereas Lsm2-8 complex is localised specifically in the nucleus (Weichenrieder, 2014). Assuming conservation of the intracellular localisation of these complexes it is surprising that disruption of Lsm8 also suppressed the regulatory response (Figure 4.1.a). It may be that in *A. nidulans* Lsm8 is not exclusively active in the nucleus or alternatively that its disruption impacts on the expression and/or distribution of the other Lsm components and has an indirect effect on HU induced histone mRNA depletion.

Other components of the 5'-3' mRNA decay machinery were also investigated. Dcp1, Dcp2, Edc3 and Xrn1 are important in mRNA decapping and 5'-3' degradation. However, their disruption only partially inhibited HU induced histone mRNA regulation. Decapping enzymes, Dcp1 and Dcp2 had more impact than Edc3 and Xrn1 (Figure 4.1.a). These findings suggest that other decay pathway(s), in addition to 5'-3' decay play a significant role in histone mRNA degradation. Again this is consistent with the mammalian system, where both 5'-3' and 3'-5' degradation are implicated in the regulated degradation of histone encoding transcripts (Mullen and Marzluff, 2008).

The exosome is a large protein complex responsible for 3'-5' RNA degradation. Disruption of Rrp44, a core exosome component with nuclease activity, partially reduced the HU regulatory response, the effect being similar to that seen in the disruption of 5'-3' exonuclease, Xrn1. However, disruption of Ski3 (AN3014) had no effect which suggests that this protein is not involved in HU induced mRNA degradation pathway (Figure 4.1.a). This is consistent with the role of Ski3 in degradation of non-stop decay substrates (Krebs, Goldstein and Kilpatrick, 2017). Disruption of the exonucleolytic activity of the two catalytic components of the deadenylase complex, Ccr4 and Caf1 (Morozov et al., 2010), also partially supressed the HU response, consistent with partial stabilisation of the histone transcripts (Figure 4.1.a). The above data suggest that deadenylation and 3'-5' degradation of mRNA both play a role in histone transcript degradation but are not solely responsible.

4.2 Analysis of genetic interactions by disrupting both NMD and decay factors

The analysis of strains bearing single mutants disrupting distinct components of mRNA degradation mechanisms, suggests that multiple pathways are implicated in the HU induced histone mRNA degradation. To investigate this further we undertook to construct a range of double mutants. If the double mutant displays a phenotype which is additive, ie has a more extreme phenotype than either single mutant, the implication is that the pathways involved are distinct and independent. If the double mutant's phenotype is equivalent to the single mutants, the implication is that the two mutations are disrupting the same pathway.

A range of double mutants were constructed by crossing appropriate strains bearing single mutations in NMD and decay factors. However, some of the double mutants, *nmdA1* Δ*dhh1*,

Δdcp2 Δdhh1, *Δlsm1 Δlsm8*, *Δlsm1 Δpat1* and *Δlsm3 Δlsm5*, were not obtained either due to the respective crosses being inviable or synthetic lethality.

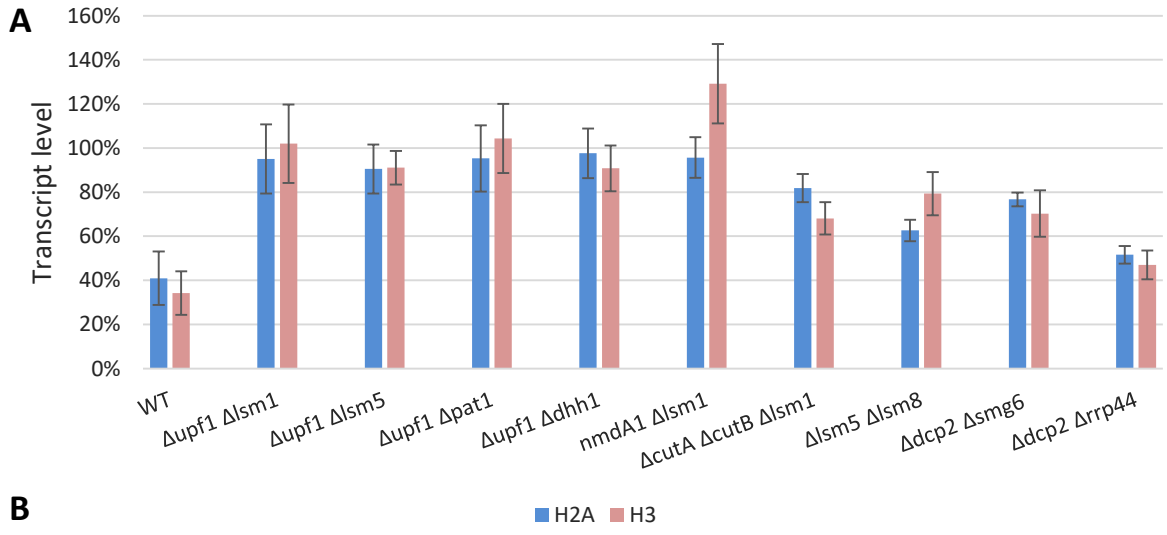

		Δupf1 Δlsm1	*Δupf1 Δlsm5*	*Δupf1 Δpat1*	*Δupf1 Δdhh1*	*nmdA1 Δlsm1*	*ΔcutA ΔcutB Δlsm1*	*Δlsm5 Δlsm8*	*Δdcp2 Δsmg6*	*Δdcp2 Δrrp44*
H2A	p-value	0.0262	0.0197	0.0241	0.0132	0.0114	0.0203	0.0857	0.0230	0.2253
		Sig.	Sig.	Sig.	Sig.	Sig.	Sig.		Sig.	
H3	p-value	0.0147	0.0052	0.0096	0.0084	0.0049	0.0256	0.0158	0.0335	0.1708
		Sig.	Sig.	Sig.	Sig.	Sig.	Sig.	Sig.	Sig.	

Figure 4.2.a The effect of double mutants on histone H2A and H3 mRNA regulation in response to HU treatment. All strains were treated with HU over a 20 minutes time course (t_0-t_{20}), to block DNA synthesis. Aliquots (10 µg) of total RNA were resolved on an agarose gel, transferred to a nylon membrane and hybridised with a ^{32}P radiolabelled probe for H2A and H3. Bar graph shows calibrated quantitative values normalised to 18S rRNA as a control, giving the relative expression levels of both H2A and H3 transcripts after a 20 minutes treatment with HU (t_{20}) compared to untreated samples (t_0) in wild-type and mutant strains. n = 3 +/- SD. (B) A t-test was performed to determine whether there was a significant difference between the HU response in mutants and in the wild-type strain. A p-value of ≤0.05 is considered statistically significant (Sig.).

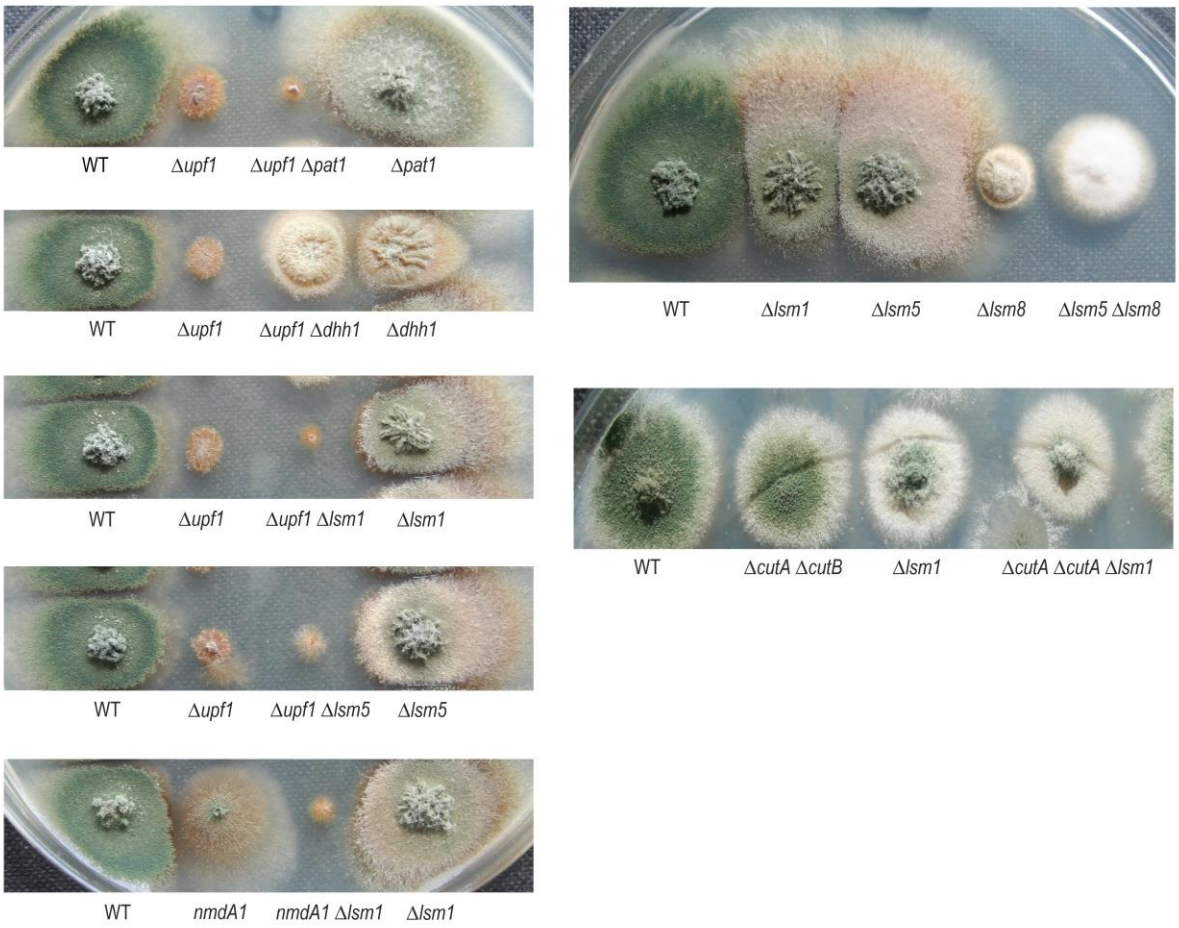

Figure 4.2.b Growth phenotype of selected double mutants affecting NMD and RNA degradation factors. Photographs of the colonies of *A. nidulans* wild-type (WT) compared to the single and double mutants as indicated. All strains were grown on solid MM with required supplement for 3 days at 37 ˚C.

The double mutants, Δ*upf1* Δ*dhh1*, Δ*upf1* Δ*lsm1*, Δ*upf1* Δ*pat1*, Δ*upf1* Δ*lsm5* and *nmdA1* Δ*lsm1* all appeared to fully disrupt the HU induced regulatory response for both H2A and H3 encoding transcripts (Figure 4.2.a). Based on this, these double mutants display additivity, consistent with loss of histone mRNA degradation. In contrast the double mutants, Δ*lsm5* Δ*lsm8*, Δ*smg6* Δ*dcp2* and the treble mutant Δ*cutA* Δ*cutB* Δ*lsm1*, displayed no additivity (Figure 4.2.a). One interpretation is that the loss of the HU response implies that at least two distinct mechanisms are involved in HU induced mRNA degradation: the NMD complex mediating one and the Lsm1-7 activated decapping pathway another. Interestingly, in Δ*dcp2*

Δ*rrp44* the regulatory response is not diminished, being similar or even closer to wild-type than that of the Δ*rrp44* single mutant.

4.3 Functional analysis of Upf1 in histone mRNA regulation

Previously we undertook a more detailed analysis of the role for specific residues within Upf1 with respect to NMD. This was done by constructing strains bearing three different Upf1 alleles: C134S, K451Q and RR811AA (Figure 3.2.f). We decided to test the effect of these mutations on histone mRNA regulation to see if the same domains have a critical role or if NMD and HU induced repression of histone mRNA or if the two processes are mechanistically distinct.

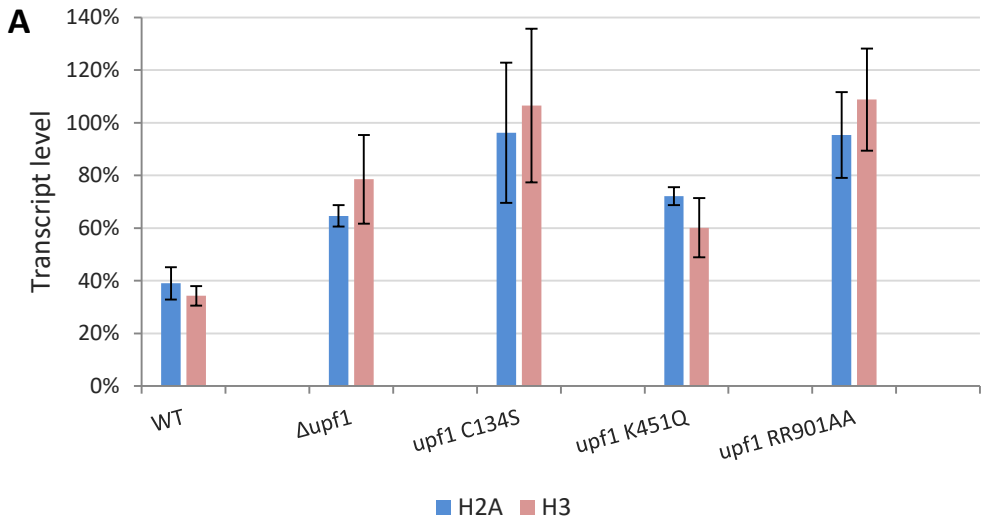

B

		Δ*upf1*	*upf1* C134S	*upf1* K451Q	*upf1* RR901AA
H2A	p-value	0.0127	0.0521	0.0090	0.0160
		Sig.		Sig.	Sig.
H3	p-value	0.0623	0.0668	0.0473	0.0317
				Sig.	Sig.

C

		upf1 C134S	upf1 K451Q	upf1 RR901AA
H2A	p-value	0.1807	0.1134	0.0710
H3	p-value	0.2266	0.2077	0.1519

Figure 4.3 The effect of Upf1 mutants on histone H2A and H3 mRNA regulation in response to HU treatment. All strains were treated with HU over a 20 minutes time course (t_0-t_{20}), to block DNA synthesis. Aliquots (10 µg) of total RNA were resolved on an agarose gel, transferred to a nylon membrane and hybridised with a ^{32}P radiolabelled probe for H2A and H3. (A) Bar graph shows calibrated quantitative values normalised to 18S rRNA as a control, giving the relative expression levels of both H2A and H3 transcripts after a 20 minutes treatment with HU (t_{20}) compared to untreated samples (t_0) in wild-type and mutant strains. n = 3 +/- SD. (B) A t-test was performed to determine whether there was a significant difference between the HU response in mutants and in the wild-type strain. (C) An additional t-test was conducted to determine if there is a significant difference in response between Upf1 mutants and Δ*upf1*. A p-value of ≤0.05 is considered statistically significant (Sig.).

Quantitative Northern analysis was again utilised to monitor the HU regulatory response for H2A and H3 transcripts. In addition to the wild-type and the Δ*upf1* mutant strain, three strains expressing mutant version of Upf1 were tested. Based on these data amino acid substitutions; C134S, K451 and RR810-811AA, all led to partial loss of HU induced repression of the histone transcripts (Figure 4.3). This is consistent with the human system, where

replication-dependent histone mRNA degradation is mainly dependent of Upf1 (Mullen and Marzluff, 2008). Interestingly, all three mutants, *upf1* C134S, *upf1* K451Q and *upf1* RR810-811AA were shown to have an effect on histone mRNA regulation. This contrasts to the effect of these mutations on NMD, where *upf1* K451Q and *upf1* RR810-811AA, disrupted the degradation response but *upf1* C134S did not have an effect (Figure 3.2.f). This implies that the underlying molecular mechanisms associated with NMD and histone mRNA regulation are distinct.

4.4 The role of endonucleolytic domain of Smg6 in histone mRNA regulation

Previously, we have shown that mutations disrupting the endonuclease PIN domain of Smg6 lead to loss of NMD in a *Δdcp2* background (Figure 3.4). Further analysis was undertaken to determine whether fidelity of the PIN domain is similarly required for regulating histone transcripts. Based on quantitative Northern analysis of histone mRNA levels in *smg6* $^{D13A\ D251A}$ strain, the result suggests that the catalytic activity of Smg6 is not required for the regulation of both H2A and H3 transcripts (Figure 4.5). These results are similar to those seen for NMD of the uaZ_{14} transcripts. This suggests that the PIN domain of Smg6, which is likely to be required for its putative endonuclease function, is not required for the regulated degradation of histone transcripts. However, the disruption of regulation associated with the Δ*smg6* allele, suggests that its role as part of the NMD complex is critical.

4.5 The role of Dcp2 and Smg6 in histone mRNA regulation

Our data indicates that the regulation of histone transcripts can potentially be initiated by deadenylation, decapping and/or endonuclease cleavage. This could then be followed by 5'-3' degradation by Xrn1, and/or 3'-5' degradation by the exosome. Functional analysis of

Upf1 uncovered the multiple roles of this factor in the regulation of normal and aberrant transcripts**.** It is possible that Upf1 has functions in mRNA regulation that act upstream of the formation of a decapping complex and/or activation of endonucleolytic domain of Smg6. We showed with respect to NMD of *uaZ*$_{14}$ mRNA, Smg6 forms an essential component within the NMD machinery which is distinct from the specific endonuclease function. The role of the Smg6 endonuclease activity was only observed in the Δ*dcp2* background, where decapping is blocked. Therefore, to check whether the HU histone response similarly required the Smg6 PIN domain functionality in the absence of decapping the *Δdcp2 smg6* $^{D13A\ D251A}$ mutant strain was tested alongside the *Δdcp2* and *smg6* $^{D13A\ D251A}$ single mutants. Northern hybridisation analysis demonstrates that the smg6 catalytic mutation, *smg6* $^{D13A\ D251A}$, was not additive with Δ*dpc2,* which as with previous data shows only partial disruption of the HU induced regulatory response (Figure 4.1.a). This suggests that the mechanisms underlying NMD and histone mRNA regulation are distinct, consistent with the Upf1 mutational analysis. Furthermore, although Smg6 is implicated in the HU induced repression of histone encoding transcripts, there is no evidence to suggest this involves the Smg6 endonuclease activity. More likely is that it is critical as part of the NMD complex involving Upf1, Upf2, Upf3 and Smg6, and deletion of Smg6 disrupts this complex.

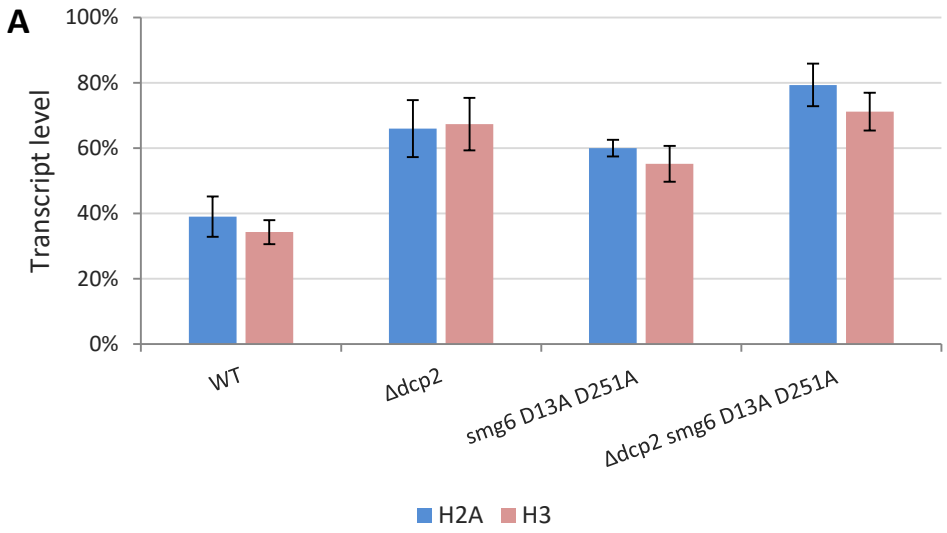

B

		Δdcp2	smg6 D13A D251A	Δdcp2 smg6 D13A D251A
H2A	p-value	0.0325	0.2746	0.0054
		Sig.		Sig.
H3	p-value	0.0101	0.0171	0.0029
		Sig.	Sig.	Sig.

C

		WT	Δdcp2	smg6 D13A D251A
H2A	p-value	0.0054	0.1440	0.0255
		Sig.		Sig.
H3	p-value	0.0029	0.3603	0.0581
		Sig.		

Figure 4.5 Characterisation of decapping and Smg6 mediated endonucleolytic cleavage in histone H2A and H3 mRNA regulation in response to HU treatment. All strains were treated with HU over a 20 minutes time course (t_0-t_{20}), to block DNA synthesis. Aliquots (10 µg) of total RNA were resolved on an agarose gel, transferred to a nylon membrane and hybridised with a ^{32}P radiolabelled probe for H2A and H3. Bar graph shows calibrated quantitative values normalised to 18S rRNA as a control, giving the relative expression levels of both H2A and H3 transcripts after a 20 minutes treatment with HU (t_{20}) compared to untreated samples (t_0) in wild-type and mutant strains. n = 3 +/- SD. (B) A t-test was performed to determine whether there was a significant difference between the HU response in mutants and in the wild-type strain. (C) An additional t-test was conducted to determine if there is a significant difference in response between Δ*dcp2 smg6* $^{D13A\ D251A}$ and the single mutants. A p-value of ≤0.05 is considered statistically significant (Sig.).

4.6 The effect of RNA degradation mutants on basal transcript levels

As transcript levels are a product of both the rate of synthesis and degradation, the observation that various mutants affect histone mRNA degradation suggests that they may also dramatically altered histone mRNA levels. However, from other systems it is known that disruption of many components involved in mRNA turnover do not have a dramatic

effect on mRNA levels, implying that there is a compensation mechanism (Houseley and Tollervey, 2009). To determine if aberrant histone mRNA levels are associated with the mutant tested we undertook comparative Northern analysis. In order to determine if any differences were specific to histone mRNA or is shared with other transcripts we investigated the *gdhA* (AN4376) mRNA levels as a comparator.

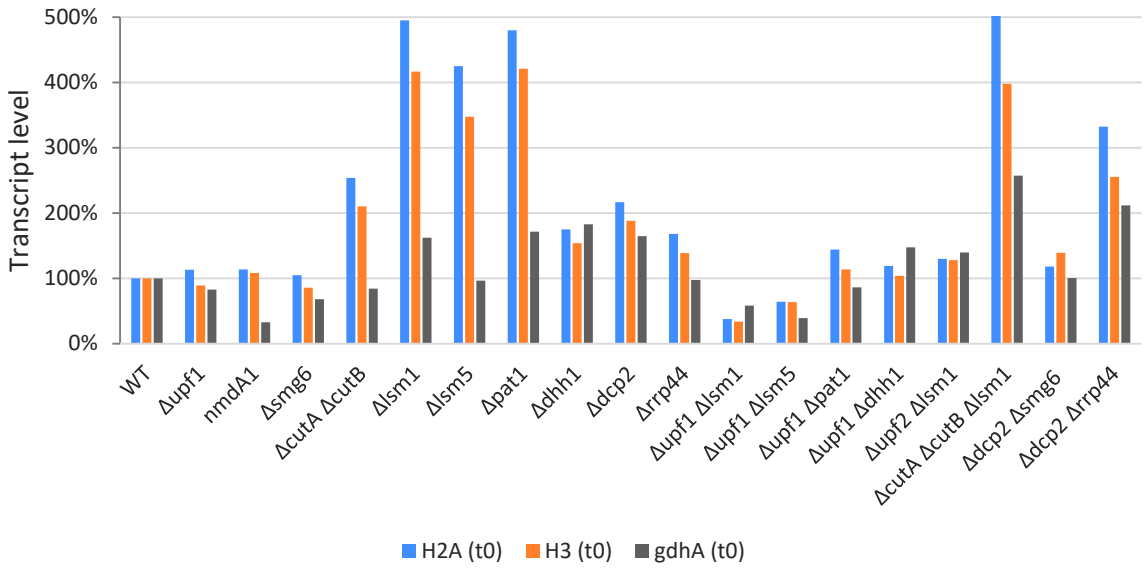

Figure 4.6 The abundance of H2A, H3 and gdhA basal mRNA in wild-type (WT) and mutant strains. The strains were grown overnight for 16 hours. Total RNA was extracted from each strain and aliquots (10 µg) of RNA were resolved on an agarose gel, transferred to a nylon membrane and hybridised with a ^{32}P radiolabelled probe for H2A, H3 and *gdhA*. Bar graph shows calibrated quantitative values normalised to 18S rRNA as a control. H2A, H3 and *gdhA* at t_0 transcript levels in mutant strains are given as a percentage of the wild-type level before treatment (t_0). n = 1.

We detected that the disruption of CutA, CutB, Pat1 and Lsm proteins individually or in pairs increased the abundance of basal mRNA levels for H2A and H3 mRNA. This dramatic shift was not generally shared with *gdhA*, although for the Δ*lsm1*, Δ*pat1* single mutants and the treble mutant Δ*cutA* Δ*cutB* Δ*lsm1*, there was an increase relative to wild-type (Figure 4.6). In the case of Δ*dcp2*, Δ*dhh1* and the Δ*dcp2* Δ*rrp44* double mutant, there was a similarly high level of all three transcripts (Figure 4.6). Interestingly, the disruption of Lsm proteins

combined with the disruption of Upf2 and particularly Upf1 significantly reduced mRNA abundance (Figure 4.6). Interpretation of these data is difficult other than to observe that there is not a simple relationship between transcript degradation and abundance and that different transcripts are affected in different ways.

4.7 Phenotype analysis of the wild-type and mutant strains

The importance of NMD effectors in cell viability and organism development varies across species (Vicente-Crespo and Palacios, 2010). The work in *S. cerevisiae* indicated, the loss of the Upf proteins has no obvious effect on growth, although PTC-containing mRNAs are stabilised in Upf mutants. It was suggested that the fact that the Upf proteins are not essential in yeast is because the regulation of targets by NMD in this organism is not required for growth (Vicente-Crespo and Palacios, 2010). Similar to the *S. cerevisiae*, deletion of *upf2* in *S. pombe* results in strains which are viable and show no apparent growth abnormality, whereas deletion of *upf1* produces abnormally long cells probably due to problems with cell cycle progression (Vicente-Crespo and Palacios, 2010). *upf1* and *upf2* knockout mice show early embryonic lethality (Vicente-Crespo and Palacios, 2010). Mutants for *A. thaliana upf1* are lethal and show metabolic, flowering, seeding and growth problems (Vicente-Crespo and Palacios, 2010). It was not clear whether this phenotype is due to lack of NMD or to some other function of the protein (Vicente-Crespo and Palacios, 2010).

The deletion of Upf1 in *A. nidulans* displays an unhealthy phenotype with reduced colonies size (growth rate) and very poor conidiation, whereas *upf1* point mutations which disrupt NMD and/or histone mRNA regulation showed relatively normal morphology (Figure 3.3). We showed the Upf1 point mutations have similar or stronger effect for both H2A and H3

mRNAs as compared with that observed with Δ*upf1* (Figure 4.3). The abundance of H2A and H3 basal mRNAs of Δ*upf1*, *upf1* ^{C134S}, *upf1* ^{K451Q} and *upf1* ^{RR811AA} are similar to that observed with the wild-type. This implies that the dramatic phenotypic effect of the Upf1 deletion might be due to its multiple roles including cellular functions other than NMD. Upf1 has roles which are important for the cell development, such as in DNA replication, telomere metabolism and genome maintenance pathways (Nicholson et al., 2014). Based on our observations and data obtained, it is clear that the role of Upf1 in other cellular processes is independent of its function in NMD.

Interestingly we observed that the double mutant, Δ*upf1* Δ*dhh1*, displayed a healthier phenotype than the Δ*upf1* single mutant (Figure 4.2.b); the implication is that the disruption of *dhh1* partially supresses the effect of *upf1* deletion. Interestingly, both Dhh1 and Upf1 are RNA helicases. One possibility is that in the absence of Upf1, Dhh1 can bind RNA that is normally associated with Upf1 and that this has a toxic effect which contributes to the poor Upf1 mutant phenotype. This would fit with the upf1 point mutations and the disruption of other NMD components not leading to the extreme mutant phenotype exhibited by Δ*upf1* strains.

The double mutants, Δ*upf1* Δ*lsm1*, Δ*upf1* Δ*lsm5*, Δ*upf1* Δ*pat1* and *nmdA1* Δ*lsm1* display an extremely poor growth phenotype in addition to loss of HU regulatory response for histone transcripts. Based on our observations and data, simultaneous disruption of both NMD and certain decay factors dramatically affect the cell viability and development. In previous studies, it has been shown that some of these factors are multifunctional, with roles ranging from transcription to mRNA decay, implicating them in a feedback loop affecting gene

transcription (Maekawa et al., 2015, Haimovich et al., 2013). Therefore, disruption of these factors may influence the expression of the genes responsible for cell development. One important possibility is that these NMD factors are also involved in general mRNA degradation (Morozov et al., 2012) and that the disruption of the two parallel mechanisms, NMD and decapping, is leading to this very poor growth phenotype**.**

4.8 The role of NMD factors in histone mRNA 3' tagging

Previously, it was demonstrated that disruption of both the ribonucleotidyltransferases, CutA and CutB led to loss of mRNA 3' tagging in *A. nidulans* (Morozov et al, 2012). However, disruption of both CutA and CutB did not have a major effect on the HU induced repression of histone transcripts, whereas disruption of Upf1, Upf2 and strikingly, Smg6 resulted in a partial suppression of this response (Figure 4.1.a). Initial data indicated that HU treatment induced uridylation of H2A mRNA and that this was dependent on CutA and CutB, and regulated by Upf1 (Morozov and Caddick, unpublished data). To investigate the possible role of NMD components in histone mRNA 3' tagging, DNase I treated total RNA was digested by alkaline phosphatase to remove 5'-phosphate group from the mRNA cap structure. Dephosphorylated mRNA was treated with tobacco acid pyrophosphatase (TAP) to remove the 5' cap structure, exposing a mono-phosphate group for subsequent ligation. The resulting decapped 5'-phosphorylated terminus and 3'-hydroxylated terminus were ligated using T4 RNA Ligase. The distribution of 5' and 3' ends of decapped histone transcripts in the respective mutant strains was assessed by circularised reverse transcriptase PCR (cRT-PCR) followed by sequencing.

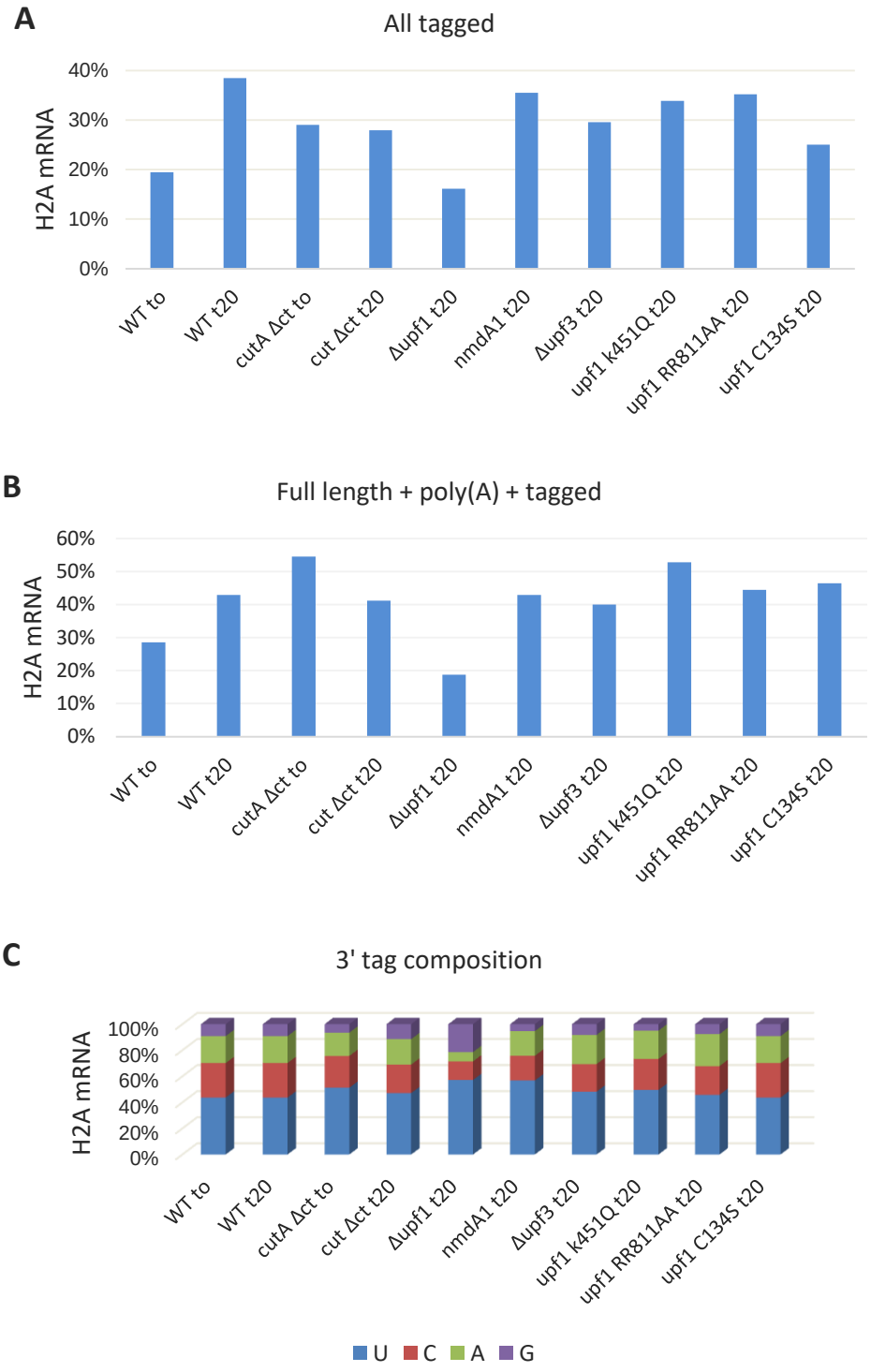

Figure 4.8 cRT-PCR analysis of histone mRNA. The strains were grown overnight for 16 hours. HU was added to the cultures, 20 minutes prior to sampling (t_{20}). Total RNA was extracted from each strain. The RNA samples were treated with alkaline phosphatase prior to decapping with tobacco acid pyrophosphatase. Sequences were obtained by cRT-PCR using a primer complementary to H2A transcripts. Between 31 and 100 transcripts were analysed from each strain. Sequence data analyses indicated the number of tagged transcripts (A), tagged full length transcripts + poly(A) tail (B) and the distribution of U, C, A and G nucleotides associated with mRNA 3' tagging in the wild-type and mutant strains (C).

From these data, it is clear that a high frequency of mRNA 3' tagging is induced by HU treatment in the wild-type strain (Figure 4.8 A and B). This is consistent with previous studies (Morozov and Caddick, unpublished data) and the situation in human cells (Mullen and Marzluff, 2008). These data indicated that the deletion of Upf1 leads to retardation of H2A mRNA 3' tagging (Figure 4.8 A and B). This is consistent with published data where Δ*upf1* lead to reduced tagging for wild-type *gdhA* mRNA and the NMD substrate, uaZ_{14} mRNA (Morozov et al, 2012). Interestingly, the Upf1 point mutations did not have an effect on tagging (Figure 4.8 A and B), whereas the *upf1* mutant strains *upf1* ^{C134S}, *upf1* ^{K451Q} and *upf1* ^{RR811AA} had a similar or more extreme effect than the deletion of Upf1 with respect to the regulatory response of histone transcripts to HU treatment (Figure 4.3).

Additionally, the frequency of tagging of the capped transcripts is not diminished, relative to wild-type, in the *nmdA1* and Δ*upf*3 strains unlike the Δ*upf1* strain (Figure 4.8 A and B). These data suggest that Upf1 plays a role in mediating HU induced histone mRNA tagging, which is distinct from its role as part of the NMD complex and mRNA degradation in *A. nidulans*. This is consistent with the minor impact that deletion of both *cutA* and *cutB* have no HU induced repression of H2A and H3 mRNA. However, this opens the question as to the primary role of tagging, if it is not to trigger transcript degradation.

CutA has a long C-terminal unstructured domain. Such domains are commonly associated with protein-protein interactions and modulation of activity (He and Jacobson, 2015). Preliminary work had indicated that a mutation, *cutA*-ΔCT, leading to C-terminal truncation (residues 578 to 1000) results in a high frequency of tagging for the *gdhA* mRNA consistent with deregulation and possible constitutive activation. It is possible that the C-terminal

domain of CutA contains the regulatory elements for its activity. Our data supports this with high levels of tagging being observed for H2A mRNA independently of HU treatment (Figure 4.8 A and B).

The distribution of nucleotides associated with mRNA 3' tagging are displayed in Figure 4.8 C. These data are consistent with other systems where U > C > A > G (Chang et al., 2014). This distribution is similar before and after treatment with HU in the wild-type strain. However, disruption of Upf1 resulted in an altered distribution with a high frequency of tagging with G and a very low frequency of A tags compared to the wild-type strain (Figure 4.8 C). Interestingly, the Upf1 point mutations did not appear to alter tagging composition (Figure 4.8 C). This is consistent with these mutations not impacting on the regulation of tagging, unlike Δ*upf1* (Figure 4.8 A and B). *in vitro* analysis of CutA showed that ATP, UTP and CTP are all substrates (Kobyłecki et al., 2017). CutA is processive for ATP, leading to polyadenylation but only short tracts of C or U, consistent with short tags normally observed and terminating in C or U nucleotides (Kobyłecki et al., 2017).

Previously, it was demonstrated that disruption of both CutA and CutB led to loss of mRNA 3' tagging in *A. nidulans* (Morozov et al., 2012). Disruption of Upf1 leads to significant retardation of mRNA 3' tagging compared to other NMD factors. Based on these findings it is likely that, in the absence of Upf1, both CutA and CutB are still being recruited to the histone transcripts but in the wild-type, Upf1 stimulates their recruitment or activity during HU induced degradation. This is consistent with the human system where Upf1 is implicated in recruiting the decay factors (Mullen and Marzluff, 2008).

4.9 Summary

Our previous results (Chapter 3) clearly demonstrated that the assembly of the active NMD machinery requires Upf1, Upf2, Upf3 and Smg6 to stimulate both decapping and cleavage of transcripts that terminate at a PTC. Based on other systems it is highly plausible that phosphorylated Upf1 facilitates Smg6 recruitment to the EJC through Upf2 and Upf3 (Nicholson et al., 2014). However, we found that the disruption of the catalytic PIN domain of Smg6 was not required where the decapping complex, Dcp1-Dcp2 was present. Importantly, in the absence of this active complex the endonuclease domain of Smg6 is required. This shows that both means of cleaving the NMD substrate, ie decapping and endonuclease cleavage, are utilised in *A. nidulans*, as in mammalian systems (Huntzinger et al., 2008).

Our data demonstrate that the NMD components, Upf1, Upf2 and Smg6, all play a major role in histone mRNA regulation but this is mechanistically distinct from NMD. With respect to smg6, HU induced regulatory response of histone coding mRNA is not dependent on fidelity of the PIN domain in the Δ*dcp2* background. Based on this distinction between NMD and histone mRNA regulation we conclude that the histone transcripts are unlikely to be cleaved by Smg6, but this protein probably plays a critical role as part of a protein complex involving other NMD components, which is also important for NMD itself.

Additionally, our results clearly indicated that Upf3 is required for NMD but not essential for histone transcripts regulation. Finally, Upf1 mutational analysis demonstrated that specific residues in both the HD and CH-domain are essential for histone regulation, whereas those

in the Upf1 HD disrupted NMD, consistent with a fundamental difference between the two processes.

Disruption of both CutA and CutB, did not have a major effect on the HU induced repression of histone transcripts. This is consistent with the pervious results where the *uaZ*$_{14}$ transcript was not stabilised by disruption of either gene (Morozov et al., 2012). However, our data indicates that the deletion of *upf1* leads to reduced histone mRNA tagging. This is consistent with published data where Δ*upf1* led to reduced tagging for wild-type *gdhA* mRNA and the NMD substrate, *uaZ*$_{14}$ mRNA (Morozov et al, 2012). Interestingly, the Upf1 point mutations that affected NMD and/or histone mRNA regulation, did not have an effect on tagging. Regarding these observations, what remains unclear is the primary function of mRNA 3' tagging; as it appeared that the absence of tagging had no major impact on the regulation of both *uaZ*$_{14}$ and histone transcripts.

Chapter 5: Characterising the role of 3' tagging

Introduction

In *A. nidulans*, the 3' tagging of mRNA involves the catalytic activity of a CutA and CutB. Our data indicated that HU treatment increases 3' tagging of histone transcripts. This is consistent with 3' tagging playing a role in the regulation of histone mRNAs in *A. nidulans*, as has been observed in human cells (Mullen and Marzluff, 2008). In human cells, it was demonstrated that histone mRNAs with oligouridylated 3' ends are likely to recruit the Lsm1-7 complex (Mullen and Marzluff, 2008), which is a known activator of decapping and translational repression (Wu et al., 2013). Our data indicated that disruption of a number of factors involved in decapping, including Lsm1 and the decapping enzyme Dcp2, reduced histone mRNA degradation induced by HU treatment. This implies that activation of decapping plays a direct role in the HU induced regulation of histone mRNA abundance and that CutA and CutB mediated 3' tagging is an integral component, helping to trigger this regulatory mechanism. Furthermore, Δ*lsm1* Δ*cutA* Δ*cutB* treble mutant's phenotype is equivalent to the single mutants with respect to histone mRNA regulation (Figure 4.2.a); this implies that Lsm1, CutA and CutB mutations are disrupting the same pathway.

Based on analysis of the effect of mutations disrupting *cutA* or *cutB*, it appears that defects in 3' tagging result transcripts subject to NMD accumulating in ribosomal fractions (Morozov et al., 2012). This suggests that 3' tagging occurs prior to dissociation of transcripts from ribosomes and that it has a role in translational repression and/or the dissociation of ribosomes from the transcript after termination. In *A. nidulans* 3' tagging has also been linked to deadenylation dependent mRNA degradation. This transition, which correlates with mRNA decapping, occurs when the poly(A) tail reaches a threshold length of A_{15} and in

A. nidulans this is also the point at which 3' tagging occurs (Morozov et al., 2012). This is consistent with tagging being closely linked to the point of transition for translation of a functional transcript to translational repression and degradation. All these pieces of evidence indicate that CutA and CutB may be associated with the ribosomes. Furthermore, confocal microscopy analysis was undertaken to locate fluorescently tagged CutA and CutB proteins. CutA was observed mainly in cytoplasm whereas CutB localised primarily to the nucleus, although a significant proportion was found in the cytoplasm (Bharudin, 2017). Interestingly, the amount of CutA in nucleus increased when CutB was disrupted (Bharudin, 2017). Thus, it was postulated that both proteins, CutA and CutB, may shuttle between the nucleus and the cytoplasm.

Based on these observations, further analysis was undertaken to check whether CutA and CutB are associated with ribosomes, consistent with their proposed role in the regulation of transcript functionality and stability.

5.1 CutA and CutB association with ribosomes and their link to Lsm1

5.1.1 Ribosomal analysis of CutB:S-tag

CutB was tagged at its C-terminus with the S-tag. This was achieved by homologous integration of a linear construct in which the 3' coding region of *cutB* was fused to the S-tag coding region and *Af-pyrG*, a selectable marker (Nayak et al., 2005). Downstream for *Af-pyrG* was the 3' UTR of *CutB*. Putative transformants were screened by PCR to confirm integration of the tagging cassette. The resulting *CutB:S-tag* strain was subjected to Western analysis (Figure 5.1.a). Three bands were observed for *cutB:S-tag* strain, but not with the wild-type. The lower doublet had an approximate size of ≥70kDa, which is consistent with

the expected size of 77kDa for the CutB protein. The two forms with showing very similar migration would be consistent with post-translational modification such as phosphorylation. The larger form had an approximate size of ≥100kDa. This may be due to a second isoform via different mRNA splicing and/or post-translational modifications (Ahmad et al., 2011). As this is a denaturing SDS-PAGE, it is unlikely to be a result of multimerisation.

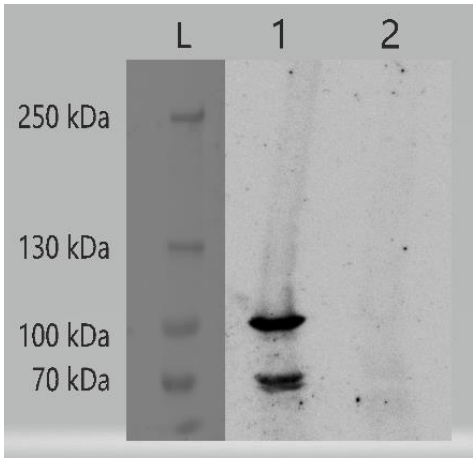

Figure 5.1.a CutB Western analysis. The whole cell lysates from wild-type (Lane 2) and *cutB:S-tag* (Lane 1) strains were subjected to Western blot using S-tag antibody against CutB:S-tag. Two bands were visualised for CutB:S-tag with approximate sizes of ≥70kDa and ≤100kDa. The expected size of CutB is 77kDa. The PageRuler™ Plus (Thermo Scientific) protein ladder image taken from the membrane is superimposed on the Western blot image in order to estimate the size of protein bands identified (L).

To determine if CutB associates with ribosomes we undertook Western analysis of the ribosomal fractions obtained by sucrose density gradient centrifugation. Additionally, we investigated the effect of *lsm1* deletion to assess if this had an effect on abundance or distribution. In order to do this *cutB:S-tag* allele was crossed into the Δ*lsm1* background. *cutB:S-tag* and Δ*lsm1 cutB:S-tag* strains were cultured in liquid media and prior to harvesting were treated with cycloheximide (CHX) for 10 minutes to block ribosome elongation and run-off. Cell free extracts were then fractioned using sucrose density gradient analysis. The resulting ribosomal profile was monitored by UV absorbance and

distinct fractions including polysomes, monosomes and ribosomal subunits were collected. The ribosome-associated proteins from gradient fractions were resolved by SDS-PAGE then probed with an antibody against the S-tag to determine the presence of CutB in the ribosomal fractions. The experiments were performed at least three times, and typical results are shown (Figure 5.1.b). Based on our observation, it was found that CutB is associated with polysomes, monosomes but the major proportion was associated with the 40S and 60S ribosomal subunits. This is consistent with CutB putative role in the modification of mRNA 3' end to promote decapping by recruiting the Lsm1-7 complex (Morozov et al., 2010). Based on this analysis, it seems that disruption of Lsm1 leads to an increase in the accumulation of CutB in the polysomal fraction. This is consistent with there being a direct functional link between CutB and the cytoplasmic Lsm complex, which fits with the putative role of 3' tagging in the recruitment of Lsm1-7 complex to initiate mRNA degradation (Mullen and Marzluff, 2008).

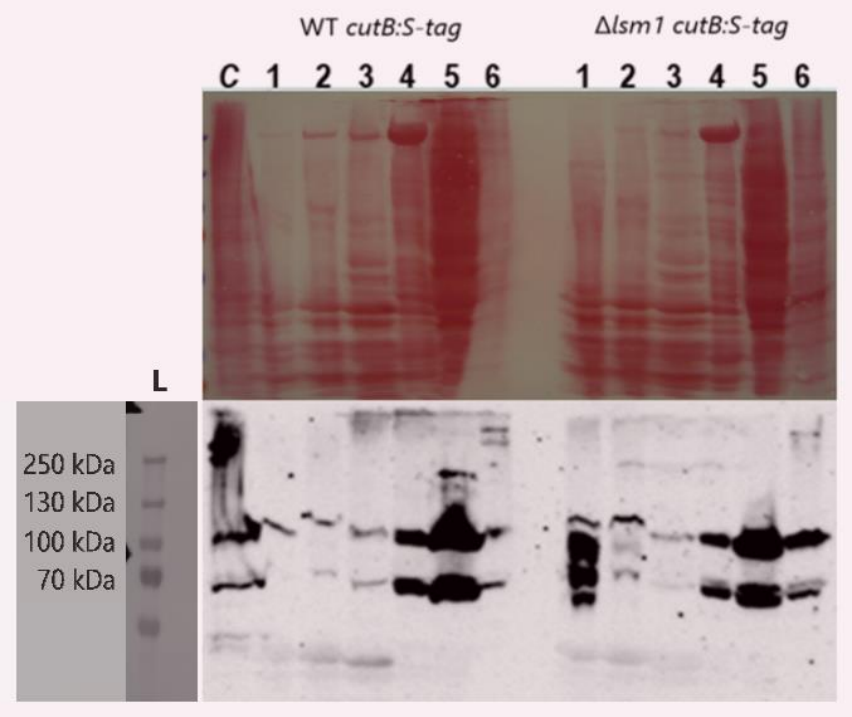

Figure 5.1.b CutB association with ribosomes. The whole cell lysates from cutB:S-tag and Δ*lsm1* cutB:S-tag strains were subjected to ribosome profiling using sucrose density centrifugation. Polysomes (Fraction 1), disome and trisomes (Fraction 2), monosome (Fraction 3), 60S subunit (Fraction 4) and 40S subunit (Fraction 5) and free soluble proteins (Fraction 6) fractions were separated according to size in a 10-50% sucrose gradient and the absorbance at 254 nm along the gradient was monitored. Membranes were stained with ponceau red to assess gel loading (Top panel) before they were analysed by Western blot with anti-S-tag antibody (Bottom panel).Two major bands were visualised for CutB:S-tag with approximate sizes of ≥70kDa and ≤100kDa consistent with the Western analysis of whole cell extract control (C). The PageRuler™ Plus (Thermo Scientific) protein ladder image taken from the membrane is superimposed on the Western blot image in order to estimate the size of protein bands identified (L).

5.1.2 Ribosomal analysis of CutA:S-tag

Further analysis was undertaken to determine whether CutA was also present in the ribosomal fractions. CutA was tagged at its C-terminus with the S-tag. Tagging was achieved as described for CutB. The resulting *cutA:S-tag* strain was subjected to Western analysis to confirm the size of CutA (Figure 5.1.c). A major band with an approximate size of ≥100kDa was observed for *cutA:S-tag* strain which contrasts with the expected size of 121kDa. Minor bands were also observed which may represent degradation products. Western analysis of protein extracted from polysome fractions gave a band with similar size, based on electrophoretic mobility. Surprisingly, CutA:S-tag was only found associated with the polysome fraction and not the other ribosomal fractions (Figure 5.1.d).

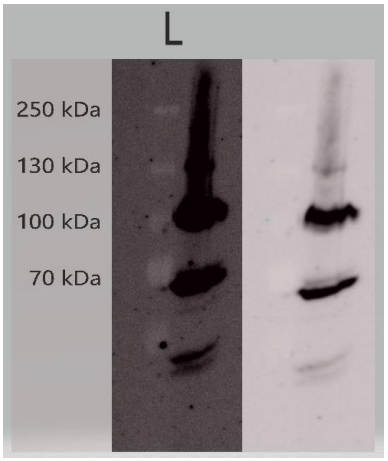

Figure 5.1.c CutA Western analysis. The whole cell lysates from *CutA:S-tag* strain was subjected to Western blot using S-tag antibody against CutA:S-tag. A band with approximate size of ≤100kDa was observed for *cutA:S-tag* strain. The PageRuler™ Plus (Thermo Scientific) protein ladder image taken from the membrane is superimposed on the Western blot image in order to estimate the size of protein bands identified (L).

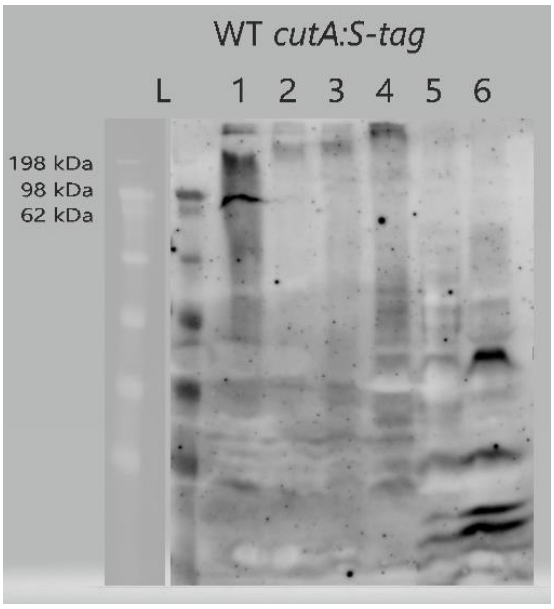

Figure 5.1.d CutA association with ribosomes. The whole cell lysates from *cutA:S-tag* was subjected to ribosome profiling using sucrose density centrifugation. Polysomes (Fraction 1), disome and trisomes (Fraction 2), monosome (Fraction 3), 60S subunit (Fraction 4), 40S subunit (Fraction 5) and free soluble proteins (Fraction 6) fractions were separated according to size in a 10-50% sucrose gradient and the absorbance at 254 nm along the gradient was monitored. Fractions were analysed by Western blotting using an S-tag antibody against CutB:S-tag. One band was visualised for CutA:S-tag with approximate size of ≥100kDa consistent with the size observed for CutA using whole cell extract (Figure 5.1.c). The SeeBlue® Plus2 (Thermo Scientific) protein ladder image taken from the membrane is superimposed on the Western blot image in order to estimate the size of protein bands identified (L).

5.2 CutA and CutB interaction

Pull-down assay was used to determine if there is a physical interaction between CutA and CutB. To elucidate their interaction, the *cutA:GFP* strain was crossed with a *cutBS-tag* strain to construct *cutA:GFP cutBS-tag* mutant strain. The total cell lysate was incubated with the anti-GFP antibody (AB) to immobilise CutA:GFP on agarose beads. The eluted proteins from the beads were resolved by SDS-PAGE and an antibody against the S-tag or GFP-tag was used as a probe. The pull-down results obtained clearly showed co-immunoprecipitation, indicative of an interaction between CutA and CutB proteins (Figure 5.2). However, this was very inconsistent with a number of repeat experiments being unsuccessful. Additionally, tests in which the samples were treated with RNase prior to precipitation never produced a positive result. CutA was not often found in the polysome fraction which was noted during multiple CutA polysomal analyses. Combined together, these results indicate that there is a possibility that CutA and CutB are engaged with one another but this may not be a direct interaction. These results are consistent with imaging of a strain expressing CutA:GFP CutB:RFP did not give any clear indication of colocalisation suggesting that it is only a small proportion of the two proteins that interact at any one time (Bharudin, 2017).

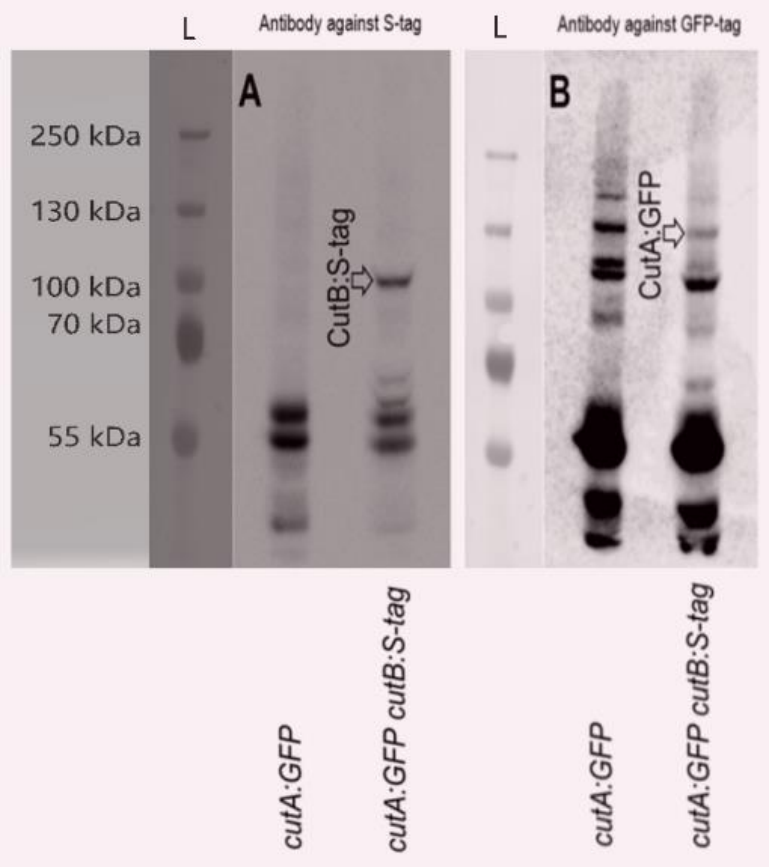

Figure 5.2 CutA interacts with CutB. Pull-down experiment was performed to determine if CutA:GFP and CutB:S-tag interact. Whole cell lysate of *cutB:S-tag cutA:GFP* strain and *cutA:GFP* as a control were incubated with anti-GFP antibody and protein A/G agarose beads. The beads were washed and subsequently the proteins were eluted from the beads, subjected to SDS-PAGE and transferred onto nitrocellulose membrane. The membranes were incubated with the primary antibody: anti S-tag (A) or anti GFP (B). Membranes were washed and incubated with HRP coupled secondary antibody and then visualised using ImageQuant LAS 4000 scanner. One band was visualised for CutB:S-tag with the size of ≤100kDa (A); and when re-probed with anti-GFP-tag, the expected bands for CutA at ~130kDa and >130kDa. These data are consistent with the sizes observed for CutA and CutB, using cell free extract (Figure 5.1.a and 5.1.c). The PageRuler™ Plus (Thermo Scientific) protein ladder image taken from the membrane is superimposed on the Western blot image in order to estimate the size of protein bands identified (L).

5.3 The effect of HU on histone mRNA engaged with ribosomes in Δ*lsm1* and Δ*cutA* Δ*cutB*

NMD relies on translation in order to scan and asses the functionality of transcripts. Through this mechanism transcripts with premature termination codons are recognised leading to translational repression and degradation, allowing cells to avoid the synthesis of aberrant proteins. Translation of mRNA starts with the association of a small ribosomal subunit (40S)

and a large ribosomal subunit (60S) to form a complete ribosome (monosome) (Lorsch, 2013). As the ribosome moves along the mRNA during translation elongation, additional ribosomes can initiate translation on the same mRNA forming, polysomes (Lorsch, 2013). The rate of translation is reflected in the polysome to monosome ratio (Lorsch, 2013). The loss of polysomes results in an associated increase in the number of free 80S ribosomes (monosomal peak) (Lorsch, 2013). However, polysomal analysis simply monitors the association of ribosomes with an mRNA and this necessarily does not mean that the mRNA is translated (Michel and Baranov, 2013). Therefore, ribosomes may be stalled on the transcript without generating a protein (Michel and Baranov, 2013).

HU induced histone mRNA degradation data indicated that the disruption of both *cutA* and *cutB* led to only limited stabilisation of histone mRNA levels (Figure 4.1.a). Moreover, the disruption of Lsm1 resulted in an increase in the accumulation of CutB in the polysomal fraction (Figure 5.1.b). This suggests a functional link during the translation.

To check the effect of these factors on histone translation and/or ribosome association of the transcript after HU treatment, the cells from wild-type, Δ*lsm1* and Δ*cutA* Δ*cutB* strains were harvested after both 10 minutes of treatment with CHX (t_0), and 10 minutes with HU prior to CHX treatment (t_{20}). Ribosome-associated transcripts were separated by sucrose density gradient centrifugation. Northern analysis was used subsequently to evaluate the relative level of histone transcripts engaged with polysomes, monosomes and ribosomal subunits.

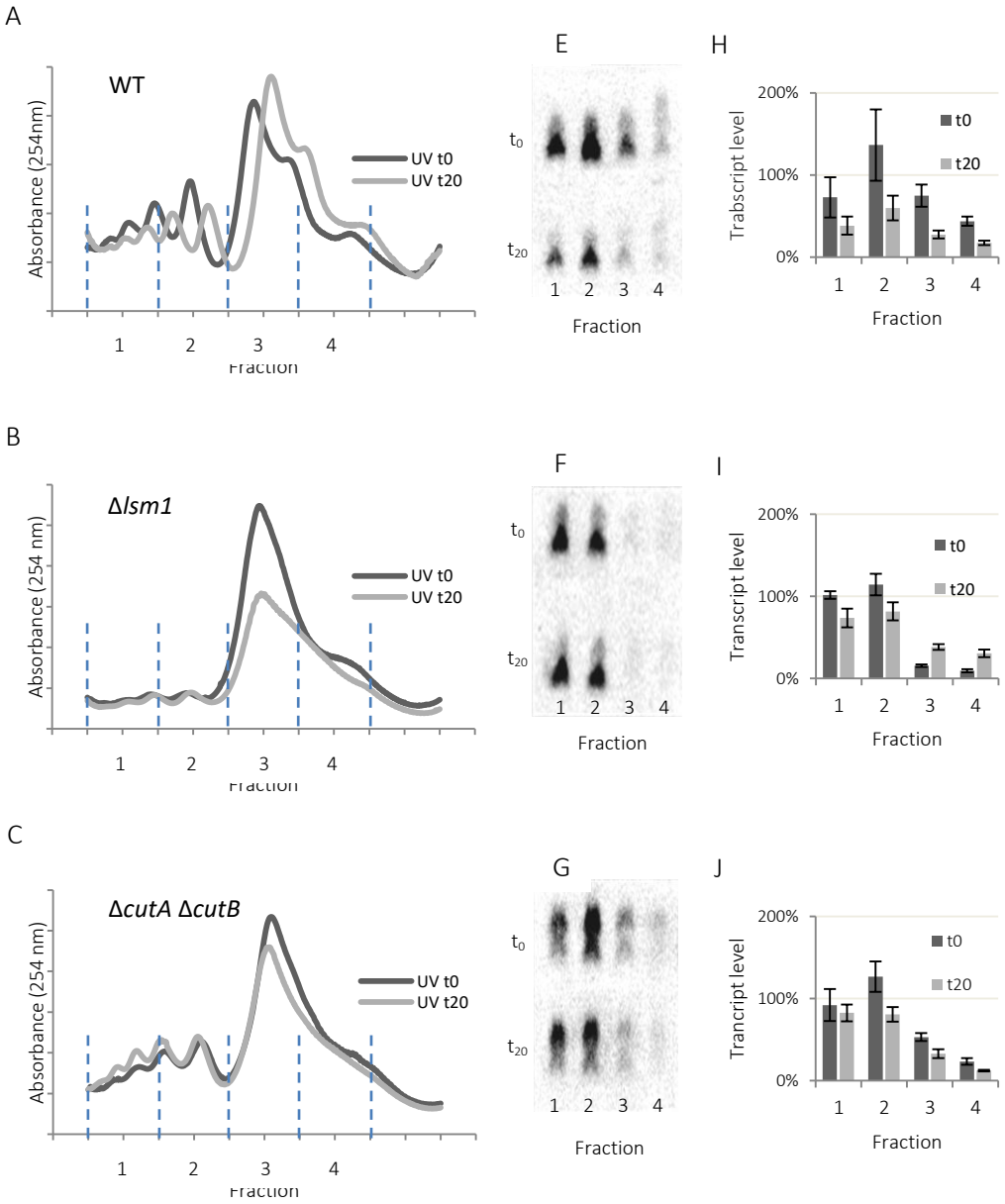

Figure 5.3.a Polysomal profile and Northern analysis of the response to HU treatment. Wild-type (WT), Δ*lsm1* and Δ*cutA* Δ*cutB* cell cultures were treated 10 minutes with CHX (t_0), or 10 minutes with HU prior to 10 minutes of CHX treatment (t20). Cellular extracts were subject to differential centrifugation and the positions of the ribosomal subunits, monosomes and polysomes determined by representative 254 nm absorbance profiles (A - D). Each 8 ml gradient was separated into polysomes (Fraction 1), disome and trisomes (Fraction 2), monosomes (Fraction 3) and ribosomal subunits (Fraction 4). Total RNA was extracted from each fraction and resolved by agarose gel electrophoresis and subjected to Northern blot analysis using a probe for H3 mRNA and 18S RNA (E – G). Bar graph shows calibrated quantitative values for H3 mRNA in each fraction, normalising against 18S as a control. n = 3 +/- SD (H – J).

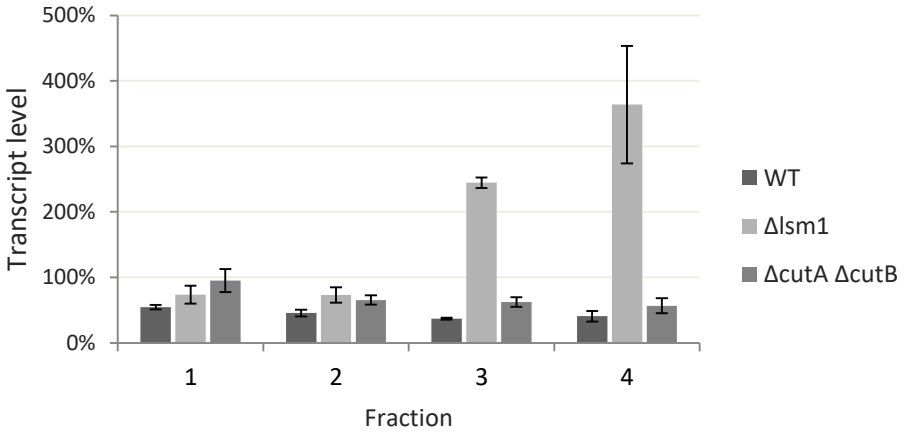

Figure 5.3.b The effect of CutA/B and Lsm1 proteins on translational regulation of histone mRNA in response to HU treatment. Graph shows quantitative data based on Northern analysis, giving the relative levels of H3 transcripts in the polysomes (Fraction 1), the disome and trisome (Fraction 2), the monosome (Fraction 3) and the subunit (Fraction 4) fractions, after a 10 min treatment with HU prior to 10 minutes of CHX treatment (t_{20}) compared to 10 minutes of treatment with CHX (t_0) in wild-type (WT), Δ*lsm1* and Δ*cutA* Δ*cutB* strains. n = 3 +/- SD.

In comparison to the wild-type strain at t_0, the *cutA cutB* double deletion resulted in a similar ratio of polysome to monosome fractions (Figure 5.3.a C). Lsm1 deletion had reduced polysomal fraction indicative of generally reduced translation (Figure 5.3.a B) consistent with the poor growth phenotype. HU treatment in wild-type strain led only to a marginal change in the profile, the polysomal proportion decreased relative to the monosomal fraction (Figure 5.3.a A). However, the disruption of Lsm1 and CutA/B had little effect on their polysomal proportion. Interestingly, in Δ*lsm1* strain we observed a noticeably high monosomal peak which almost halved at t_{20}, whereas in Δ*cutA* Δ*cutB* strain the monosomal peak declined slightly. The resulting absorbance profiles reflect the whole transcriptome associated with ribosomes. Therefore it is difficult to interpret the effect of HU treatment on the absorbance profiles.

Northern blot analysis was conducted to monitor any change in the distribution of H3 mRNA within the ribosomal profile (Figure 5.3.a). These data were quantified (Figure 5.3.b) and this demonstrated a clear change in levels of histone mRNA within polysomes, monosomes and ribosomal subunits after HU treatment for the wild-type, which is consistent with the reduced level of H3 mRNA observed by Northern analysis after 20 minutes of HU treatment (Figure 4.1.a). Interestingly, deletion of Lsm1 resulted in an increase in the proportion of transcripts within the monosome and subunit fractions after HU treatment (Figure 5.3.a I). Importantly, Northern blot analysis revealed that double deletion of *cutA* and *cutB* led to a dramatic stabilisation of histone mRNA engaged with polysomes (Fraction 1) (Figure 5.3.a J). This supports our previous data, where CutA was found only in the polysome fraction (Figure 5.1.d). These data demonstrate the link between the 3' tagging and the transcripts engaged in active translation.

5.4 The effect of CutA/B and Lsm1 on eRF3 association with ribosomes

In eukaryotes, during translation, eRF3 is recruited to ribosomes stalled at the termination codon, by eRF1 (Morozov et al., 2012). The interaction between eRF3 and Pab1 facilitates ribosome recycling and the repeated rounds of translation (Morozov et al., 2012). However, when translational termination occurs at a premature termination codon, eRF3 is unable to interact with Pab1, this allows Upf1 to be recruited (Singh, Rebbapragada and Lykke-Andersen, 2008) which induces mRNA 3' tagging in addition to NMD (Morozov et al., 2012). NMD induced termination complexes are known to be more recalcitrant than those at a native termination codons (Popp and Maquat, 2013), suggesting translational termination and/or ribosome recycling are delayed. It has also been proposed that for transcripts that have been deadenylated to the threshold length of A_{15}, eRF3 recruited to the terminating

ribosome will also be unable to interact with Pab1 and may therefore recruit Upf1, signalling mRNA 3' tagging and promoting rapid degradation (Morozov et al., 2012). This would explain the reduced 3' tagging observed for wild-type transcripts in a Δ*upf1* strain (Morozov et al., 2012). Again, these termination complexes may be more stable than those present on polyadenylated transcripts.

Tagging is known to facilitate removal of NMD substrates from the ribosomes, and possibly dissociation of the termination complex. As 3' tagging is known to help recruit the Lsm1-7 complex to the transcripts (Mullen and Marzluff, 2008) it is possible that this complex is directly involved in dissociation of the termination complex. Thus, it was postulated that the disruption of Lsm1, CutA and CutB proteins may result in eRF3, which should be associated with the termination complex, being retained for longer by the ribosomes if ribosome dissociation is delayed. This also fits the apparent increase in the monosome fraction, which may represent the stalled terminating ribosomes.

To test this an *eRF3:S-tag* strain was constructed by introducing eRF3:S-tag cassette into the wild-type strain. This strain was crossed with Δ*lsm1* and Δ*cutA* Δ*cutB* strains to obtain the respective double and triple mutants. Ribosome profiling was conducted using differential centrifugation and Western analysis was used to evaluate the abundance of eRF3 engaged with ribosomal fractions. Based on our observation, it seems that the amount of eRF3 in the polysomal fractions of Δ*lsm1* and the wild-type is very similar (Figure 5.4). This contrasts with our expectations, where we postulated a significant increase in the level of eRF3 in the monosomal fraction for the Δ*lsm1* strain. However, it appears that gel electrophoresis pattern for eRF3 in samples derived from the Δ*cutA* Δ*cutB* strain is different to those

observed for the wild-type and Δ*lsm1* strains, where the double mutant results in one prominent band for the eRF3 in the polysome fraction (Fraction 1). These different forms may result from post-translational modification. These data would be consistent with CutA and CutB having a role in the transition for translation of a functional transcript to translational repression and transcript degradation. Thus further investigation into whether this mutation has an effect on eRF3 post translational modification is necessary.

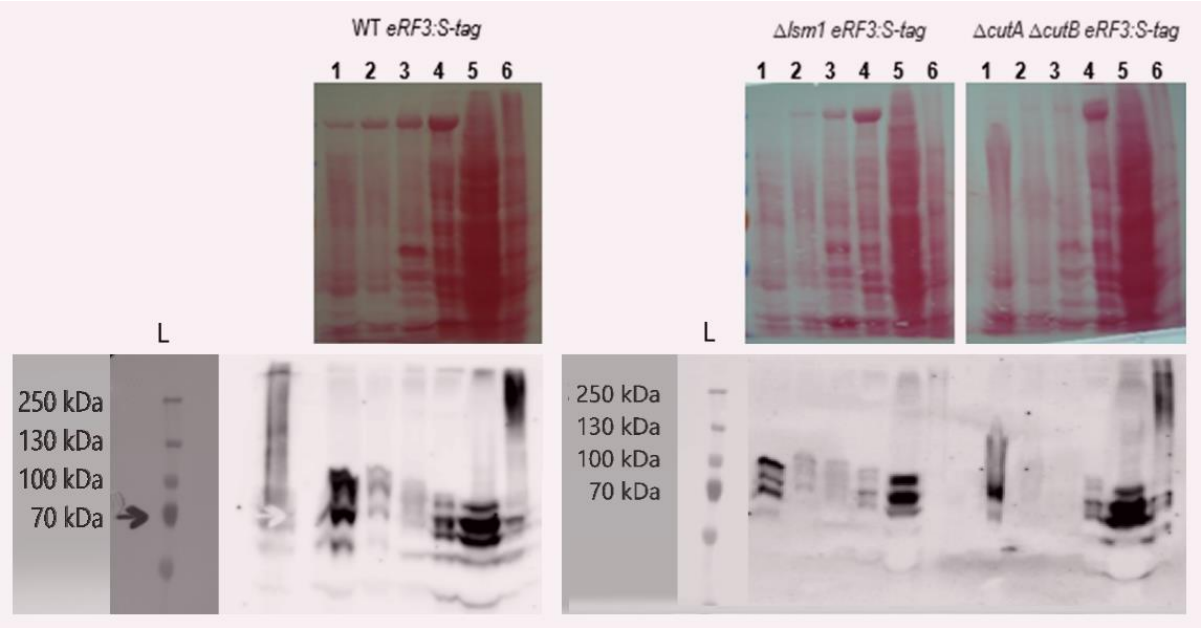

Figure 5.4 eRF3 association with ribosomes. Cell extracts from wild-type (WT) *eRF3:S-tag*, Δ*lsm1 eRF3:S-tag* and Δ*cutA* Δ*cutB eRF3:S-tag* strains were subject to ribosome profiling using sucrose density centrifugation. Polysomes, 80S, 60S and 40S were separated according to size in a 10-50% sucrose gradient and the absorbance at 254 nm along the gradient was monitored. Fractions subjected to SDS-PAGE and transferred onto nitrocellulose. Membranes were stained with ponceau red to assess gel loading (Top panel) before they were analysed by Western blot with anti-S-tag antibody (Bottom panel). The PageRuler™ Plus (Thermo Scientific) protein ladder image taken from the membrane is superimposed on the Western blot image in order to estimate the size of protein bands identified (L).

5.5 Summary

Three bands were observed for *cutB:S-tag* strain in Westerns. The lower doublet had an approximate size of ≥70kDa, which is consistent with the expected size of 77kDa for the CutB protein. The larger form had an approximate size of ≥100kDa which seems to be the one interacting with the CutA based on the pull-down assay results. Polysomal analysis showed that CutA is only in the polysome fraction whereas CutB was detected in all fractions. Compared to wild-type, double deletion of CutA and CutB caused an almost two-fold increase in stabilisation of histone mRNA engaged with polysomes (Figure 5.3.a). This is consistent with previous data, where it has been shown that for transcripts subjected to NMD, disruption of 3' tagging results in transcript accumulation in ribosomal fractions obtained by sucrose density gradient (Morozov et al., 2012). This suggests that, disruption of tagging results in a delay in ribosomes clearance and possibly histone transcript degradation becomes dependent on deadenylation.

Regarding HU induced histone mRNA degradation data it was demonstrated that the disruption of CutA and CutB had a low impact on the histone mRNA degradation rate, whereas their disruption had a major impact on histone transcripts within polysomes. This Suggests that CutA and CutB enzymes are possibly involved in regulating translationally active histone transcripts and their disruption results in extension of histone mRNA half-life in the polysomes (Figure 5.3.a G and J).

Tagging is known to help recruit the Lsm1-7 complex (Chowdhury, Mukhopadhyay and Tharun, 2007) which has been postulated to be directly involved in removal of NMD substrates from the ribosomes and dissociation of the termination complex (Morozov et al.,

2012). Based on this model, the disruption of Lsm1, CutA and CutB should result in an increased level of eRF3 bound to the termination complex in ribosomal fractions. The results contrast with our expectations; however, it appeared that the eRF3 in the polysome fraction of the Δ*cutA* Δ*cutB* strain is different to those observed for the wild-type and Δ*lsm1* strains. This suggests that the tagging factors may have an in/direct role in the post-translational modification of eRF3.

Chapter 6: Discussion

6.1 The role of NMD factors in *uaZ$_{14}$* mRNA regulation

Our results indicated that mutations disrupting the putative NMD factors Upf3 and Smg6 had a strong effect on the *uaZ$_{14}$* transcript level. This is consistent with their predicted function in NMD and similar to mutations disrupting the previously characterised loci, upf1 and nmdA (upf2) (Morozov et al., 2006). In previous studies in eukaryotes, Smg6 has been characterised as an endonuclease that cleaves transcripts harbouring an EJC associated with Upf2 and Upf3 proteins downstream from the PTC (Metze et al., 2013). EJC-enhanced NMD is a possibility in this case as there are introns positioned 3' to the PTC in *uaZ$_{14}$* (Morozov et al., 2012). Additionally, EJC components have been shown to play an important part in NMD for another filamentous ascomycete, *N. crassa*.

We have shown that both endonuclease cleavage and decapping are essential for NMD in *A. nidulans*, which distinguishes it from *S. cerevisiae* where decapping is essential. However, this is more like mammalian systems where both decapping and Smg6 cleavage are both involved in NMD. It has been shown that the human Smg6 protein cannot bind to mRNA itself. Assuming this is the case in *A. nidulans*, it is highly plausible that phosphorylated Upf1 recruits Smg6 to the EJC through Upf2 and Upf3, adding extra specificity to the Smg6 recruitment process (Nicholson et al., 2014).

We found that Upf1 and Smg6 are required for both decapping and cleavage of PTC-containing *uaZ$_{14}$* transcript. Moreover, our results indicated that both Upf1-K451Q and Upf1-RR811AA disrupt NMD, whereas Upf1-C134S had no major effect on *uaZ$_{14}$* mRNA stability. K451Q and RR811AA are located in the HD, whereas C134S is located in the CH-

domain of Upf1. Our results confirm the key role of Upf1 HD is highly likely that Upf1-Smg6 interaction is required to trigger NMD; the Upf1 HD may be involved in forming this complex.

Based on *in vitro* studies in human cells, Upf1 interacts with CBP80 via its HD to interact with the mRNA cap structure (Benhabiles, Jia and Lejeune, 2016). This direct interaction with CBP80 promotes the recruitment of Upf1 to the EJC (Hosoda et al., 2005). Additionally, Smg1 associated with Smg5-7 and Smg6 (Benhabiles, Jia and Lejeune, 2016). However, CBP80 only co-precipitated with Upf1 in the absence of RNaseA, whereas Smg5-7 and Smg6 were co-precipitated with phosphorylated Upf1 in the presence of RNase A (Okada-Katsuhata et al., 2011). It was suggested that decapping and endo-cleavage occurs when Smg5, Smg6 and Smg7 have all bound to Upf1 and Upf1 ATPase is activated, since Upf1 ATPase activity may regulate the decapping and Smg6 endonuclease activity (Okada-Katsuhata et al., 2011). This is consistent with our results where it is possible that a Upf1-Smg6 association is required for both decapping and Smg6 PIN domain activation for the regulation of uaZ_{14} transcript.

6.2. The role of NMD components in histone mRNA regulation and tagging

6.2.1. Smg6

It has been found in various studies amongst eukaryotes that the relative contribution of endo- and exo-nucleolytic mRNA decay pathways is variable between transcripts (Metze et al., 2013). This is in agreement with our data, where the eliminating components of both the 5'-3' and 3'-5' decay pathways, does not fully overcome but partially reduces the regulatory response of histone mRNA to an HU induced block in DNA replication. This indicates that the

response is at least partially dependent on transcript degradation and that both 5’ and 3’ decay pathways contribute to histone mRNA degradation in *A. nidulans*. These data are consistent with a model in which HU treatment induces rapid histone mRNA degradation through both 3’-5’ and 5'-3' pathways in human cells (Mullen and Marzluff, 2008).

In addition to the 5’ and 3’ decay pathways, the enzyme Smg6 has been implicated as an endonuclease involved in an alternative deadenylation-independent mRNA decay pathway (Nicholson et al., 2014). Endonucleases are particularly potent since they can avoid both the 5’ cap structure and poly(A) tail that serve as structural mRNA stabilising components. The subsequent 5’ and 3’ cleavage products are then degraded in both the 3’-5’ and 5’-3’ directions, respectively.

Histone mRNA regulation data presented here indicates that despite the elimination of Dcp1, Dcp2, Xrn1 or, components of 3’-5’ exosome complex, mRNA degradation is still observed. This potentially underestimates the role of the decapping complex in *A. nidulans*. In addition, the disruption of Smg6 resulted in a dramatic stabilisation of histone mRNA, which emphasised the possibility of Smg6 being involved in an endonucleolytic cleavage of histone mRNAs. For instance, in *D. melanogaster*, which lacks Smg7, degradation is mainly mediated by the Smg6-mediated endonuclease pathway (Palacios, 2012), where Smg7 is believed to link NMD and mRNA decay by interacting with Smg5 and Upf1 (Unterholzner and Izaurralde, 2004). Further analysis was undertaken to confirm the role of Smg6 during histone mRNA regulation. The results suggested that cleavage of histone transcripts by Smg6 was not required as point mutations disrupting the PIN domain did not have an effect in either the wild-type or Δ*dcp1* background. The role of Smg6 in histone mRNA regulation

not being dependent on its nuclease activity would suggest a general role as part of a complex involving Upf1. This possibility is in line with the fact that Smg6 may be involved in dephosphorylation/phosphorylation cycle of Upf1 (Fukuhara et al., 2005). This clearly indicates that the mechanism of histone transcript regulation is different to that of NMD although many of the same components are implicated.

In addition to Smg6, recent studies have revealed the novel role of Rrp44 in endo- and exo-nucleolytic mRNA degradation (Schneider and Tollervey, 2014). Northern data indicates Rrp44 had an effect on the histone mRNA stability but not as dramatic as Smg6. Rrp44 is a catalytic subunit of the exosome involved in both endonucleolytic and exonucleolytic digestions of RNAs (Shoemaker and Green, 2012). It therefore remains a formal possibility that endonuclease activity does play some part in histone mRNA degradation.

6.2.2 Upf1

Phosphorylation of Upf1 as a consequence of replication stress is the starting point for the histone mRNA translational termination and subsequent rapid degradation in human cells (Choe, Ahn and Kim, 2014). A phosphorylated Upf1 is required as a starting point for mRNA decay pathways that have been reported so far (Nicholson et al., 2014). Upf1 binds with its N-terminal region rich in CH-domain to C-terminal region of Upf2 which interacts with Upf3 and thus represents the bridge between Upf1 and Upf3 (Metze et al., 2013). Initial data clearly indicates that Upf1, Upf2 and Smg6 are important in the regulation of histone transcripts. Our data shows that the Upf1 can have a profound influence on the regulation of histone transcripts, although suggesting that other factors may compensate for the role of the absent Upf1 in the regulation of histone transcripts in *A. nidulans*.

Upf1 point mutants, C134S, K451Q and RR811AA led to loss of HU induced repression of the histone transcripts. This shows that both HD and CH-domain are critical in Upf1 activity. However, this contrasts to the effect of these mutations on NMD, where only mutations of the Upf1 HD were critical. This indicates that Upf1 functions differently in NMD and histone mRNA regulation.

6.2.3 Dhh1

The interaction between the eIF4G of the cap-binding complex and the Pab1 of the poly(A) tail enhances translation and protects the transcript from degradation (Huch and Nissan, 2014). It has been shown that mutations in the cap-binding complex leads to enhanced mRNA decay by increasing the rates of deadenylation and decapping (Huch and Nissan, 2014). It has been suggested that the replacement of translational initiation factors with mRNA decay factors including Dhh1 and Scd6 is an initial step in mRNA degradation (Huch and Nissan, 2014). Our results demonstrated that apart from the NMD factors, Dhh1 has the strongest effect on histone mRNA levels among the decay factors. It is likely that Dhh1 acts upstream of other decay factors by employing additional trans-acting factors that reinforce repression and concomitantly stimulate both 5' and 3' decay pathways of histone mRNA in *A. nidulans*. For example, the decapping activators Dhh1 and Pat1 are able to interact with and recruit deadenylases in yeast and other eukaryotes (Huch and Nissan, 2014). Moreover, the deletion of *scd6* in *A. nidulans* displayed a relatively normal morphology, whereas deletion of *Dhh1* showed a poor growth phenotype (Figure 4.1.b). This may suggest the multifunctional role of Dhh1 within and/or outside the NMD complex.

In *S. cerevisiae*, it has been shown that decapping and 5'-3' degradation of mRNA can occur when the transcripts are associated with actively translating ribosomes, in this way, the final polypeptide translated is full length and functional before the transcript is destroyed (Hu et al., 2009). It has also been proposed that mRNA decapping *in vivo* occurs predominantly on polyribosomes, with the ribosomes blocking the 5'-3' degradation mediated by Xrn1 (Huch and Nissan, 2014). Therefore, preventing further ribosome loading onto transcript seems essential to promote mRNA degradation. Furthermore, various studies have shown that using the drug CHX blocks the elongation of ribosomes on mRNA which supports a model that elongating ribosomes inhibit mRNA degradation (Huch and Nissan, 2014).

Finally, In the HU induced histone mRNA degradation pathway, histone transcript degradation occurs because of inhibition of DNA replication and not through the recognition of a PTC. Therefore EJCs would be removed by the first round of translation. It has been shown that an EJC located approximately thirty nucleotides downstream from the NTC acts as an important trans-acting enhancer of NMD (Metze et al., 2013). This is consistent with both Upf2 and Upf3 having important roles in NMD as they associate with the EJC. Interestingly, our results clearly show that Upf3 is important for NMD-mediated decay however, we found that Upf3 does not play a major role in histone mRNA regulation. This difference may therefore relate to the absence of a role for the EJC in histone mRNA regulation.

6.3 Characterising the role of 3' tagging

As previous reports have linked transcript 3' modification with transcript accelerated degradation, it was surprising that the double deletion of CutA and CutB which are

responsible for 3' tagging did not have a daramatic effect on the histone transcript regulation. The same has been previously observed with PTC-containing uaZ_{14} transcript, where it was shown that the disruption of CutA or CutB had no inhibiting effect on NMD (Morozov et al., 2012).

Our Western analysis data demonstrating that CutA and CutB co-elute with active ribosomal fractions. This is consistent with the association of the CutA and CutB enzymes with translationally active transcripts. Moreover, the histone mRNA tagging was increased by HU treatment in the wild-type strain. Therefore, it is possible that CutA and CutB are involved in tagging translationally active histone transcripts. These results are consistent with a model in which the tagging factors may interact with the terminating ribosome, to promote the engagement of the Lsm1-7 complex which facilitates decapping and translational repression. This is consistent with our preliminary data that suggests the Δ*cutA* Δ*cutB* double deletion has an effect on eRF3 post-translational modification in the polysome fraction (Figure 5.4). Moreover, we found that both forms of CutB (≥70kDa and ≤100kDa) are engaged with the ribosomes however, only the larger form of CutB was shown to interact with CutA (Figure 5.2).

Appendix 1a - Buffers and solutions for general molecular biology

0.5 M disodium EDTA (1 litre):

168.1 g disodium EDTA

NaOH (adjust the pH to 8.0)

1X Tris-EDTA (TE) buffer (1 litre):

0.01 M EDTA, 0.1 M Tris-HCl, pH7.5, autoclave

50X Tris Acetate EDTA buffer (1 litre):

2 M Tris base, 0.95 M Glacial acetic acid, 100 ml 0.5 M EDTA (pH8.0)

20X Sodium citrate (SSC) buffer (1 litre):

3 M NaCl, 0.34 M Sodium citrate, pH7.0, autoclave

10X MOPS (1 litre):

0.2 M MOPS, 0.05 M NaAc, 0.01 M EDTA, autoclave

10X Gel-Loading buffer (RNA electrophoresis):

50 ml glycerol, 25 ml 1.0 M EDTA (pH8.0), 100 mg bromophenol blue

Appendix 1b - Fungal solutions and media

Aspergillus Salt Solution (1 litre):

KCl (0.35 M)

$MgSO_4.7H_2O$ (0.1 M)

KH_2PO_4 (0.056 M)

Trace elements solution (50 ml)

Solution stored at 4˚C

Vitamin solution (1 litre):

$_p$-aminobenzoic acid (PABA) (0.003 M)

Calcium pantothenate (Panto) (0.003 M)

Pyridoxine (Pyro) (0.001 M)

Riboflavin (Ribo) (0.0003 M)

Trace elements solution (1 litre):

Sodium tetraborate (0.0002 M)

Cupric sulphate (0.002 M)

Ferric orthophosphate (0.005 M)

Manganese sulphate (0.005 M)

Sodium molybdate (0.004 M)

Zinc sulphate (0.05 M)

Complete medium (CM) (1 litre):

Glucose (0.056 M)

Aspergillus salt solutions (20 ml)

Vitamin solution (10 ml)

Yeast extract (0.004 M)

Peptone (2 g)

Casamino acids (0.0047 M)

Adenine (0.0006 M)

NaOH (adjust pH to 6.5)

Minimum medium (MM) (1 litre):

Glucose (0.056 M)

Aspergillus salt solutions (20 ml)

NaOH (adjust pH to 6.5)

For solid media, granulated agar was added at either 1% or 3% (w/v)

All media were autoclaved for 20 minutes at 15 psi and stored at 4˚C

Appendix 1c - SDS-PAGE buffers and gels

Resolving gel buffer:

Tris (1.5 M)

MQ-H_2O (make up to 1 litre)

HCl (adjust pH to 8.8)

Stacking gel buffer:

Tris (0.14 M)

MQ-H_2O (make up to 250 ml)

HCl (adjust pH to 6.8)

10% SDS:

SDS (5 g)

MQ-H_2O (make up to 50 ml)

10X SDS electrophoresis buffer:

Tris (0.25 M)

Glycine (1.92 M)

SDS (0.035 M)

MQ-H_2O (make up to 1 litre)

3X loading buffer for precipitated samples:

187.5 mM Tris-HCl, pH 6.8

2 % (v/v) SDS

30 % (v/v) glycerol

300 mM DTT

0.06 % (v/v) bromophenol blue

Solubilisation buffer

50 mM Tris-HCl, pH8.0

2 % (w/v) SDS

Transfer buffer (1 Litre):

Glycine (0.192 M)

Tris (0.025 M)

Methanol (200 ml)

1X TBST buffer (1 litre):

Tris (0.02 M)

NaCl (0.15 M)

HCl (adjust the pH to 7.5)

Tween® 20 (1 ml)

10% acrylamide gel (1.5 mm glass plate) for SDS-PAGE:

Resolving gel:

Acrylamide/Bisacrylamide (2.5 ml)

Resolving gel buffer (2.5 ml)

10% SDS (50 µl)

MQ-H_2O (4.9 ml)

10% APS (100 µl)

TEMED (10 µl)

Stacking gel:

Acrylamide/Bisacrylamide (0.66 ml)

Stacking gel buffer (1.26 ml)

10% SDS (50 µl)

MQ-H_2O (3 ml)

10% APS (50 µl)

TEMED (5 µl)

Appendix 2

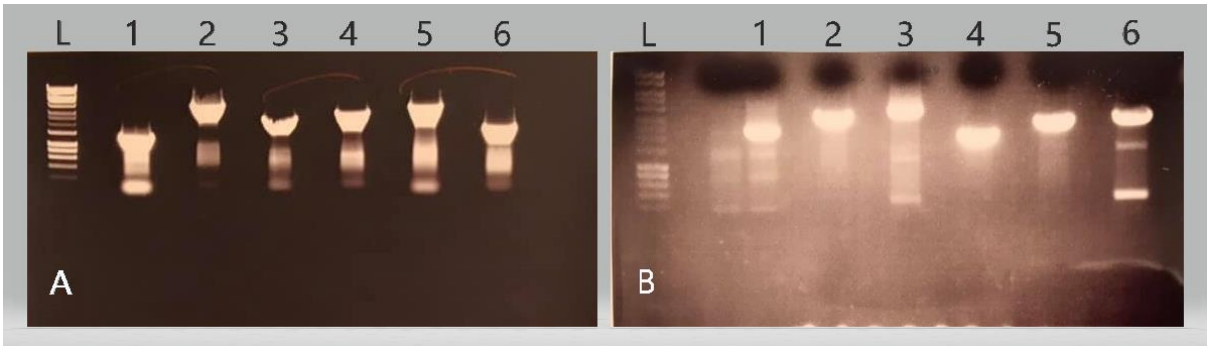

PCR images of Upf1 mutant gene construction. (A) Two gene fragments with ~25 bp overlapping region were produced by PCR for each *upf1* mutant allele. (B) DNA bands with the correct size were gel-purified and fused together to extend the overlapping region (A1+A2→B1+B2; A3+A4→B3+B4; A5+A6→B5+B6). (L) DNA Ladder (Hyperladder1). Primer sequences used in this experiment are listed in Table 2.1.1.

Appendix 3

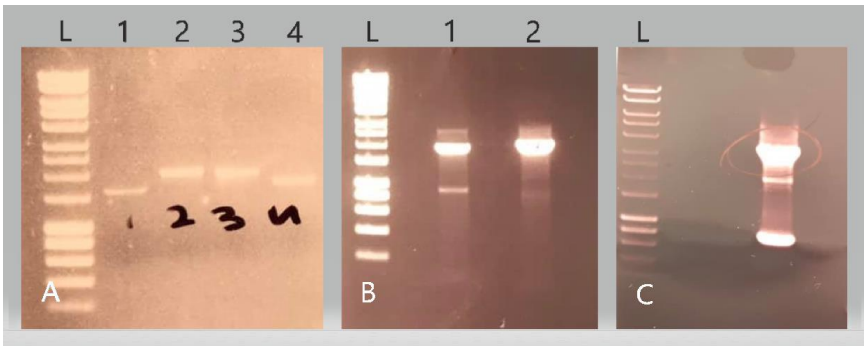

PCR images of Smg6 double mutant gene construction. (A) Two gene fragments with ~25 bp overlapping region were produced by PCR for each *smg6* mutant allele. (B) DNA bands with the correct size were gel-purified and fused together (A1+A2→B1 and A3+A4→B2). (C) The two resulting fragments (B1 and B2), each containing one of the point mutations were fused together to obtain the full length Smg6 gene with an approximate size of 3.5 kbp harbouring both mutations. (L) DNA Ladder (Hyperladder1). Primer sequences used in this experiment are listed in Table 2.1.1.

References

Ahmad, Y., Boisvert, F., Lundberg, E., Uhlen, M. and Lamond, A. (2011). Systematic analysis of protein pools, isoforms, and modifications affecting turnover and subcellular localization. *Molecular & Cellular Proteomics*, 11(3), pp.M111.013680.

Allan Drummond, D. and Wilke, C. (2009). The evolutionary consequences of erroneous protein synthesis. Nature Reviews Genetics, 10(10), pp.715-724.

Antic, S., Wolfinger, M., Skucha, A., Hosiner, S. and Dorner, S. (2015). General and MicroRNA-mediated mRNA degradation occurs on ribosome complexes in Drosophila Cells. *Molecular and Cellular Biology*, 35(13), pp.2309-2320.

Annunziato, A. (2008). DNA Packaging: nucleosomes and Chromatin. Nature education, 1(1), p.26.

Araújo, A., Melo, T., Maciel, E., Pereira, C., Morais, C., Santinha, D., Tavares, J., Oliveira, H., Jurado, A., Costa, V., Domingues, P., Domingues, M. and Santos, M. (2018). Errors in protein synthesis increase the level of saturated fatty acids and affect the overall lipid profiles of yeast. PLOS ONE, 13(8), p.e0202402.

Azzalin, C. and Lingner, J. (2006). The double life of UPF1 in RNA and DNA stability pathways. *Cell Cycle*, 5(14), pp.1496-1498.

Benhabiles, H., Jia, J. and Lejeune, F. (2016). *Nonsense mutation correction in human diseases: an approach for targeted medicine*. Academic Press.

Bhuvanagiri, M., Schlitter, A., Hentze, M. and Kulozik, A. (2010). NMD: RNA biology meets human genetic medicine. *Biochemical Journal*, 430(3), pp.365-377.

Braun, K. and Young, E. (2014). Coupling mRNA synthesis and decay. *Molecular and Cellular Biology*, 34(22), pp.4078-4087.

Celik, A., Kervestin, S. and Jacobson, A. (2015). NMD: At the crossroads between translation termination and ribosome recycling. *Biochimie*, 114, pp.2-9.

Chakrabarti, S., Jayachandran, U., Bonneau, F., Fiorini, F., Basquin, C., Domcke, S., Le Hir, H. and Conti, E. (2011). Molecular Mechanisms for the RNA-Dependent ATPase Activity of Upf1 and Its Regulation by Upf2. *Molecular Cell*, 41(6), pp.693-703.

Chang, H., Lim, J., Ha, M. and Kim, V. (2014). TAIL-seq: Genome-wide Determination of Poly(A) Tail Length and 3' End Modifications. Molecular Cell, 53(6), pp.1044-1052.

Cheng, Z., Muhlrad, D., Lim, M., Parker, R. and Song, H. (2006). Structural and functional insights into the human Upf1 helicase core. *The EMBO Journal*, 26(1), pp.253-264.

Choe, J., Ahn, S. and Kim, Y. (2014). The mRNP remodeling mediated by UPF1 promotes rapid degradation of replication-dependent histone mRNA. *Nucleic Acids Research*, 42(14), pp.9334-9349.

Choe, J., Kim, K., Park, S., Lee, Y., Song, O., Kim, M., Lee, B., Song, H. and Kim, Y. (2012). Rapid degradation of replication-dependent histone mRNAs largely occurs on mRNAs bound by nuclear cap-binding proteins 80 and 20. *Nucleic Acids Research*, 41(2), pp.1307-1318.

Chowdhury, A., Mukhopadhyay, J. and Tharun, S. (2007). The decapping activator Lsm1p-7p-Pat1p complex has the intrinsic ability to distinguish between oligoadenylated and polyadenylated RNAs. *RNA*, 13(7), pp.998-1016.

Cooper, G. (2000). *The Cell: A Molecular Approach*. 2nd ed. Sinauer Associates Inc.

da Costa, P., Menezes, J. and Romão, L. (2017). The role of alternative splicing coupled to nonsense-mediated mRNA decay in human disease. *The International Journal of Biochemistry & Cell Biology*, 91, pp.168-175.

Deutscher, M. (2006). Degradation of RNA in bacteria: comparison of mRNA and stable RNA. *Nucleic Acids Research*, 34(2), pp.659-666.

Dunn, E. (2005). Yeast poly(A)-binding protein, Pab1, and PAN, a poly(A) nuclease complex recruited by Pab1, connect mRNA biogenesis to export. *Genes & Development*, 19(1), pp.90-103.

Durand, S., Franks, T. and Lykke-Andersen, J. (2016). Hyperphosphorylation amplifies UPF1 activity to resolve stalls in nonsense-mediated mRNA decay. *Nature Communications*, 7, p.12434.

EPICENTRE, (2004) Forum 11(5), 23.

Fillman, C. and Lykke-Andersen, J. (2005). RNA decapping inside and outside of processing bodies. *Current Opinion in Cell Biology*, 17(3), pp.326-331.

Fiorini, F., Bonneau, F. & Hir, H.L. (2012). Biochemical characterization of the RNA helicase UPF1 involved in nonsense-mediated mRNA decay. *Methods in Enzymology RNA helicases*, pp.255–274.

Fiorini, F., Boudvillain, M. and Le Hir, H. (2012). Tight intramolecular regulation of the human Upf1 helicase by its N- and C-terminal domains. *Nucleic Acids Research*, 41(4), pp.2404-2415.

Fourati, Z., Kolesnikova, O., Back, R., Keller, J., Charenton, C., Taverniti, V., Plesse, C., Lazar, N., Durand, D., van Tilbeurgh, H., Séraphin, B. and Graille, M. (2014). The C-Terminal Domain from S. cerevisiae Pat1 Displays Two Conserved Regions Involved in Decapping Factor Recruitment. *PLoS ONE*, 9(5), p.e96828.

Fromont-Racine, M. & Saveanu, C. (2014). mRNA Degradation and Decay. *Fungal RNA Biology*, pp.159–193.

Fukuhara, N., Ebert, J., Unterholzner, L., Lindner, D., Izaurralde, E. and Conti, E. (2005). SMG7 Is a 14-3-3-like adaptor in the nonsense-mediated mRNA decay pathway. *Molecular Cell*, 17(4), pp.537-547.

Gardner, L. (2010). Nonsense-mediated RNA decay regulation by cellular stress: implications for Tumorigenesis. *Molecular Cancer Research*, 8(3), pp.295-308.

Garre, E., Romero-Santacreu, L., De Clercq, N., Blasco-Angulo, N., Sunnerhagen, P. and Alepuz, P. (2012). Yeast mRNA cap-binding protein Cbc1/Sto1 is necessary for the rapid reprogramming of translation after hyperosmotic shock. *Molecular Biology of the Cell*, 23(1), pp.137-150.

Gleghorn, M. and Maquat, L. (2011). UPF1 learns to relax and unwind. *Molecular Cell*, 41(6), pp.621-623.

González-Almela, E., Williams, H., Sanz, M. and Carrasco, L. (2018). The initiation factors eIF2, eIF2A, eIF2D, eIF4A, and eIF4G are not Involved in translation driven by Hepatitis C virus IRES in human cells. *Frontiers in Microbiology*, 9.

Gout, J., Li, W., Fritsch, C., Li, A., Haroon, S., Singh, L., Hua, D., Fazelinia, H., Smith, Z., Seeholzer, S., Thomas, K., Lynch, M. and Vermulst, M. (2017). The landscape of transcription errors in eukaryotic cells. Science Advances, 3(10), p.e1701484.

Haimovich, G., Medina, D., Causse, S., Garber, M., Millán-Zambrano, G., Barkai, O., Chávez, S., Pérez-Ortín, J., Darzacq, X. and Choder, M. (2013). Gene expression is circular: factors for mRNA degradation also foster mRNA synthesis. *Cell*, 153(5), pp.1000-1011.

Han, X., Wei, Y., Wang, H., Wang, F., Ju, Z. and Li, T. (2017). Nonsense-mediated mRNA decay: a 'nonsense' pathway makes sense in stem cell biology. *Nucleic Acids Research*, 46(3), pp.1038-1051.

Harigaya, Y. and Parker, R. (2012). Global analysis of mRNA decay intermediates in Saccharomyces cerevisiae. Proceedings of the National Academy of Sciences, 109(29), pp.11764-11769.

He, F. and Jacobson, A. (2015). Control of mRNA decapping by positive and negative regulatory elements in the Dcp2 C-terminal domain. *RNA*, 21(9), pp.1633-1647.

Hir, H., Saulière, J. and Wang, Z. (2015). The exon junction complex as a node of post-transcriptional networks. *Nature Reviews Molecular Cell Biology*, 17(1), pp.41-54.

Hosoda, N., Kim, Y., Lejeune, F. and Maquat, L. (2005). CBP80 promotes interaction of Upf1 with Upf2 during nonsense-mediated mRNA decay in mammalian cells. *Nature Structural & Molecular Biology*, 12(10), pp.893-901.

Houseley, J. and Tollervey, D. (2009). The many pathways of RNA degradation. *Cell*, 136(4), pp.763-776.

Hu, J., Li, Y. and Li, P. (2013). MARVELD1 inhibits nonsense-mediated RNA decay by repressing serine phosphorylation of UPF1. *PLoS ONE*, 8(6), p.e68291.

Hu, W., Petzold, C., Coller, J. and Baker, K. (2010). Nonsense-mediated mRNA decapping occurs on polyribosomes in Saccharomyces cerevisiae. *Nature Structural & Molecular Biology*, 17(2), pp.244-247.

Hu, W., Sweet, T., Chamnongpol, S., Baker, K. and Coller, J. (2009). Co-translational mRNA decay in Saccharomyces cerevisiae. *Nature*, 461(7261), pp.225-229.

Hu, Y., Qin, Y. and Liu, G. (2018). Collection and Curation of Transcriptional Regulatory Interactions in Aspergillus nidulans and Neurospora crassa Reveal Structural and Evolutionary Features of the Regulatory Networks. *Frontiers in Microbiology*, 9.

Huch, S. and Nissan, T. (2014). Interrelations between translation and general mRNA degradation in yeast. *Wiley Interdisciplinary Reviews: RNA*, 5(6), pp.747-763.

Hug, N., Longman, D. and Cáceres, J. (2016). Mechanism and regulation of the nonsense-mediated decay pathway. *Nucleic Acids Research*, 44(4), pp.1483-1495.

Huntzinger, E., Kashima, I., Fauser, M., Sauliere, J. and Izaurralde, E. (2008). SMG6 is the catalytic endonuclease that cleaves mRNAs containing nonsense codons in metazoan. *RNA*, 14(12), pp.2609-2617.

Hwang, J., Sato, H., Tang, Y., Matsuda, D. and Maquat, L. (2010). UPF1 association with the cap-binding protein, CBP80, promotes nonsense-mediated mRNA decay at two distinct steps. *Molecular Cell*, 39(3),pp.396-409.

Imamachi (2012). Up-frameshift protein 1 (UPF1): Multitalented entertainer in RNA decay. *Drug Discoveries & Therapeutics*.

Ishigaki, Y., Li, X., Serin, G. and Maquat, L. (2001). Evidence for a pioneer round of mRNA translation. Cell, 106(5), pp.607-617.

Isken, O. and Maquat, L. (2008). The multiple lives of NMD factors: balancing roles in gene and genome regulation. *Nature Reviews Genetics*, 9(9), pp.699-712.

Jamar, N., Kritsiligkou, P. and Grant, C. (2017). The non-stop decay mRNA surveillance pathway is required for oxidative stress tolerance. *Nucleic Acids Research*, 45(11), pp.6881-6893.

Kaygun, H. and Marzluff, W. (2005). Regulated degradation of replication-dependent histone mRNAs requires both ATR and Upf1. *Nature Structural & Molecular Biology*, 12(9), pp.794-800.

Kervestin, S. and Jacobson, A. (2012). NMD: a multifaceted response to premature translational termination. *Nature Reviews Molecular Cell Biology*, 13(11),pp.700-712.

Kiledjian, M. (2015). Twenty years of RNA and mRNA decay. *RNA*, 21(4), pp.664-666.

Kim, K., Cho, H., Choi, K., Kim, J., Kim, B., Ko, Y., Jang, S. and Kim, Y. (2009). A new MIF4G domain-containing protein, CTIF, directs nuclear cap-binding protein CBP80/20-dependent translation. *Genes & Development*, 23(17), pp.2033-2045.

Kim, W., Yun, S., Kwon, Y., You, K., Shin, N., Kim, J. and Kim, H. (2017). mRNAs containing NMD-competent premature termination codons are stabilized and translated under UPF1 depletion. *Scientific Reports*, 7(1).

Kobyłecki, K., Kuchta, K., Dziembowski, A., Ginalski, K. and Tomecki, R. (2017). Biochemical and structural bioinformatics studies of fungal CutA nucleotidyltransferases explain their unusual specificity toward CTP and increased tendency for cytidine incorporation at the 3'-terminal positions of synthesized tails. *RNA*, 23(12), pp.1902-1926.

Kramer, S. (2017). The ApaH-like phosphatase TbALPH1 is the major mRNA decapping enzyme of trypanosomes. *PLOS Pathogens*, 13(6), p.e1006456.

Krebs, J., Goldstein, E. and Kilpatrick, S. (2017). *Lewin's genes XII*. 12th ed. Jones & Bartlett Learning, pp.555-560.

Kufel, J., Bousquet-Antonelli, C., Beggs, J. and Tollervey, D. (2004). Nuclear pre-mRNA decapping and 5' degradation in yeast require the Lsm2-8p Complex. *Molecular and Cellular Biology*, 24(21), pp.9646-9657.

Langley, R. (2015). Aspergillus nidulans Upf1: putative role of conserved active sites in ribosome recycling and 3' end mRNA tagging. *Bioscience Horizons*, 8(0), pp.hzv004-hzv004.

Laribee, R., Hosni-Ahmed, A., Workman, J. and Chen, H. (2015). Ccr4-not regulates RNA polymerase I transcription and couples nutrient signaling to the control of ribosomal RNA biogenesis. *PLOS Genetics*, 11(3), p.e1005113.

Lee, Y. and Rio, D. (2015). Mechanisms and regulation of alternative pre-mRNA splicing. *Annual Review of Biochemistry*, 84(1), pp.291-323.

Li, G. and Xie, X. (2011). Central dogma at the single-molecule level in living cells. *Nature*, 475(7356), pp.308-315.

Li, Y., Xu, Y. and Ma, Z. (2017). Comparative Analysis of the Exon-Intron Structure in Eukaryotic Genomes. Yangtze Medicine, 01(01), pp.50-64.

Lim, J., Ha, M., Chang, H., Kwon, S., Simanshu, D., Patel, D. and Kim, V. (2014). Uridylation by TUT4 and TUT7 marks mRNA for degradation. *Cell*, 159(6), pp.1365-1376.

Lloyd, J. and Davies, B. (2013). SMG1 is an ancient nonsense-mediated mRNA decay effector. *The Plant Journal*, 76(5), pp.800-810.

Lorsch, J. (2013). *Laboratory methods in enzymology: RNA*. 1st ed. Amsterdam: Elsevier, Acad. Press.

Maekawa, S., Imamachi, N., Irie, T., Tani, H., Matsumoto, K., Mizutani, R., Imamura, K., Kakeda, M., Yada, T., Sugano, S., Suzuki, Y. and Akimitsu, N. (2015). Analysis of RNA decay factor mediated RNA stability contributions on RNA abundance. *BMC Genomics*, 16(1), p.154.

McCulloch, S. and Kunkel, T. (2008). The fidelity of DNA synthesis by eukaryotic replicative and translesion synthesis polymerases. Cell Research, 18(1), pp.148-161.

Melero, R., Uchiyama, A., Castaño, R., Kataoka, N., Kurosawa, H., Ohno, S., Yamashita, A. and Llorca, O. (2014). Structures of SMG1-UPFs Complexes: SMG1 Contributes to Regulate UPF2-Dependent Activation of UPF1 in NMD. *Structure*, 22(8), pp.1105-1119.

Metze, S., Herzog, V., Ruepp, M. and Muhlemann, O. (2013). Comparison of EJC-enhanced and EJC-independent NMD in human cells reveals two partially redundant degradation pathways. *RNA*, 19(10), pp.1432-1448.

Meyerovich, M., Mamou, G. and Ben-Yehuda, S. (2010). Visualizing high error levels during gene expression in living bacterial cells. Proceedings of the National Academy of Sciences, 107(25), pp.11543-11548.

Michel, A. and Baranov, P. (2013). Ribosome profiling: a Hi-Def monitor for protein synthesis at the genome-wide scale. *Wiley Interdisciplinary Reviews: RNA*, 4(5), pp.473-490.

Miller, J. and Pearce, D. (2014). Nonsense-mediated decay in genetic disease: friend or foe?. *Mutation Research/Reviews in Mutation Research*, 762, pp.52-64.

Mohler, K. and Ibba, M. (2017). Translational fidelity and mistranslation in the cellular response to stress. Nature Microbiology, 2(9), p.17117.

Morozov, I., Jones, M., Gould, P., Crome, V., Wilson, J., Hall, A., Rigden, D. and Caddick, M. (2012). mRNA 3' tagging is induced by nonsense-mediated decay and promotes ribosome dissociation. *Molecular and Cellular Biology*, 32(13), pp.2585-2595.

Morozov, I., Negrete-Urtasun, S., Tilburn, J., Jansen, C., Caddick, M. and Arst, H. (2006). Nonsense-mediated mRNA decay mutation in Aspergillus nidulans. *Eukaryotic Cell*, 5(11), pp.1838-1846.

Muers, M. (2013). mRNA decay factors regulate transcription. *Nature Reviews Genetics*, 14(7), pp.444-444.

Muir, V., Gasch, A. and Anderson, P. (2017). The Substrates of Nonsense-Mediated mRNA Decay in Caenorhabditis elegans. G3: Genes|Genomes|Genetics, 8(1), pp.195-205.

Mullen, T. and Marzluff, W. (2008). Degradation of histone mRNA requires oligouridylation followed by decapping and simultaneous degradation of the mRNA both 5' to 3' and 3' to 5'. *Genes & Development*, 22(1), pp.50-65.

Nayak, T., Szewczyk, E., Oakley, C., Osmani, A., Ukil, L., Murray, S., Hynes, M., Osmani, S. and Oakley, B. (2005). A versatile and efficient gene-targeting system for Aspergillus nidulans. *Genetics*, 172(3), pp.1557-1566.

Nicholson, P., Josi, C., Kurosawa, H., Yamashita, A. and Mühlemann, O. (2014). A novel phosphorylation-independent interaction between SMG6 and UPF1 is essential for human NMD. *Nucleic Acids Research*, 42(14), pp.9217-9235.

Norbury, C. (2013). Cytoplasmic RNA: a case of the tail wagging the dog. *Nature Reviews Molecular Cell Biology*, 14(10), pp.643-653.

Okada-Katsuhata, Y., Yamashita, A., Kutsuzawa, K., Izumi, N., Hirahara, F. and Ohno, S. (2011). N- and C-terminal Upf1 phosphorylations create binding platforms for SMG-6 and SMG-5:SMG-7 during NMD. *Nucleic Acids Research*, 40(3), pp.1251-1266.

Ottens, F. and Gehring, N. (2016). Physiological and pathophysiological role of nonsense-mediated mRNA decay. *Pflügers Archiv - European Journal of Physiology*, 468(6), pp.1013-1028.

Palacios, I. (2012). Nonsense-mediated mRNA decay: from mechanistic insights to impacts on human health. *Briefings in Functional Genomics*, 12(1), pp.25-36.

Parker, R. (2012). RNA degradation in Saccharomyces cerevisae. *Genetics*, 191(3), pp.671-702.

Peccarelli, M. and Kebaara, B. (2014). Regulation of natural mRNAs by the nonsense-mediated mRNA decay pathway. *Eukaryotic Cell*, 13(9), pp.1126-1135.

Popp, M. and Maquat, L. (2013). Organizing principles of mammalian nonsense-mediated mRNA decay. *Annual Review of Genetics*, 47(1), pp.139-165.

Rissland, O. and Norbury, C. (2009). Decapping is preceded by 3’ uridylation in a novel pathway of bulk mRNA turnover. *Nature Structural & Molecular Biology*, 16(6),pp.616-623.

Rissland, O., Subtelny, A., Wang, M., Lugowski, A., Nicholson, B., Laver, J., Sidhu, S., Smibert, C., Lipshitz, H. and Bartel, D. (2017). The influence of microRNAs and poly(A) tail length on endogenous mRNA–protein complexes. *Genome Biology*, 18(1).

Roy, B. and Jacobson, A. (2013). The intimate relationships of mRNA decay and translation. *Trends in Genetics*, 29(12), pp.691-699.

Saito, S., Hosoda, N. and Hoshino, S. (2013). The Hbs1-Dom34 protein complex functions in non-stop mRNA decay in mammalian cells. *Journal of Biological Chemistry*, 288(24), pp.17832-17843. (Saito, Hosoda and Hoshino, 2013)

Schneider, C. and Tollervey, D. (2014). Looking into the barrel of the RNA exosome. *Nature Structural & Molecular Biology*, 21(1), pp.17-18.

Sesma, A. and Haar, T. (2014). *Fungal RNA biology*. 1st ed. Springer, pp.179-180.

Shen, B. (2004). Uridine addition after microRNA-directed cleavage. *Science*, 306(5698), pp.997-997.

Shi, M., Zhang, H., Wang, L., Zhu, C., Sheng, K., Du, Y., Wang, K., Dias, A., Chen, S., Whitman, M., Wang, E., Reed, R. and Cheng, H. (2015). Premature termination codons are recognized in the nucleus in a reading-frame-dependent manner. *Cell Discovery*, 1(1).

Shoemaker, C. and Green, R. (2012). Translation drives mRNA quality control. *Nature Structural & Molecular Biology*, 19(6), pp.594-601.

Singh, G., Rebbapragada, I. and Lykke-Andersen, J. (2008). A competition between stimulators and antagonists of Upf complex recruitment governs human nonsense-mediated mRNA decay. *PLoS Biology*, 6(4), p.e111.

Smith, C., Blencowe, B. and Graveley, B. (2008). Alternative splicing in the postgenomic era. *RNA*, 14(12), pp.2460-2461.

Song, M. and Kiledjian, M. (2007). 3' Terminal oligo U-tract-mediated stimulation of decapping. *RNA*, 13(12), pp.2356-2365.

Stajich, J., Dietrich, F. and Roy, S. (2007). Comparative genomic analysis of fungal genomes reveals intron-rich ancestors. Genome Biology, 8(10), p.R223.

Sun, X., Zhu, J., Bao, L., Hu, C., Jin, C., Harris, S., Liu, H. and Li, S. (2013). pyrG is required for maintaining stable cellular uracil level and normal sporulation pattern under excess uracil stress in Aspergillus nidulans. *Science China Life Sciences*, 56(5), pp.467-475.

Tian, M., Yang, W., Zhang, J., Dang, H., Lu, X., Fu, C. and Miao, W. (2017). Nonsense-mediated mRNA decay in Tetrahymena is EJC independent and requires a protozoa-specific nuclease. *Nucleic Acids Research*, 45(11), pp.6848-6863.

Unterholzner, L. and Izaurralde, E. (2004). SMG7 Acts as a Molecular Link between mRNA Surveillance and mRNA Decay. *Molecular Cell*, 16(4), pp.587-596.

Valentin-Hansen, P., Eriksen, M. and Udesen, C. (2004). The bacterial Sm-like protein Hfq: a key player in RNA transactions. *Molecular Microbiology*, 51(6), pp.1525-1533.

Vicente-Crespo, M. and Palacios, I. (2010). Nonsense-mediated mRNA decay and development: shoot the messenger to survive?. *Biochemical Society Transactions*, 38(6), pp.1500-1505.

von der Haar, T., Ball, P. and McCarthy, J. (2000). Stabilization of eukaryotic initiation factor 4E binding to the mRNA 5'-cap by domains of eIF4G. *Journal of Biological Chemistry*, 275(39), pp.30551-30555.

Weichenrieder, O. (2014). RNA binding by Hfq and ring-forming (L)Sm proteins. *RNA Biology*, 11(5), pp.537-549.

Wu, D., Muhlrad, D., Bowler, M., Jiang, S., Liu, Z., Parker, R. and Song, H. (2013). Lsm2 and Lsm3 bridge the interaction of the Lsm1-7 complex with Pat1 for decapping activation. *Cell Research*, 24(2), pp.233-246.

Zhang, Y. and Sachs, M. (2015). Control of mRNA stability in fungi by NMD, EJC and CBC factors through 3'UTR introns. *Genetics*, 200(4), pp.1133-1148.

Zhao, P., Liu, Q., Miller, W. and Goss, D. (2017). Eukaryotic translation initiation factor 4G (eIF4G) coordinates interactions with eIF4A, eIF4B, and eIF4E in binding and translation of the barley yellow dwarf virus 3' cap-independent translation element (BTE). *Journal of Biological Chemistry*, 292(14), pp.5921-5931.

Zhou, L., Hang, J., Zhou, Y., Wan, R., Lu, G., Yin, P., Yan, C. and Shi, Y. (2013). Crystal structures of the Lsm complex bound to the 3' end sequence of U6 small nuclear RNA. *Nature*, 506(7486), pp.116-120.

Zhou, L., Zhou, Y., Hang, J., Wan, R., Lu, G., Yan, C. and Shi, Y. (2014). Crystal structure and biochemical analysis of the heptameric Lsm1-7 complex. *Cell Research*, 24(4), pp.497-500.